In vitro assessment of aspalathin-enriched Rooibos (*Aspalathus linearis*) extract treatment in statin-induced hepatotoxicity

By

Danielle Ann Millar

Manuscript presented in fulfilment of the requirements for the degree of Masters in Science (Medical Physiology) in the Faculty of Medicine and Health Sciences at Stellenbosch University

Supervisor: Prof Christo Muller
Co-supervisors: Dr Sandra Bowles
Dr Shantal Windvogel

April 2019

Declaration

By submitting this thesis electronically, I declare that the entirety of the work contained therein is my own, original work, that I am the sole author thereof (save to the extent explicitly otherwise stated), that reproduction and publication thereof by Stellenbosch University will not infringe any third party rights and that I have not previously in its entirety or in part submitted it for obtaining any qualification.

Danielle Ann Millar April 2019

Acknowledgements

I would like to acknowledge the South African Medical Research Council and Johan Louw for the funding of this project and the use of research facilities and equipment.

I would like to acknowledge the following people for the use of reagents and their contribution to my thesis: Oelfah Patel, Nokulunga Hlengwa, Nonkululeko Mchunu, Rabia Johnson, and Phiwayinkosi Dludla.

I would like to acknowledge and thank Charna Chapman, Desmond Linden, and Ruzayda van Aarde for their countless hours of assistance.

I would like to acknowledge my supervisor, Christo Muller, and my co-supervisors, Sandi Bowles and Shantal Windvogel, for their time, guidance, and for showing me the kind of researcher I will strive to be.
Shantal, thank you for being a voice of calm and kindness throughout this project.
Sandi, thank you for being an incredible mentor and for always going above and beyond.
Christo, your expertise has been invaluable, and I am honoured to have learned from you.
I would also like to acknowledge Nireshni Chellan for the use of reagents, a second opinion, and an unofficial co-co-supervisor position.

I would like to acknowledge and thank Nélla Boshoff and Simoné Nel for keeping me laughing. I have had a richer experience for having you two by my side.

I would like to acknowledge my parents – Lasni and Tanya Millar – and my brother – Matthew Tanner – for their constant support. Without their love and encouragement, I would never have been able to achieve even a fragment of what I have achieved.

Outputs of the Study

- Millar, D.A., Bowles, S.L., Windvogel, S., & Muller, C.J.F. *In vitro* assessment of aspalathin-enriched Rooibos (*Aspalathus linearis*) extract treatment in statin-induced hepatotoxicity. **Oral presentation**, South African Medical Research Council Biomedical Research and Innovation Platform Annual Research Symposium, Cape Town, South Africa, October 2017

- Millar, D.A., Bowles, S.L., Windvogel, S., & Muller, C.J.F. *In vitro* assessment of aspalathin-enriched Rooibos (*Aspalathus linearis*) extract treatment in statin-induced hepatotoxicity. **Oral presentation**, 62nd Faculty of Medicine and Health Sciences Annual Academic Day, Tygerberg, South Africa, August 2018

- Millar, D.A., Bowles, S.L., Windvogel, S., & Muller, C.J.F. *In vitro* assessment of aspalathin-enriched Rooibos (*Aspalathus linearis*) extract treatment in statin-induced hepatotoxicity. **Poster presentation**, First Conference of Biomedical and Natural Sciences and Therapeutics, Stellenbosch, South Africa, October 2018

- Millar, D.A., Bowles, S.L., Windvogel, S., & Muller, C.J.F. *In vitro* assessment of aspalathin-enriched Rooibos (*Aspalathus linearis*) extract treatment in statin-induced hepatotoxicity. **Oral presentation**, South African Medical Research Council Biomedical Research and Innovation Platform Annual Research Symposium, Cape Town, South Africa, October 2018

Table of Contents

List of Abbreviations

ABCB1:	ATP-binding cassette (ABC) efflux transporter, subfamily B, member 1; P-gp
ADME:	Absorption, distribution, metabolism, and excretion
ADP:	Adenosine diphosphate
AGE:	Advanced glycation end-products
ALP:	Alkaline phosphatase
ALT:	Alanine transferase
AMPK:	5' adenosine monophosphate-activated protein kinase
apo:	Apolipoprotein
AST:	Aspartate transferase
ATCC:	American Type Culture Collection
ATP:	Adenosine triphosphate
ATV:	Atorvastatin
AU:	Arbitrary units
Bcl-2:	B-cell lymphoma 2
Bcl-XL:	B-cell lymphoma-extra large
BSEP:	Bile salt export pump
BSA:	Bovine serum albumin
CCl_4^-:	Carbon tetrachloride
CETP:	Cholesterol ester transfer protein
C_{max}:	Maximum plasma concentration
CO_2:	Carbon dioxide
CoQ:	Co-enzyme Q; ubiquinone
CVD:	Cardiovascular disease
CYP3A4:	CYP450 isoform 3A4
CYP450:	Cytochrome P450
DCF:	2', 7'-dichlorofluorescin
DCFDA:	2', 7'-dichlorofluorescin diacetate
DILI:	Drug-induced liver injury
DMSO:	Dimethyl sulfoxide
DNA:	Deoxyribonucleic acid
DPBS:	Dulbecco's phosphate-buffered saline
ECAR:	Extracellular acidification rate
EFSA:	European Food Safety Authority

ELISA:	Enzyme-linked immunosorbent assay
EMEM:	Eagle's Minimum Essential Medium
ER:	Endoplasmic reticulum
ETC:	Electron transport chain
eWAT:	Epididymal white adipose tissue
FATP:	Fatty acid transport protein
FBS:	Foetal bovine serum
FDA:	Food and Drug Administration
GAPDH:	Glyceraldehyde 3-phosphate dehydrogenase
GRT:	Afriplex GRT™ aspalathin-enriched green Rooibos extract
GSH:	Glutathione
GSSG:	Glutathione disulfide
H_2O_2:	Hydrogen peroxide
HDL:	High-density lipoprotein
HMG-CoA:	Hydroxymethylglutyral-coenzyme A
HRP:	Horseradish peroxidase
IC_{50}:	Half maximal inhibitory concentration
IDL:	Intermediate-density lipoprotein
IL:	Interleukin
ILLUMINATE:	Investigation of lipid level management to understand its impact in atherosclerotic events
JC-1:	5, 5', 6, 6'-Tetrachloro-1, 1', 3, 3'-tetraethylbenzimidazolylcarbocyanine iodide
LDL:	Low-density lipoprotein
$LDLr^{-/-}$:	Low-density lipoprotein receptor deficient
LPS:	Lipopolysaccharide
MAPK:	Mitogen-activated protein kinases
MRP3:	Multidrug resistance-associated protein 3
MTT:	3-(4, 5-dimethylthiazol-2-yl)-2, 5-diphenyltetrazolium bromide
NAC:	N-acetyl cysteine
NADPH:	Nicotinamide adenine dinucleotide phosphate
NAFLD:	Non-alcoholic fatty liver disease
$NaHCO_3$:	Sodium bicarbonate
NCD:	Non-communicable disease
NFκB:	Nuclear factor kappa-light-chain-enhancer of activated B cells
O_2^-:	Oxygen
OATP:	Organic anion transporting protein

OCR:	Oxygen consumption rate
PA:	Pyrrolizidine alkaloid
PAI-1:	Plasminogen activator inhibitor
PARP:	Poly ADP ribose polymerase
P-gp:	P-glycoprotein; ABCB1
PI:	Propidium iodide
PKC:	Protein kinase C
PMSF:	Phenylmethylsulfonyl fluoride
PS:	Phospholipid phosphatidylserine
PXR:	Pregnane X receptor
RIPA:	Radioimmunoprecipitation assay
RLU:	Random luminescence units
RNA:	Ribonucleic acid
RNS:	Reactive nitrogen species
ROS:	Reactive oxygen species
SDS:	Sodium dodecyl sulphate
SLCO:	Solute carrier organic anion transporter
SOD:	Superoxide dismutase
T25:	25 cm^2 culture flask
T2DM:	Type 2 diabetes mellitus
T75:	75 cm^2 culture flask
t-BHP:	*tert*-butyl hyroperoxide
TBS-T:	1 x Tris-buffered saline with 0.1% Tween 20
TLR4:	Toll-like receptor 4
TNF-α:	Tumour necrosis factor-α
UCP-2:	Uncoupling protein 2
UPR:	Unfolded protein response
VLDL:	Very low-density lipoprotein
WHO:	World Health Organisation

List of Figures

List of Tables

Abstract

Rooibos (*Aspalathus linearis*) has been shown to have various health benefits including antidiabetic, lipid-lowering, and hepatoprotective properties. Although anecdotally Rooibos consumption is regarded as safe, recently, two case studies have associated chronic consumption of Rooibos with conventional prescription medications, such as atorvastatin, with hepatotoxicity. The cholesterol-lowering drugs, statins, act by competitively inhibiting hydroxymethylglutaryl-coenzyme A (HMG-CoA) reductase, a rate-limiting enzyme in cholesterol synthesis. Although rare in occurrence, statins are potentially hepatotoxic. The safety of the concurrent use of Rooibos and statins thus needs to be elucidated.

This study aims to investigate the interaction between the potential hepatoprotective effects of Rooibos and statin-induced hepatotoxicity using an *in vitro* C3A liver cell model.

C3A liver cells, in both normal and hyperlipidaemic conditions, were exposed to atorvastatin (ATV; 10 µM and 25 µM) and Afriplex GRT™ (green Rooibos extract; 0.01 mg/mL and 0.1 mg/mL) and a combination thereof. Pre-treatment with palmitate (500 µM) for 24 hours was used to induce a hyperlipidaemic condition *in vitro*. The effects of the co-treatment on cell viability, oxidative stress, apoptosis, mitochondrial integrity and cellular ROS production were assessed in a C3A liver cell culture model. In addition, 3D culture was used to produce C3A liver spheroids, and the effect of the treatments in a chronic culture was then assessed.

GRT was not cytotoxic at any of the concentrations tested, whereas ATV showed time- and concentration-dependent cytotoxicity in C3A cells. A significant increase in ROS production was observed in C3A cells exposed to 25 µM ATV and palmitate (353.10% ± 262.70 vs. 1431.00% ± 504.2). Similar results were seen following ATV and GRT combination therapy (845.00% ± 589.60 vs. 1493.00% ± 278.4). Under hyperlipidaemic conditions, ATV induced significant increases in apoptosis (19.50% ± 3.56 vs. 52.83% ± 7.14) which was not ameliorated by GRT co-treatment (13.83% ± 2.79). The results of the 3D culture showed complementary results. Treatment with palmitate and ATV was toxic to the spheroids and treatment with GRT was unable to attenuate this toxicity. A decrease in cellular ATP was found in the ATV and ATV+GRT treated spheroids (1.45 AU/µm^3 ± 1.00, and 3.79 AU/µm^3 ± 2.32, respectively, vs control, 161.02 AU/µm^3 ± 55.26) as well as decreased glucose utilisation calculated from the increased remaining glucose in the treatment media (91.83% and 94.68%, respectively, vs control,100%).

The culmination of experiments showed that ATV was hepatotoxic. This effect was exacerbated by exposing the cells to palmitate intended to mimic a hyperlipidaemic condition. GRT co-treatment did not show any modulating effects on ATV-induced hepatotoxicity under the acute or chronic conditions tested.

Opsomming

Rooibos (*Aspalathus linearis*) besit verskeie gesondheidsvoordele insluitend antidiabetiese, lipiedverlagende eienskappe en bied beskerming teen lewertoksisiteit. Alhoewel die verbruik van Rooibos anekdoties as veilig beskou word, het twee gevallestudies onlangs hepatotoksisiteit, geassosieer met die gesamentlike gebruik van Rooibos met konvensionele kroniese voorskrifmedisyne, insluitend die statien, atorvastatien. Die cholesterolverlagende statiene, is mededingende inhibeerders van hidroksielmetielglutaryl-koënsiem A (HMG-CoA) reduktase, 'n tempo-beperkende ensiem in cholesterolsintese. Alhoewel dit selde voorkom, is statiene soms hepatotoksies. Die veiligheid van rooibos en statiene se gelyktydige gebruik moet dus getoets word.

Hierdie studie het ten doel om die potensiële beskermings-interaksie tussen ‘n aspalatien-ryk groenrooibos ekstrak, Afriplex GRT™ (GRT) en statien-geïnduseerde hepatotoksisiteit in ‘n C3A lewerselkultuur model te ondersoek.

C3A lewer selle, onder beide normale en hiperlipidaemiese toestande, is behandel met atorvastatien (ATV; 10 µM en 25 µM) en GRT (0.01 mg/mL en 0.1 mg/mL) asook 'n kombinasie daarvan. ‘n Voorbehandeling met palmitaat (500 µM) vir 24 uur is gebruik om 'n hiperlipidemiese toestand *in vitro* te veroorsaak. Die gevolge van die mede-behandeling op sel- lewensvatbaarheid, oksidatiewe stres, apoptose, mitochondriale membraan-integriteit en sellulêre ROS-produksie is in C3A-lewerselkultuur ondersoek. Daarbenewens is 3D selkultuur gebruik om C3A lewersferoïede te produseer, om die kroniese effek van die behandelings op lewer weefsel na te boots.

GRT was nie sitotoksies by die konsentrasies wat getoets is nie, terwyl ATV tyd- en konsentrasie-afhanklike sitotoksisiteit in C3A-selle getoon het. 'n Beduidende toename in ROS-produksie is waargeneem in C3A-selle wat aan 25 µM ATV en palmitaat (353.10% ± 262.70 vs. 1431.00% ± 504.2) blootgestel was. Soortgelyke resultate is waargeneem met ATV- en GRT-kombinasie terapie (845.00% ± 589.60 teen 1493.00% ± 278.4). Onder hiperlipidemiese toestande het ATV beduidende toenames in apoptose (19.50% ± 3.56 teenoor 52.83% ± 7.14) veroorsaak wat nie deur GRT-mede-behandeling verbeter is nie (13.83% ± 2.79). Die resultate van die 3D-kultuur het komplementêre resultate getoon. 'n Afname in sellulêre ATP is gevind in die ATV- en ATV + GRT-lewersferoïede (1.45 AU/µm^3 ± 1.00 en 3.79 AU/µm^3 ± 2.32, onderskeidelik). Glukoseverbruik is ook verminder, soos bereken uit die oorblywende glukose in die behandelingsmedia (91.83% en 94.68%, onderskeidelik).

Behandeling met palmitaat en ATV was toksies vir die lewersferoïede en behandeling met GRT kon nie hierdie toksisiteit ophef nie.

Die resultate van die eksperimente het getoon dat ATV hepatotoksies was. Hierdie effek is vererger deur die selle aan palmitaat bloot te stel, wat gebruik was om 'n hiperlipidemiese toestand na te boots. Die GRT-medebehandeling was oneffektief om die selle teen die ATV-geïnduseerde hepatotoksisiteit onder die akute of kroniese toestande te beskerm.

1 Introduction

Aspalathus linearis, also known as Rooibos, is a shrub indigenous to South Africa, and is recognised for its health benefits. Rooibos has been shown to have beneficial effects on metabolic diseases, including having antidiabetic (Son *et al*, 2013) and lipid-lowering properties (Beltrán-Debón *et al*, 2011). Furthermore, Rooibos has been shown to confer hepatoprotective properties (Uličná *et al*, 2003; Kucharská *et al*, 2004; Ajuwon *et al*, 2013; Canda *et al*, 2014) in multiple studies. The unabated pandemic of metabolic disease and associated co-morbidities has fuelled the demand for alternative and complementary medicines, which are perceived to be effective without adverse side-effects.

Pharmaceutical agents, although clinically proven to be effective, are often associated with side-effects. Currently, the increase in public health awareness has caused an increase in the use of alternative therapeutic options to treat chronic conditions, either in conjunction with prescription medicines or as an alternative treatment, often without consulting health practitioners. Given the growing popularity in the use of natural health products to enhance health, the likelihood of supplementing chronic prescriptions with natural medications is increasing. However, information on the safety of combining natural products and pharmaceutical products is sparse and the potential for herb-drug interactions is becoming a serious concern. Research into potential herb-drug interactions is therefore becoming increasingly urgent.

Atorvastatin is considered a “blockbuster drug” as the best-selling prescription drug in history, with lifetime sales of USD 148 744 million between 1996 and 2016 (editorial in The Lancet, 2011; Forbes, 2013). Statins are a major chronic prescription worldwide and are administered to lower increased cholesterol levels in patients who are at increased risk of developing cardiovascular disease. They act by competitively inhibiting hydroxymethylglutaryl-coenzyme A (HMG-CoA) reductase, the first and key rate-limiting enzyme of the cholesterol biosynthetic pathway (Björnsson *et al*, 2012). As with all chronic and prescription medication, the risk for the development of side-effects exists. Although rare, statin usage has resulted in serious side-effects in some patients, the most severe of which include new-onset diabetes, myalgia and myopathy, as well as the potential of rhabdomyolysis or hepatotoxicity. The presence of these side-effects or even the potential thereof, often causes patients to cease statin treatment and pursue alternative treatment options. Up to 32% of patients on statins cease taking the drug within the first six months. The changing of one’s diet, for example, may act as a preventative measure. However, this alone is unlikely to significantly improve one’s

cardiovascular risk-profile and prevent the necessity of statin treatment in the long run. Similarly, in order to lessen the statin dosage and mitigate the risk of side-effects, patients may be self-medicating with supplements that exert their own health and risk-profile modulating effects, Rooibos supplementation, as an example.

Several natural products, including Rooibos, have been shown to infer metabolic benefits. Findings by the Biomedical Research and Innovation Platform at the South African Medical Research Council have demonstrated that an aspalathin-enriched unfermented Rooibos extract (GRT) improves glycaemia and dyslipidemia in various diabetic models (Mazibuko *et al*, 2013; Dludla *et al*, 2014; Mazibuko *et al*, 2015; Johnson *et al*, 2016), including non-human primates. Controversially, two case studies exist that show that supplementing maintenance treatment of rituximab and daily administration of prednisolone with Rooibos (Sinisalo *et al*, 2010), or a Rooibos and Buchu combination in conjunction with oral steroids as well as long-term atorvastatin use (Engels *et al*, 2013), have been associated with the development of hepatotoxicity. This highlighted the gap in knowledge of whether or not Rooibos increases the risk of adverse herb-drug interactions. However, pre-clinically it has been shown that Rooibos is hepatoprotective against chemically-induced hepatotoxicity and hepatic injury (i.e. through administration of CCl_4^-, LPS, or *t*-BHP). It is unknown whether or not this hepatoprotective effect can be conferred in the case of ATV-induced toxicity. It is therefore important to understand whether these interactions could pose an added risk for hepatotoxicity, or, contrastingly, whether Rooibos is able to ameliorate ATV-induced hepatotoxic damage.

To address this, a combination of aspalathin-enriched Rooibos and ATV treatment was used to assess whether the ATV-induced hepatotoxicity could be ameliorated by the hepatoprotective effects of GRT. In terms of clinical and therapeutic relevance, both acute and chronic models were assessed, by using 2D and 3D culture of liver cells, respectively.

The use of conventional cell culture allows for the assessments of mechanistic and acute effects of a treatment on a cell line. The present study assessed cell viability using an MTT assay, mitochondrial integrity in terms of ROS production, using a DCF assay, and mitochondrial membrane potential, using a JC-1 dual emission stain assessed using flow cytometry. Secondly, markers of apoptosis were assessed: annexin V/PI staining, assessed with flow cytometry, showed the differentiation between viable, and early and late apoptotic cells, while a caspase 3/7 assay showed the activation of the apoptotic pathway. All of these parameters were assessed in the normal and a palmitate-induced hyperlipidaemic condition.

This study further investigated the usefulness of using a 3D culture model to assess the potential of chronic or accumulative toxicity of ATV and co-treatment with GRT. The value of this experimental approach is two-fold. Firstly, although the technique is still in its experimental or developmental phase, it is intended to act as an intermediate between *in vitro* and *in vivo* studies and is ethically justified as it potentially reduces the number of animals used for pharmaceutical and cosmeceutical experimentation. Secondly, rodents, such as mice and rats, lack certain human isozymes of important drug metabolising enzymes such as CYP3A4 which is a primary metabolising enzyme for both ATV and GRT. Cell lines, such as HepG2/C3A, are used to produce liver spheroids. The spheroids produced are representative of human liver tissue (see *Chapter 5: Results: 5.9 Transmission electron micrographs*) as they are a long-term culture that avoids cell passaging. As the cell lines are human-derived, human metabolising enzymes are expressed, offering the opportunity for demonstrating herb-drug interactions relevant to hepatotoxicity

Initial cytotoxicity was performed on GRT and ATV, illustrating the effects of the treatments on the cells at a range of dosages. The concentration selection for GRT was literature-relevant (Muller *et al*, 2012; Mazibuko *et al*, 2013; Mazibuko *et al*, 2015), while the dose selection of ATV was chosen as concentrations below the calculated mitochondrial dehydrogenase activity IC_{50} values of ATV, with the lower dose being non-toxic and the higher dose being significantly toxic after 24 hours.

Palmitate pre-treatment was added to the study design in order to induce a hyperlipidaemic condition *in vitro*. The presence of these metabolic alterations leaves the liver cells more susceptible to further injury than normal/untreated liver cells (Koh *et al*, 2011). The palmitate concentrations selected (500 µM) was within a literature-relevant range (Mazibuko *et al*, 2015; Abu-Baker & Tan, 2017; Zezina *et al*, 2018). Further, the palmitate concentration was indicative of a severe dyslipidaemic state, rendering the cells extensively vulnerable to additional injury by ATV.

Mitochondrial stress and dysfunction, and oxidative stress are closely linked and form a feed-forward relationship: increased mitochondrial stress results in increased ROS generation and oxidative stress, and vice-versa. The ROS-induced cytotoxic environment created, results in the initiation of apoptosis, the cleavage of executioner caspases and, ultimately, cell death. Mitochondrial membrane potential was assessed using a JC-1 assay, which was confirmed with a DCF assay assessing ROS generation. Positive results in these assays were confirmed in terms of apoptosis activation, with specific consideration on membrane integrity (annexin V/PI staining) and caspase activation.

As mentioned previously, 3D cell culturing is a culturing technique that allows for chronic, long-term assessment of treatments on specialised human-derived cells. In this single observational study, the focus was on creating a microgravitational environment for C3A liver spheroids whereby the environment created in the acute model could be extrapolated and applied to a chronic culturing setting. The microwell base of the wells of the AggreWell™ plates allows for the reproducible formation of 3D cell clusters in large quantities per well. As such, multiple spheroids are used and sampled per treatment and time point assessed, yielding multiple technical repeats within a single experimental repeat.

Assessment of basic functional parameters was demonstrative of the effects of treatment on the spheroids. Average diameter measurements and ultrastructural morphology confirmed changes in spheroid and cellular integrity. These results were correlated with the assessment of glucose utilisation, cellular ATP, and adenylate kinase which indicates the alterations in cellular functioning.

2 Literature Review

2.1 Rooibos

Aspalathus linearis, or Rooibos, (English: “red bush”) is a legumous fynbos shrub indigenous to the Cederberg region in the Western Cape Province of South Africa (*Figure 2.1.1*). Typically fermented and brewed as a tea, Rooibos gets its characteristic ‘red’ look from the ‘fermentation’ (oxidation) process. Customarily, fermented leaves and stems are used to produce a mild tasting tisane, free of caffeine, containing few tannins, while being rich in polyphenolic compounds. Compared to its fermented counterpart, unfermented, or ‘green’, Rooibos contains higher concentrations of polyphenolic compounds, including aspalathin, a dihydrochalcone *C*-glucoside exclusive to this plant species (Uličná *et al*, 2003; McKay & Blumberg, 2007).

Rooibos, as a tea, first became a commodity in 1904 through marketing by a Clanwilliam merchant, Benjamin Ginsberg. Ginsberg acquired the tea from Khoi descendants who had been crudely processing the stems and leaves during the warm summer months (Joubert & De Beer, 2011).

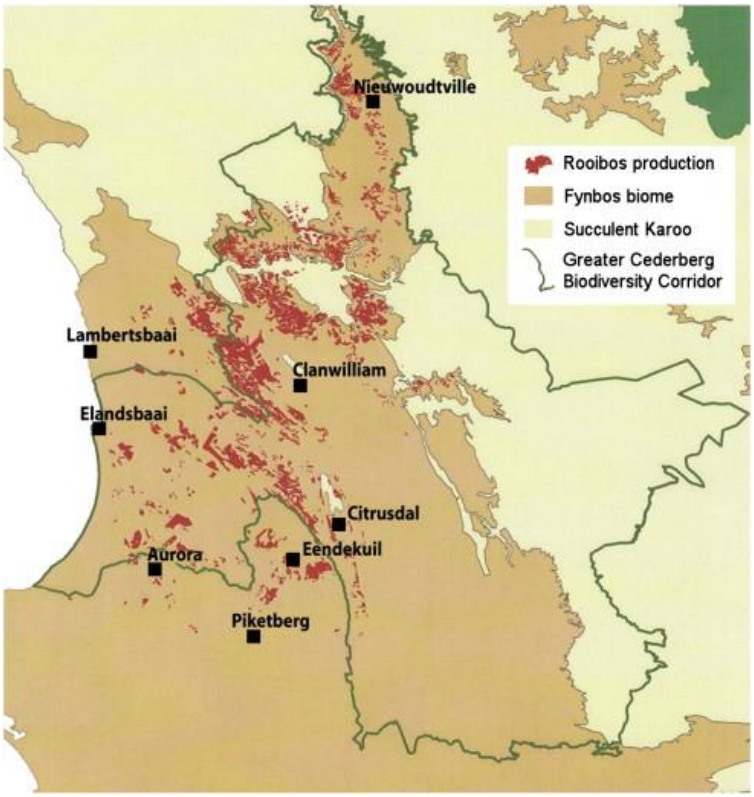

Figure 2.1.1: Production areas of Aspalathus linearis in and around the Greater Cederberg Biodiversity Corridor (map supplied by SARC). *(Adopted from Joubert & De Beer, 2011).*

Figure 2.1.2: Rooibos plantation in the Clanwilliam area. *(A) Seeding plantation; (B) Seedlings ready for transplantation; (C) Full-grown Rooibos plantation. (Images supplied by S. Bowles).*

2.1.1 Biological Characteristics

Scientific evidence confers multiple health benefits to Rooibos, such as anti-inflammatory (Lee & Bae, 2015), antioxidant (Joubert *et al*, 2004), hepatoprotective (Kucharská *et al*, 2004; Ajuwon *et al*, 2014; Canda *et al*, 2014), lipid-lowering (Bursill *et al*, 2007; Marnewick, *et al*, 2011), anti-diabetic (Son *et al*, 2013), and hypoglycaemic (Kawano, 2009; Johnson *et al*, 2016)

effects. These health benefits are contributed widely to the presence of various polyphenolic compounds (Ulicná *et al*, 2003; McKay & Blumberg, 2007; Ajuwon *et al*, 2013) (*Table 2-1*).

Table 2-1: Contents of major phenolic compounds in green and fermented Aspalathus linearis plant material (means±SD; g/100 g dry matter). *(Adapted from Joubert & De Beer, 2011)*

Structures	Compounds	Green (n=3)	Fermented (n=3)
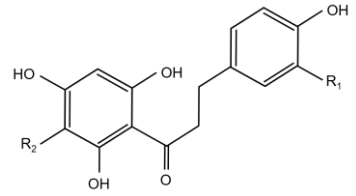	Dihydrochalcones		
	aspalathin (R_1=OH; R_2=*C*-glucosyl)	2.559±0.699	0.421±0.017
	nothofagin (R_1=*C*-glucosyl; R_2=OH)	0.251±0.230	0.040±0.022
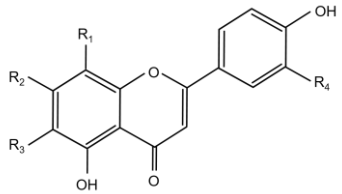	Flavones		
	orientin (R_1=*C*-glucosyl; R_2,R_4=OH; R_3=H)	0.263±0.087	0.202±0.026
	iso-orientin (R_1=H; R_2,R_4=OH; R_3=*C*-glucosyl)	0.450±0.163	0.329±0.049
	vitexin (R_1=*C*-glucosyl; R_2=OH; R_3,R_4=H)	0.042±0.020	0.035±0.009
	isovitexin (R_1,R_4=H; R_2=OH; R_3=*C*-glucosyl)	0.049±0.029	0.035±0.012
	luteolin (R_1,R_3=H; R_2,R_4=OH)	0.007±0.006	0.010±0.005
	luteolin-7-*O*-β-D-glucoside (R_1,R_3=H; R_2=*O*-glucosyl; R_4=OH)	0.015±0.008	0.015±0.008
	chrysoeriol (R_1,R_3=H; R_2=OH; R_4=OCH_3)	0.003±0.001	0.007±0.002
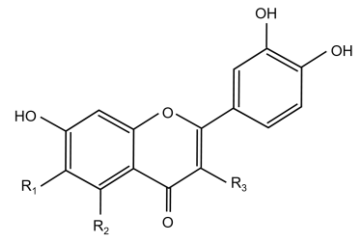	Flavonols		
	quercetin (R_1=H; R_2,R_3=OH)	0.001±0.001	0.010±0.001
	hyperoside (R_1=H; R_2=OH; R_3=*O*-galactosyl)	0.021±0.012	0.016±0.015
	rutin (R_1=H; R_2=OH; R_3=*O*- rutinosyl)	0.245±0.141	0.173±0.016

It has been well documented that the many polyphenols naturally occurring in plant extracts, such as tea extracts, act complementarily with one another to exert beneficial effects (Singh *et al*, 2009). The composition of flavonoids in Rooibos is predominantly dihydrochalcones, flavonols, and flavones, with the two most notable flavonoids in Rooibos being aspalathin, and nothofagin; the two bioactive dihydrochalcones (McKay & Blumberg, 2007; Gelderblom *et al*, 2017). Aspalathin is a dihydrochalcone *C*-glucoside, to date, found uniquely in *Aspalathus* species. Nothofagin, a rare dihydrochalcone *C*-glucoside, is the 3-deoxy analogue of aspalathin and is present in Rooibos in lower quantities than aspalathin, and has only been

previously reported to have been found in the bark of a Chinese medicinal plant, *Schoepfia chinensis* (Huang *et al*, 2008), and *Nothofagus fusca* (Hillis & Inoue, 1967) (McKay & Blumberg, 2007; Joubert & de Beer, 2011; Lee & Bae, 2015)

A study by Marnewick, *et al*, (2011) showed that dietary intervention with Rooibos modulates serum lipid profiles in humans, with results supporting studies by Bursill *et al* (2007) and Koo and Noh (2007), describing the low-density lipoprotein (LDL)-lowering capabilities of phenolic-rich beverages. It is unclear if the mechanism of action proposed included upregulation of LDL receptors, or inhibition of cholesterol synthesis and lipid absorption (Marnewick, *et al*, 2011). Irrespective of the mechanism, such findings contribute to the likelihood of concomitant therapy of chronic medication by phytotherapeutic supplements. One such chronic medication, particularly in terms of targeting dyslipidaemia, is statins.

2.2 Metabolic Perturbations

Endogenous antioxidant systems defend the body under conditions of oxidative stress. It has been confirmed that antioxidant defense systems participate in hepatoprotection in these instances, however the exact mechanisms thereof have not yet been fully elucidated (Degli Esposti *et al*, 2012; Li *et al*, 2015). Several models have shown where Rooibos exerts hepatoprotective effects (McKay & Blumberg, 2007; Ajuwon *et al*, 2013), and that the antioxidant potential of Rooibos extracts and infusions depends on its total polyphenolic profile, which is subject to method of preparation batch-to-batch variability of the plant material (McKay & Blumberg, 2007).

Lee and Bae (2015) assessed the effect of intravenous treatment with nothofagin and aspalathin on lipopolysaccharide (LPS)-mediated vascular inflammatory responses. Aspalathin and nothofagin were found to inhibit LPS-mediated expression of Toll-like receptor 4 (TLR4) as well as protecting the cellular barrier integrity, confirmed both *in vitro* and *in vivo*. Nothofagin exhibited reduced LPS-mediated inflammatory inhibitory ability compared to aspalathin. The difference in their antioxidant capabilities is postulated to be as a result of the conformational differences between the polyphenols, and nothofagin's lack of the catechol moiety. Nothofagin's decreased anti-inflammatory effectiveness as compared to its aspalathin counterpart is in agreement with other studies. Irrespective of the differences, both nothofagin and aspalathin are considered potent antioxidants and consequently both may be regarded as potential therapeutic agents in treating severe vascular inflammatory diseases (Lee & Bae, 2015).

There are many adaptive mechanisms employed by cells to promote survival in stressful situations (Yang *et al*, 2000). A compensatory mechanism – the unfolded protein response (UPR) cascade – is activated in the endoplasmic reticulum (ER) under nutrient excessive conditions, such as overwhelming fatty acid content in a cell, or hypoxia. The ER is the sensor of nutrients and cholesterol, as well as being crucial in *de novo* protein synthesis and protein folding. Changes in the redox state, calcium concentration alterations sensed by the ER, or accumulation of unfolded or misfolded proteins in the ER lumen are all possible triggers of the UPR (Wei *et al*, 2006; Wei *et al*, 2007; Schenk *et al*, 2008). Often in liver injury and disease, the ER stress is too great for the UPR to overcome, activating caspase activity and apoptosis (Wang *et al*, 2006; Wei *et al*, 2007). The chronic exposure to apoptotic stresses results in cellular adaptations which may, in fact, potentiate necrosis (Yang *et al*, 2000). One such modification is the increase in uncoupling protein-2 (UCP-2) expression, which leads to increased mitochondrial electron transport and decreased mitochondrial membrane integrity. The partial uncoupling of the mitochondrial membrane by UCP-2 and the consequent decrease in adenosine triphosphate (ATP) synthesis renders the cells particularly susceptible to further insult. Because of the already compromised nature of the cells, the addition of a stressor may cause necrosis, despite not being severe enough to do so in healthy cells (Yang *et al*, 2000).

Chronic exposure to oxidative stress, as a result of chronic hyperlipidaemic conditions, contributes to mitochondrial adaptations (Yang *et al*, 2000). Zezina *et al* (2018) suggests that in macrophages, mitochondrial fission is a protective adaptation in response to fatty acid overexposure, as opposed to being caused by fatty acids. The fragmentation of the mitochondrial network allows for the decrease in mitochondrial reactive oxygen species (ROS) production. Yang *et al* (2000) showed that mitochondria of fatty livers produce increased levels of O_2^- and H_2O_2, supporting the notion that chronic ROS production and consequent oxidative stress contributes to mitochondrial modifications and dysfunction in fatty livers of *ob*/*ob* C57BL/6 mice compared to their lean controls. The same study went on to suggest that, given the similarities between their results and tumour necrosis factor α (TNF-α)-induced apoptosis as well as nuclear factor kappa-light-chain-enhancer of activated B cells (NFκB) activation and the consequent increase in anti-apoptotic genes such as B-cell lymphoma 2 (Bcl-2) and B-cell lymphoma extra-large (Bcl-XL), and increased ROS production in the hepatocytes shows a paradoxical effect. The combination of the activation of these two mechanisms by H_2O_2 seem to balance one another out, leaving the hepatocytes vulnerable to future insult, but viable under normal conditions (Yang *et al*, 2000).

The unusual balance between pro- and anti-apoptotic markers found by Yang *et al* (2000) was also found by Selzner *et al* (2000). Activation of the apoptotic pathway was dysfunctional in fatty Zucker rats compared to their lean controls, evident by the significantly decreased levels of the apoptotic mediators caspase-8, caspase-3, and cytochrome *c*. As caspase-8 is an early marker of the apoptotic pathway, its inactivity shows an impairment in the activation of the cascade. However, there was extensive necrotic cell death in the fatty rats, suggesting a preference of necrosis in fatty rats when exposed to a stressor as opposed to apoptosis which is found in the lean controls. Further, despite the high levels of apoptosis in the lean controls, there was still an increased propensity for viability, whereas the high levels of necrosis in the fatty rats resulted in a high rate of mortality, emphasizing the irreparable damage caused by necrosis (Selzner *et al*, 2000). Taken together, these results show that, in fatty livers, necrosis is the major mechanism of cell death when exposed to an insult.

Chronic oxidative stress and the resulting mitochondrial, and deoxyribose nucleic acid (DNA) damage, as well as apoptotic changes in different organ systems, could lead to multiple organ failure (Soory, 2009; Degli Esposti *et al*, 2012). As such, cellular dysfunction serves as a contributing factor in the pathogenesis of the majority of liver pathologies as well as degenerative diseases such as cancer, cardiovascular disease, diabetes, and neurodegenerative disorders (Cesaratto *et al*, 2004; Degli Esposti *et al*, 2012). Observational studies have shown that an inverse relationship exists between the consumption of diets rich in flavonoids and cellular damage via direct radical scavenging of reactive species, chelating metal ions, or challenging enzymatic systems responsible for free radical production (McKay & Blumberg, 2007; Calitz *et al*, 2015).

A study by Kucharská *et al* (2004) compared the liver antioxidant capabilities, redox state of coenzyme Q_9, and oxidative stress in rats exposed to Rooibos tea for 7 days before carbon tetrachloride (CCl_4^-)-induced liver damage. The synthetic antioxidant N-acetyl-L-cysteine (NAC) was used as a positive control for comparison. Ubiquinone (coenzyme Q or CoQ; specifically, the dominant isoform CoQ_9 in rodents and CoQ_{10} in humans) is involved in the mitochondrial respiratory chain (electron transport chain; ETC), and its reduced form (CoQ_9H_2) is a potent lipid-soluble antioxidant, synthesised in the liver. Apart from restoring CoQ_9H_2 in rats, to levels comparable to those of healthy controls, the Rooibos treatment was also shown to prevent lipid peroxidation more effectively than NAC. Kucharská *et al* (2004) therefore suggested that antioxidant treatment is important for the prevention of liver disease, however treatment with natural antioxidants, such as Rooibos, may be more beneficial than the use of synthetic antioxidants.

2.2.1 Rooibos Treatment and Lipotoxicity

Ageing and diabetes have both been shown to cause the accumulation of glycated proteins in several tissues in the body. Kinae *et al* (1994) showed that Rooibos extract and polyphenol supplementation decreased advanced glycation end-product (AGE) production in human serum albumin, inferred to be as a result of the radical scavenging capabilities of Rooibos polyphenols (Kinae, *et al*, 1994; Kawano, 2009; Son *et al*, 2013).

The presence of the enzymes alanine transaminase (ALT) and aspartate transaminase (AST) in serum are well-established markers of hepatocellular damage. This is because they are found in abundance within hepatocytes and in low levels everywhere else in the body. As a result, the leakage of these enzymes into the serum occurs when hepatocytes are damaged or injured. The ratio of serum AST/ALT is also used as an indicator of hepatic fibrosis and the extent of fibrosis-related hepatic disorders (Giboney, 2005). Monsees and Opuwari (2017) showed that ALT levels in rats were significantly decreased compared to healthy controls when treated with unfermented Rooibos, while AST levels were significantly increased, in rats treated with fermented Rooibos, compared to healthy controls. It was concluded that Rooibos maintains serum, kidney, and liver antioxidant levels and that no adverse reactions were observed *in vivo* in female rats subjected to 21 days of exposure to Rooibos as the sole substitute for water. Further, it was suggested that Rooibos may have oestrogenic potential and, pending further confirmation, may have positive effects on female fertility (Monsees & Opuwari, 2017).

Beltrán-Debón *et al* (2011) assessed the continuous administration of an aqueous Rooibos extract on male low-density lipoprotein receptor deficient ($LDLr^{-/-}$) mice. This model was chosen as it has been shown to be a representative model of aspects of intense metabolic alterations typical of metabolic syndrome in humans (Rodríguez-Sanabria *et al*, 2010). Beltrán-Debón *et al* (2011) demonstrated that lipoprotein metabolism was significantly altered by consumption of an aqueous Rooibos extract, resulting in distinct lipid-lowering effects. This effect was strictly diet-related. The study showed that mice fed a high fat diet that received the Rooibos extract showed significant reductions in serum triglycerides, cholesterol, and free fatty acids. The triglyceride reduction was found in very low-density lipoproteins (VLDL), while the cholesterol reduction was evident in all lipoprotein particles. These results suggested that possible molecular targets of Rooibos polyphenols are located mainly in the liver and adipose tissue. Further assessment of both tissues, however, showed that an aqueous Rooibos extract significantly activated the AMP-activated protein kinase (AMPK) in the liver but not in the

epididymal white adipose tissue (eWAT), irrespective of the type of diet (Beltrán-Debón *et al*, 2011).

Under normolipidaemic conditions, there is a homeostatic balance between lipids, their oxidation, and transport, whereas dyslipidaemia results in increased concentrations of free fatty acids in circulation. Increased levels of circulating free fatty acids contributes to the pathogenesis of cardiovascular disease, atherosclerosis, metabolic syndrome, and obesity (Feldstein *et al*, 2004; Wei *et al*, 2006; Wei *et al*, 2007; Li *et al*, 2008). It has been shown that increased levels of saturated fatty acids, specifically, a likely cause of lipotoxicity, is a risk factor for serious metabolic disease, including T2DM (Feldstein *et al*, 2004; Wei *et al*, 2006; Wei *et al*, 2007; Li *et al*, 2008). One of these saturated fatty acids is hexadecanoic acid, otherwise known as ‘palmitate’ or ‘palmitic acid’, which is the first fatty acid produced during fatty acid synthesis.

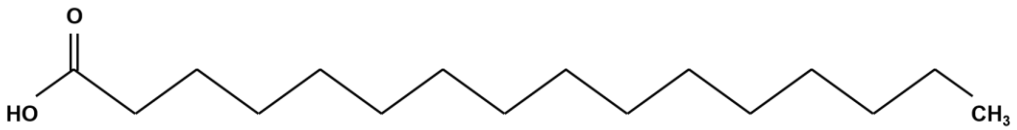

Figure 2.2.1: Chemical structure of palmitate.

Lipotoxicity, the impairment of normal cellular functioning occurs due to an imbalance between the rate of lipid production and influx and the rate of lipid expenditure. Diets rich in saturated fats have been shown to increase LDL and total cholesterol levels (Alkhouri *et al*, 2009; Unger *et al*, 2010). Free fatty acids enter hepatocytes passively, or actively through fatty acid transport proteins (FATPs), such as fatty acid translocase, also known as CD36. Once in the cell, fatty acids are converted to different types of lipids for storage, the most neutral of which is triacylglycerol. Fatty acids can also be converted to ceramides, diacylglycerol, or fatty acyl-CoAs, all of which are considered lipid intermediates and can alter normal cellular functioning and ultimately cause lipotoxicity (Schenk *et al*, 2008; Alkhouri *et al*, 2009; Unger *et al*, 2010; Alkhouri *et al*, 2011).

Excess free fatty acid storage in tissues other than adipose tissue may trigger the activation pathways that have deleterious or destructive effects, such as inflammation, insulin resistance, and excessive fibrosis. Accumulation of free fatty acids in liver cells (steatosis), for example, plays a role in Non-Alcoholic Fatty Liver Disease (NAFLD). Further, the extent of lipotoxicity is determined by the type of fatty acids present as opposed to their quantity. In hepatocytes,

liver damage and apoptosis occur as a result of an imbalance in the ratio of monounsaturated fatty acids and saturated fatty acids (Nehra *et al*, 2001; Wei *et al*, 2006; Alkhouri *et al*, 2009; Akhmedov & Berdeaux, 2013). The excess of fatty acids cause cell damage and death through any of several mechanisms, such as apoptosis pathway activation, death receptor activation, or initiating a cellular stress response in the endoplasmic reticulum (Wei *et al*, 2006; Li *et al*, 2008; Schenk *et al*, 2008; Alkhouri *et al*, 2009; Akhmedov & Berdeaux, 2013).

A study by Marnewick, *et al*, (2011) showed that dietary intervention with Rooibos modulates serum lipid profiles in humans, with results supporting studies by Bursill *et al* (2007) and Koo and Noh (2007), describing the LDL-lowering capabilities of phenolic-rich beverages. It is unclear of the mechanism of action; however proposed mechanisms include upregulation of LDL receptors, or inhibition of cholesterol synthesis and lipid absorption (Marnewick, *et al*, 2011). Irrespective of the mechanism, such findings contribute to the likelihood of concomitant therapy of chronic medication by natural and herbal supplements. One such chronic medication, particularly in terms of targeting dyslipidaemia, is statins.

2.3 Herb-Drug Interactions

A review by Awortwe *et al* (2018) illustrated that the majority of the cases recorded in the study showed patients taking statins and/or warfarin for the treatment of cardiovascular complications reported clinically significant complications after concomitant therapy with herbal products, including green tea.

Controversially, it is widely accepted that commercially available alternative and complementary medicines of natural origin are safe and effective as they have been successful in maintaining good health or used for treating certain diseases. There is an inherent trust in alternative and complementary medicines, although this trust is often misplaced as there is a lack of standardisation and regulation for these products. The lack of standardisation and regulatory control for these products is of concern to clinicians. One such concern is chemical composition of plants used for formulation of such medicines, as well as quality of the product and batch variation due many factors such as: geographical area of growth, storage and processing conditions, time of harvest, part of the plant utilised, contamination or misidentification, which may contribute to the possibility of herb-drug interactions and potential toxicity (Fugh-Berman, 2000; Antwi-Baffour *et al*, 2014; Gouws & Hamman, 2018).

A December 2017 report by Research and Markets showed that there is a growing demand for alternative and complementary medicine, in part, due to the rising burden of noncommunicable diseases and the increasing cost of healthcare, which further drives product demand. The report forecast that, by 2025, the global nutraceutical market is projected to reach USD 578.23 billion (Research and Markets, 2018).

As part of their endogenous protective mechanisms, many plants produce secondary metabolites which may be toxic (Calitz *et al*, 2015; Gum *et al*, 2017). The toxic metabolites are characterised in general as 'phytoprotectants' or 'phytoanticipins' and cannot necessarily be distinguished from therapeutically relevant ingredients (Calitz *et al*, 2015). *Atropa belladonna*, commonly known as deadly nightshade, contains tropane alkaloids, used as anticholinergics in homeopathic remedies and Food and Drug Administration (FDA)-approved drugs. High doses of these alkaloids are neurotoxic (Kwakye *et al*, 2018) and the European Food Safety Authority (EFSA) has placed a warning on Rooibos for pyrrolizidine alkaloid (PA) contamination as a potential health risk. A 2017 study by the EFSA Panel on Contaminants in the Food Chain (CONTAM) showed that, between the infusions and teas tested, including green tea and black tea infusions, Rooibos leaves had the highest concentrations of PA (Knutsen *et al*, 2017). A 2017 study by Van Wyk *et al*, however, showed that Rooibos does not produce any PAs but has been shown to grow in close contact – sometimes even entwined – with a weed (*Senecio angustifolius*) that does. The authors suggested that the shared soil is a means by which PAs are transferred to the Rooibos plant, as well as poor discerning between the plants at harvest, resulting in *Senecio angustifolius* contamination of the harvested batch of Rooibos (Van Wyk *et al*, 2017). The toxicity of these secondary metabolites depends on the metabolism of natural products by the organism (Gum *et al*, 2017). There are highly conserved biological similarities between taxa of humans and herbivorous insects, such as most pathways involving carbohydrate, protein, nucleic acid, and lipid metabolism. As a result, some phytochemicals that defend plants against herbivorous insects may also be harmful to humans (Calitz *et al*, 2015).

Similarly to pharmaceutical drugs, alternative and complementary medicines can dose-dependently be therapeutic or toxic. The potential exists for all ingested substances to interact with the same metabolising enzymes, drug transporters, as well as other components of the mixture of ingested substances. As a result, concurrent use of herbs may exacerbate, mimic, or counteract the effect of pharmaceuticals (Fugh-Berman, 2000) causing herb-drug interactions (Awortwe *et al*, 2018). As co-administration of alternative and complementary medicines can alter the pharmacodynamics and pharmacokinetics of the drug and possibly culminate in adverse effects, herb-drug interactions have become particularly significant

clinically. These interactions could lead to the concentrations of a drug in the tissue being either decreased, thereby limiting the efficacy and potentially leading to the failure of the treatment, or could be increased, leading to toxicity (Joubert *et al*, 2008; Gouws & Hamman, 2018).

2.3.1 Drug and Xenobiotic Metabolism

Xenobiotics are chemical substances found in an organism that are extrinsic to the normal metabolism of the organism. Xenobiotics are constantly introduced and eliminated by all life forms. They are typically lipophilic, synthetic or naturally occurring, and can be dose-dependently beneficial or harmful. Beneficial xenobiotics may be used during biological processes to provide energy, or even by acting as a precursor in the synthesis of macromolecules. However, xenobiotics may also be detrimental to the cell by interfering with metabolic pathways, DNA, ribose nucleic acid (RNA), or proteins (Vrbanac & Slauter, 2017). These interactions could induce cell damage and even cell death, thereby disturbing normal cellular functions and causing the onset of an array of toxic effects (Wetzel *et al*, 1994; Abrahams, 2011).

Numerous metabolic enzymes are responsible for eliminating exogenous and endogenous compounds from the body. Phase I and phase II metabolic reactions are catalysed by these enzymes. Some of the enzymes responsible for phase I reactions are the enzymes in the CYP450 metabolic system, found in the endoplasmic reticulum of gastrointestinal epithelial cells and hepatocytes (Na *et al*, 2011; Thomford *et al*, 2016). Herbal medicines consist of complex phytochemical mixtures which interact and exert multiple synergistic effects (Gum *et al*, 2017; Gouws & Hamman, 2018). The CYP450 enzyme system is vulnerable to induction or inhibition by xenobiotics, particularly these complex combinations. The resulting herb-drug interactions, often due to enzyme modulation, are of particular importance with respect to drugs with a narrow therapeutic window as even a relatively small alteration in blood plasma concentrations could cause ineffectiveness, or toxic effects (Budzinski *et al*, 2000; Gouws & Hamman, 2018).

A well-known example of adverse interactions between natural products and drugs, due to altered drug bioavailability, is the interaction between grapefruit juice and the drug felopidine which, at the time, was an accidental find. The pharmacokinetics of various drugs are altered when administered with grapefruit juice, notably calcium channel blockers, antibiotics, and statins (Mertens-Talcott *et al*, 2006). These adverse interactions, specifically herb-drug interactions, may occur through either of two significant mechanistic routes: activation of gene

transcription, or inhibition of enzyme action (Plant, 2007). The first major mechanism of the induction of the grapefruit-drug interaction is due to reduced “first-pass” metabolism by inhibition of the intestinal cytochrome P450 isozyme CYP3A4 (Mertens-Talcott *et al*, 2006).

The metabolism of the majority of therapeutic drugs and xenobiotics relies on the isoenzyme CYP3A. This enzyme is of particular interest as it has been shown that Rooibos flavonoids selectively induce CYP450 isozymes, notably CYP3A4 which metabolises numerous drugs, including statins. It has been shown that expression of CYP3A was upregulated in the intestines in rats exposed to two weeks of continuous administration of Rooibos tea, as well as a significant decline in the area under the concentration curve (AUC) and C_{max} of midazolam, a short-acting benzodiazepine derivative known to be a sensitive probe of CYP3A function (Matsuda *et al*, 2007). The induction of CYP3A as a result of exposure to Rooibos suggests that, given long-term consumption of Rooibos, the possibility of herb-drug interaction should not be overlooked (Matsuda *et al*, 2007). A similar phenomenon was found by Patel *et al* (2016) when human assessing recombinant CYP inhibition. Fermented and unfermented Rooibos extracts were assessed in terms of multiple drug-metabolising CYPs, including CYP3A4. It was shown that various polyphenols found in the Rooibos extracts were responsible for inhibiting CYP3A4, amongst others, in a time- and dose-dependent manner (Patel *et al*, 2016). These results further confirm the necessity for assessing potential herb-drug interactions, particularly with CYP3A4-metabolised drugs and nutraceuticals or supplements.

Drug transporters work in conjunction with metabolising enzymes for the disposition and metabolism of drugs. There are two types of transporters, uptake and efflux, and they are found in the intestinal enterocytes, at both the basolateral membrane and apical membrane. Efflux transporters are typically found in the brush border apical membrane of enterocytes and inhibit the complete absorption of drugs by expelling the metabolites, for example, back into the intestinal lumen (Kullak-Ublick *et al*, 2001; Chan *et al*, 2004; Ho & Kim, 2005). This results in decreased oral bioavailability of the drugs (Chan *et al*, 2004; Ho & Kim, 2005). Contrarily, uptake transporters facilitate the absorption of drugs, increasing their movement from the lumen into the enterocytes (Kullak-Ublick *et al*, 2001; Ho & Kim, 2005).

It is important to consider the effects natural products may have on the enzyme activity, however interference at the ATP-binding cassette (ABC) transporter level could also play a role in the induction and progression of adverse effects: hepatocellular excretory functions are primarily mediated by ABC transporters (Borst & Elferink, 2002; Vrbanac & Slauter, 2017). The ABC transport proteins transport substrates against a concentration gradient, utilising

ATP as an energy source (Chan *et al,* 2004). Of note is the ABC efflux transporter, subfamily B, member 1 (ABCB1), also known as P-glycoprotein (P-gp), which plays an important physiological role in detoxifying toxic metabolites (Bhardwaj *et al*, 2002; Jodoin *et al*, 2002; Patel *et al*, 2004; Del Rio *et al*, 2013; Patil *et al*, 2014). This efflux transporter's effects can either hinder or help the actions of the xenobiotic or drug. Similarly, the protein bile salt export pump (BSEP), expressed on the bile canicular membrane, is the primary facilitator of bile acid efflux in hepatocytes. Dysfunction of bile salt transporters is a mechanism by which drug-induced cholestasis occurs (Vrbanac & Slauter, 2017). Further, drugs and their metabolites have been shown to inhibit BSEP activity. The multidrug resistance-associated protein 3 (MRP3) is involved in the enterohepatic recycling of bile salts and associated with the removal of toxic organic anions under cholestatic conditions (Borst & Elferink, 2002). As a result, inhibition of liver drug transporters could potentiate adverse effects.

Organic anion transporting proteins (OATPs) belong to the *SLC* gene superfamily, with the OATP1B1 and OATP1B3 (also known as SLCO1B1 and SLCO1B3 respectively) transporters being liver-specific. Further, these transporters have been shown to have broad substrate specificity, as well as being crucial to hepatic statin uptake (Borst & Elferink, 2002; Vrbanac & Slauter, 2017). As such, up- and down-regulation in the activity of these transporters has been associated with hepatic injury. Shu *et al* (2016a) showed that the up-regulation of SLCO1B1 significantly increased the hepatic metabolism of atorvastatin and consequent hepatotoxicity.

The removal of toxic substances and prevented absorption of these substances is crucial in maintaining viability and avoiding adverse effects. However, the absorption of some toxic substances is necessary, such as in the case of cytotoxic anticancer drugs used in the treatment of malignant tumours, the efflux of which inhibits the treatment's efficacy. It has also been shown that P-gp expression and/or activity can be modulated by herbal constituents, affecting drug bioavailability (Bhardwaj *et al*, 2002; Jodoin *et al*, 2002; Mertens-Talcott *et al*, 2006; Patil *et al*, 2014). One of the nuclear receptors implicated in the regulation of P-gp expression levels as well as xenobiotic metabolising enzymes is pregnane X receptor (PXR) (Savas *et al*, 1999; Ott, *et al*, 2009).

2.3.2 Rooibos Toxicity

There have been isolated cases where idiosyncratic liver injury has been induced through the consumption of herbal products that are presumed to be safe (reviewed by Calitz *et al*, 2015). Yang *et al* (2010) reported three female patients presenting with acute hepatitis subsequent to ingestion of aloe products. *Aloe vera*, *Aloe arborescens*, and unspecified aloe extracts were

ingested daily for between 3 and 5 months at doses of between 28.5 mg to 420 mg (Yang *et al*, 2010). Similarly, Lee *et al* (2014) reported a case whereby a female patient presented with acute hepatitis consequent to 4-week ingestion of a gel preparation containing *Aloe vera*. A case study by Kocaman *et al* (2008) showed a patient, with no history of other medication, had treated flu symptoms with 1500 mg/day *Echinacea* root extract. The patient presented with fatigue and jaundice. Hepatitis, cholestasis, and eosinophilic granulocyte and portal lymphoplasmocyte infiltration were revealed by a liver biopsy. Within a month of cessation of the product, biochemical parameters were restored to within a normal range (Kocaman *et al*, 2008).

Sinisalo *et al* (2010) were the first to report an incidence of Rooibos-induced hepatotoxicity in a case study when a patient, on various chronic medications with a diagnosed stable low-grade B-cell malignancy, without clinical evidence or medical history of autoimmune or viral hepatitis or haemochromatosis, presented with elevated ALT and alkaline phosphatase (ALP) (Sinisalo *et al*, 2010). Elevated levels of these enzymes indicate diminishing hepatocellular membrane integrity and consequent enzyme leakage; a precursor to liver injury (Clarke & Mills, 2006). The patient started consuming Rooibos tea daily, two weeks prior to the test. Cessation of Rooibos consumption rectified the ALT and ALP serum levels within a week (Sinisalo *et al*, 2010). Engels *et al* (2013) reported concomitant use of a combination of Rooibos and Buchu tea with oral steroids as well as long-term statin use resulted in drug-induced liver injury (DILI). Cessation of tea intake proved to ameliorate the DILI, suggesting that the tea was possibly the direct cause of the hepatotoxicity. It is, however, note-worthy that there have been only two reports of Rooibos tea DILI and that causality was not attributed to Rooibos *per se*. Engels *et al* (2013) acknowledge that there is limited understanding of the medical interactions of herbs by clinicians – a problem which is compounded by the fact that patients are not forthcoming with the information about self-medication with herbal supplementation consumption (Engels *et al*, 2013). Similarly, Sinisalo *et al* (2010) noted that, given the excellent safety record of Rooibos tea, the patient may have had an adverse reaction to one of the multiple constituents of Rooibos, or that the tea may have been contaminated by a hepatotoxic compound – a pyrrolizidine alkaloid, for example.

2.4 Statins

In both primary and secondary prevention of cardiovascular disease (CVD), statins are the most commonly used drugs for the management of hypercholesterolemia and other CVD-associated risk factors, such as high LDL-C (Clarke & Mills, 2006; Björnsson *et al*, 2012;

Björnsson, 2016). Of these, atorvastatin and simvastatin are of the most commonly prescribed statins and are second and third most effective in lowering total and LDL cholesterol levels respectively (Schaefer & Asztalos, 2006).

The 2018 World Health Organisation's (WHO) South African Country Profile on Noncommunicable Diseases (NCDs) showed that, as of 2017, there are still many unknowns in terms of the national implementation of drug therapy to prevent heart attacks and strokes. As it stands, the following parameters for South Africa are unknown: "The proportion (%) of population with existing CVD or are at high risk for CVD, Type 2 Diabetics, and familial hypercholesterolaemia; the proportion (%) of high risk persons receiving any drug therapy and counselling to prevent heart attacks and strokes; the proportion of primary health care centres reported as offering CVD risk stratification; and [whether South Africa has] reported having [national] CVD guidelines that are utilized in at least 50% of health facilities" (Adopted from WHO, 2018).

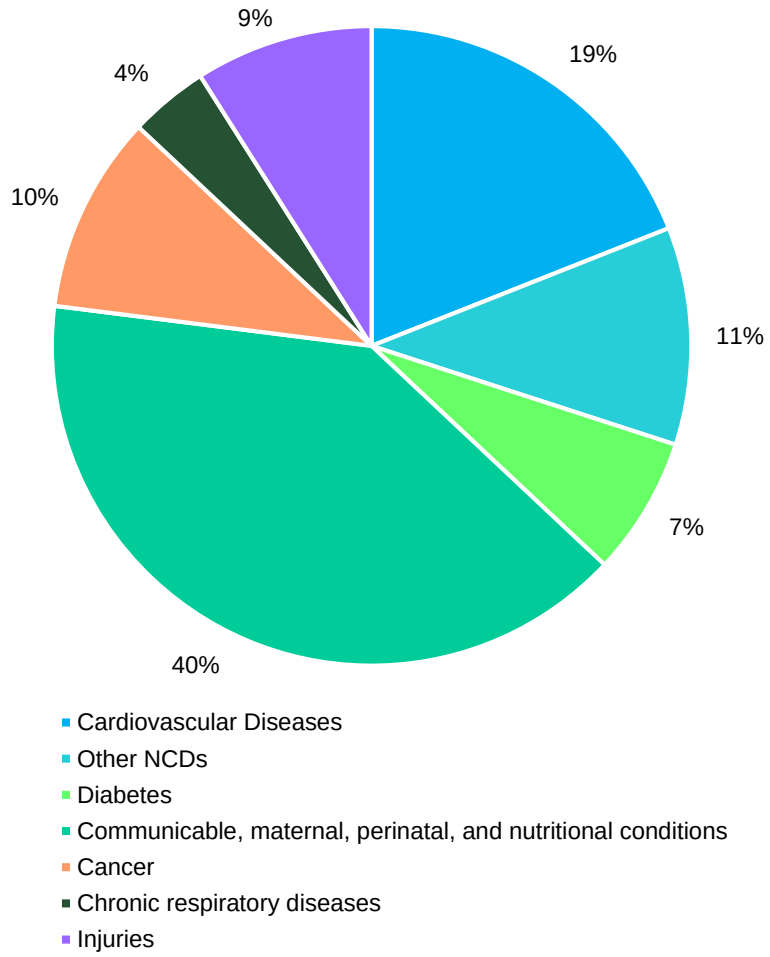

Figure 2.4.1: Proportional causes of mortality in the South African population. *(Adapted from WHO, 2018).*

These data show that it is not exactly known to what extent statins are used nationally in a South African context. While NCDs are estimated to account for 51% of deaths in South Africa, these data are uncertain approximations due to a lack of national NCD mortality data (WHO, 2018). However, data of various risk factors of NCDs are tabulated (*Table 2-2*) below:

Table 2-2: Prevalence of risk factors for NCDs in South Africa. *(Adapted from WHO, 2018).*

		Data year	Males	Females	Total
Harmful use of alcohol	Total alcohol per capita consumption, adults aged 15+ (litres of pure alcohol)	2016	16	3	9
Physical inactivity	Physical inactivity, adults aged 18+ (%)	2016	26	48	37
Salt/Sodium intake	Mean population salt intake, adults aged 20+ (g/day)	2010	7	6	6
Tobacco use	Current tobacco smoking, adults aged 15+ (%)	2016	33	8	20
Raised blood pressure	Raised blood pressure, adults aged 18+ (%)	2015	24	24	24
Diabetes	Raised blood glucose, adults aged 18+ (%)	2014	8	12	10
Obesity	Obesity, adults aged 18+ (%)	2016	15	39	27
	Obesity, adolescents aged 10-19 (%)	2016	9	13	11
Ambient air pollution	Exceedance of WHO guidelines level for annual PM 2.5 concentration (proportion)	2016	-		2
Household air pollution	Population with primary reliance on polluting fuels and technologies (%)	2016	-		15

These risk factors imply that there is a tendency towards a decline in the overall health of the South African population, suggesting that, in years to come, there will be an increase in the necessity for therapeutic and lifestyle interventions.

2.4.1 Mechanism of Action

The presence of metabolic syndrome and diabetes in patients may result in different effects of atorvastatin as compared to patients without these metabolic alterations (Koh *et al*, 2011). Within 2 to 4 hours after administration, the steady-state maximum plasma concentration (C_{max}) of multiple daily doses of atorvastatin, 2.5 to 80 mg, is 1.95 to 252 µg/L. A review by

Lea & McTavish (1997) showed that the area under the plasma concentration time curve showed values of between 25.2 to 1293 µg/(h/L). The absolute bioavailability of the drug is 12%, and is approximately 98% protein-bound in plasma, with a mean elimination half-life of about 14 hours (Lea & McTavish, 1997).

Table 2-3: Pharmacokinetic parameter values of atorvastatin acid and lactone in humans following oral administration of atorvastatin acid 20 or 40mg. *Values are means ± SD, or median (range). (Adapted from Lennernäs, 2003).*

Drug or metabolite	Dose (mg)	C_{max} (µg/L)	t_{max} (h)	$t_{½\beta}$ (h)	AUC (µg ↑ h/L)
Atorvastatin acid	40	12.7 ± 7.8	1 (0.5 – 3)	7.8 ± 3.6	61.4 ± 36.2
Atorvastatin lactone		4.2 ± 2.4	3 (1 – 8)	8.3 ± 4.1	53 ± 27.3
Atorvastatin acid	40	13.4 ± 9.5	1 (0.5 – 3)	7.0 ± 3.7	54.2 ± 24.2
Atorvastatin lactone		3.8 ± 2.6	3 (1 – 8)	9.2 ± 4.1	51.6 ± 35.1
Atorvastatin acid	20	6.9 ± 3.66	1.8 ± 1.0	13.8 ± 6.4	98.7 ± 48.4
Atorvastatin lactone		3.6 ± 2.4	3.4 ± 2.5	14.1 ± 7.7	75.1 ± 40.1

AUC = area under concentration curve (0 - ↓); C_{max} = peak plasma concentration; t_{max} = time to C_{max}; $t_{½\beta}$ = elimination half-life

As with most crucial pathways in the human body, cholesterol synthesis is highly regulated and dependent on the modulation of various genomic processes such as transcription, translation, and post-transcription. The accepted primary rate-limiting step of the cholesterol biosynthesis pathway is at the third enzyme, HMG-CoA reductase (Singh *et al*, 2009) (*Figure 2.4.2*). Statins are drugs used to decrease LDL and cholesterol in humans, achieved through the competitive inhibition of hepatic HMG-CoA. This inhibition results in decreased hepatic secretion of apolipoprotein (apo) B-100-containing lipoproteins (VLDL and intermediate-density lipoproteins (IDL)), as well as increased cellular receptor-mediated clearance of apoB-100-containing lipoproteins, particularly LDL (Schaefer & Asztalos, 2006; Björnsson *et al*, 2012; Pal *et al*, 2015; Björnsson, 2016). Taken together, this inhibition effectively lowers triglycerides by up to 40%, LDL by up to 60%, and VLDL cholesterol by up to 50%. Further, statins have been shown to increase HDL cholesterol levels by up to 15% without increasing the production of the major protein in HDL, apoA-I (Schaefer & Asztalos, 2006).

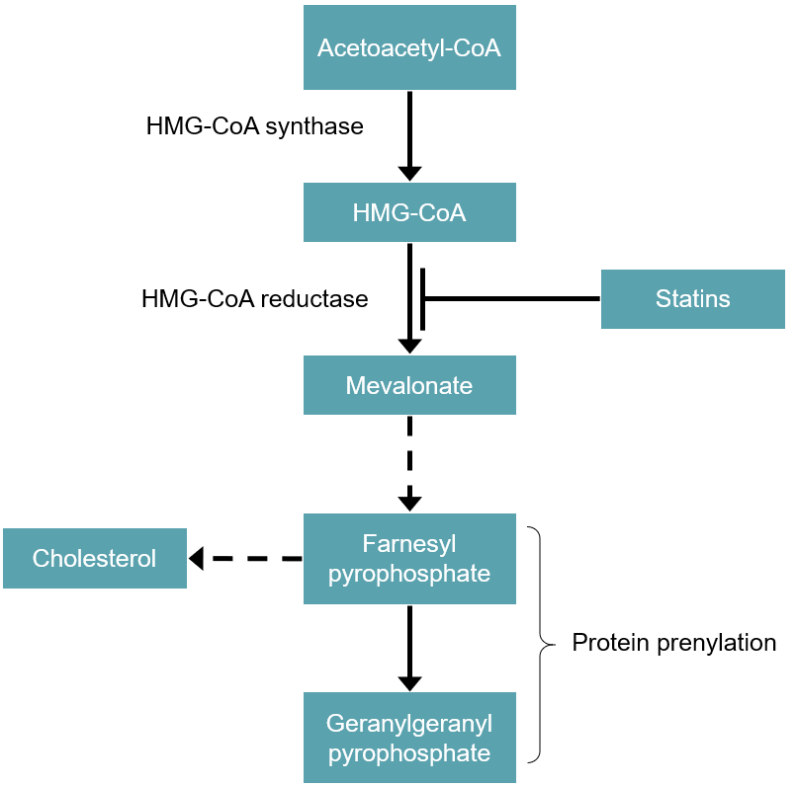

Figure 2.4.2: Statins interrupt the enzymatic reduction of HMG-CoA to mevalonate. *This inhibition prevents synthesis of cholesterol and two isoprenoids, farnesyl pyrophosphate and geranylgeranyl pyrophosphate, which post-translationally modify oncogenic proteins. Dashed arrows represent multistep transitions. HMG-CoA=hydroxymethylglutaryl-coenzyme A. (Adapted from Ahern et al, 2014).*

The active metabolites of atorvastatin results in a HMG-CoA reductase inhibition of 20 to 30 hours (Lea & McTavish, 1997). Post-translational modulation of HMG-CoA reductase results in its altered rate of degradation and phosphorylation status. Phosphorylation causes an inactivation of the enzyme allowing for rapid environmental- and cellular-dependent cholesterol synthesis modulation. The primary kinase involved in the phosphorylation-mediated inactivation of HMG-CoA reductase is AMPK, the activity of which is subject to the phosphorylation of upstream kinases (Singh *et al*, 2009). Many phenolic compounds activate AMPK, including aspalathin (Beltrán-Debón *et al*, 2011; Mazibuko *et al*, 2013; Kamakura *et al*, 2015). This inhibitory action has also been shown to inhibit monocyte activation, augmenting the vessel wall metalloprotease synthesis as well as the production of pro-inflammatory cytokines: interleukin (IL)-6, IL-1β, and TNF-α, consequently diminishing the progression of atherosclerosis (Pal *et al*, 2015).

Cholesterol synthesis is not the only end product of the mevalonate pathway and, as a result, its chronic inhibition may have other deleterious effects. Statins have been shown to decrease serum CoQ_{10} levels by up to 40% and, while, daily supplementation with CoQ_{10} has been shown to improve the antioxidant hepatic and serum CoQ_{10} levels, it is important to consider

the fundamental precursor insufficiency (Jiménez-Santos *et al*, 2014; Deichmann *et al*, 2016). Dysfunction of ubiquinone and the ETC results in decreased ATP generation and mitochondrial and cellular functioning. The inhibitory effect of the mevalonate pathway is further reaching than just CoQ_{10} levels as the inhibition also results in decreased dolichol production, affecting the fluidity and permeability of phospholipid bilayers (Lodish *et al*, 2000; Li *et al*, 2006; Deichmann *et al*, 2016; Wang & Hekimi, 2016). This suggests that the toxicity induced by ATV could be isolated to mitochondrial dysfunction and bioenergetic failure.

Independent of their HMG-CoA reductase capabilities, other pleiotropic effects of statins have been established and studied (Gum *et al*, 2017). These effects include immunomodulatory and anti-inflammatory capabilities, such as eliminating potential structural remodelling (Michalik *et al*, 2013) and altering leukocyte infiltration associated with tumours in murine models (Mira *et al*, 2013).

2.4.2 Side-effects and Toxicity

Clinically, the most common hepatic side-effects of statin use are displayed by mild-to-moderate elevations in liver transaminases, particularly ALT and AST (Clarke & Mills, 2006; Pal *et al*, 2015). Atorvastatin usage has been associated with various other side-effects, such as the manifestation of cholestatic jaundice, fulminant hepatic necrosis, cirrhosis, hepatitis, myalgia, and liver failure (Pal *et al*, 2015). A high oral daily dose (40 mg to 80 mg) is associated with an increased risk of DILI, and dose escalation of ATV has been associated with acute liver failure (Björnsson, 2016).

As it is an uncommon occurrence, the exact mechanism of atorvastatin-induced hepatotoxicity is yet to be fully elucidated, however progress has been made in establishing elements thereof. Shu *et al* (2016a) showed extensively that CYP3A4 and SLCO1B1 up-regulation occurs in a hyperlipidaemic condition *in vitro* and *in vivo*. Further, Shu *et al* (2016a) showed that the initial metabolism of atorvastatin to its metabolites, ortho- and para-hydroxy atorvastatin, results in massive ROS production which is suspected to be the point at which ATV-induced toxicity occurs. Tolosa *et al* (2015) compared six statins in terms of mitochondrial parameters in order to elucidate potential mechanisms of statin-induced hepatotoxicity. Following a one hour treatment, atorvastatin showed the lowest mitochondrial toxicity risk of six statins. In terms of mitochondrial membrane potential, atorvastatin was shown to induce hyperpolarisation. It was also shown that the proposed mechanisms of toxicity include mitochondrial superoxide production, and dysregulation of calcium homeostasis.

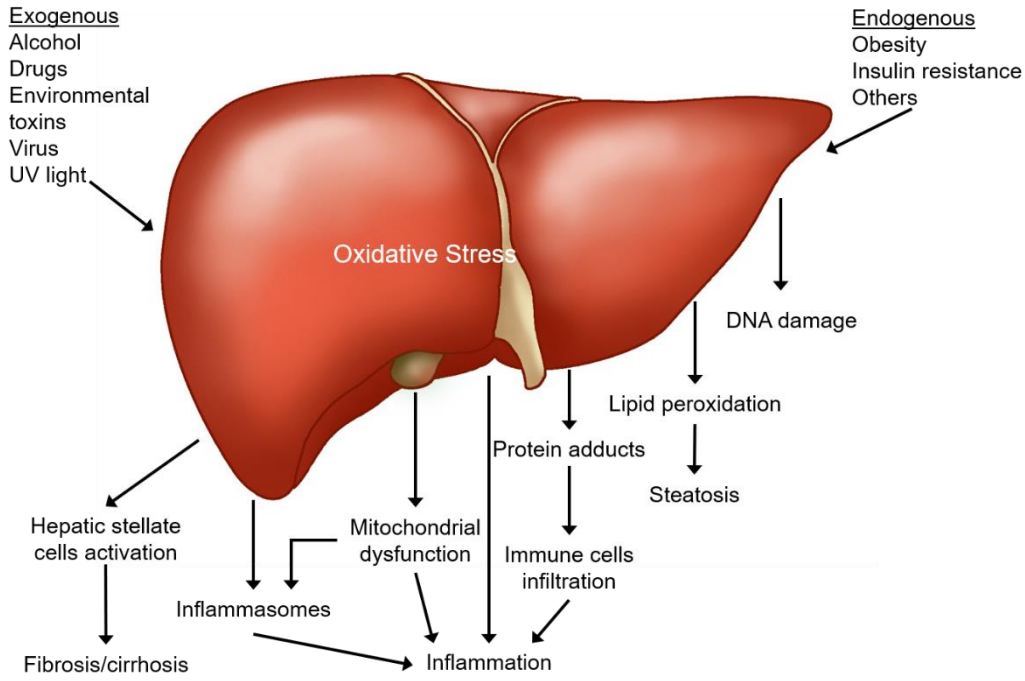

Figure 2.4.3: The general mechanism scheme of oxidative stress induced by various factors on liver disease. *(Adapted from Li et al, 2015).*

Pal *et al* (2015) showed that statin-induced hepatotoxicity is ROS-dependent and elicited by the activation of the intrinsic mitochondria-dependent pathway, ER stress, and MAPK activation (*Figure 2.4.4*). Reactive oxygen species are important and necessary in pathological conditions as it causes oxidative stress as well as contributing to retrograde redox signalling from the mitochondria to both the nucleus and the cytosol (Pal *et al*, 2015; Wang *et al*, 2015). In the same study, it was shown that hepatic tissue damage and oxidative stress as a result of ATV administration, is dose-dependent (Pal *et al*, 2015). Furthermore, ROS are known to play an integral role in ATV-induced oxidative stress. Increased ROS production causes mitochondrial and DNA damage as well as oxidative injury of the cellular membranes (Pal *et al*, 2015; Wang *et al*, 2015).

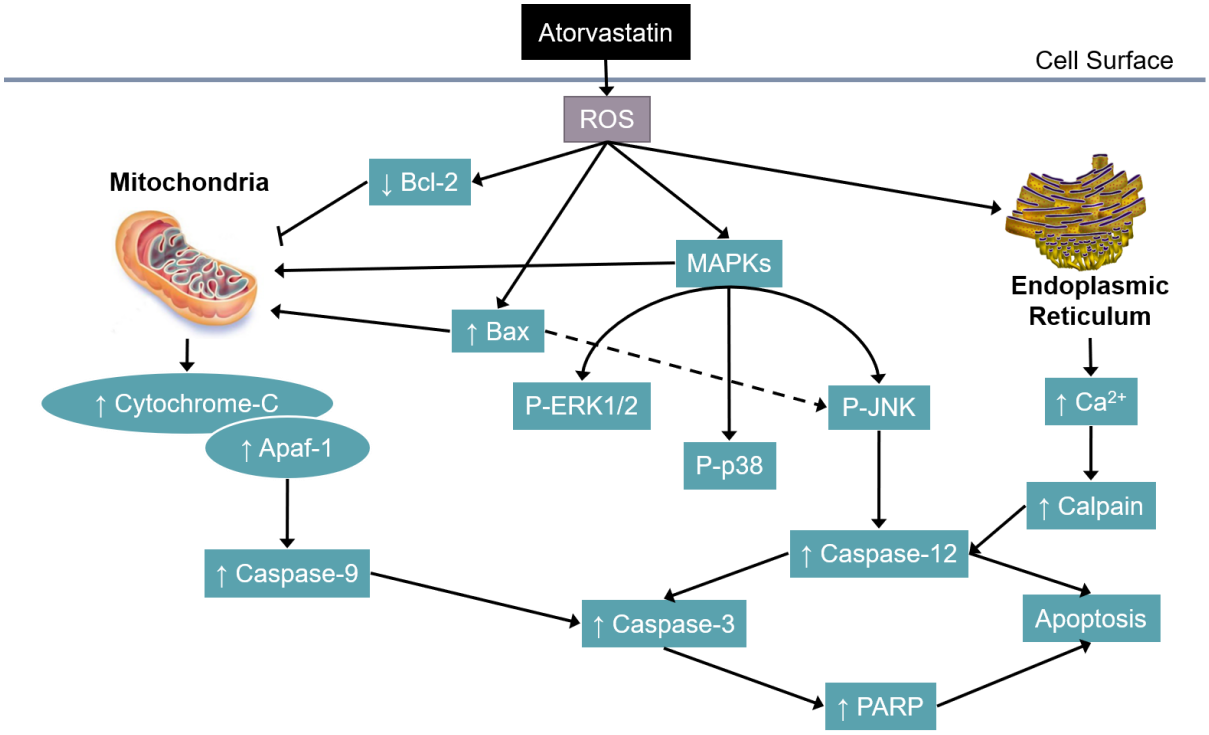

Figure 2.4.4: Schematic diagram of the ATO induced hepatic tissue toxicity in dose-dependent manner. *(Adapted from Pal et al, 2015).*

2.5 Alternative Models

Even though there are only two reported cases of hepatotoxicity associated with Rooibos, the use of herbal supplementation, specifically of Rooibos in South Africa, is high and therefore the risk for more cases increases. As such, two rare cases cannot be ignored.

Although there is rigorous and extensive testing of drugs, the extrapolation from *in vitro* to *in vivo* studies does not necessarily translate. Focus is given to five major CYP450 isozymes (CYP1A2, 2C9, 2C19, 2D6, and 3A4) in terms of drug interactions for most first line screening studies. This is because over 90% of drugs on the market are metabolised thereby (Gouws *et al*, 2017). Further, successful *in vivo* studies have failed to translate between species and to a clinical trial level. There is also the risk of the trial not translating to a clinical setting as the trials are often undertaken by young and healthy individuals (Awortwe *et al*, 2018). This can have dire consequences. One such example is the Investigation of Lipid Level Management to Understand its Impact in Atherosclerotic Events (ILLUMINATE) trial.

The ILLUMINATE trial was the assessment of one such pharmacological intervention, torcetrapib, aimed at inhibiting cholesterol ester transfer protein (CETP), increasing HDL levels, and consequently decreasing the risk of future clinical cardiovascular events in high-

risk patients. The phase III trial was terminated prematurely as the administration of torcetrapib increased the risk of morbidity and mortality as opposed to mitigating it (Barter *et al*, 2007). This contributes to the necessity for alternative, safer, more representative research models.

A cholesterol ester is a cholesterol with a fatty acid attached, and accounts for approximately 70% of all plasma cholesterol. The transfer of cholesterol esters from HDL to apoB-containing lipoproteins is instigated by CETP (*Figure 2.5.1*). Statins have been shown to mildly decrease the plasma activity of CETP, however this action is secondary to the reduction of triglyceride-rich acceptor particles. As such, raising HDL through CETP inhibition has been a therapeutic target. Increased HDL levels, combined with decreased LDL levels, would serve as a preventative measure by reducing the risk of cardiovascular disease which has been associated with low HDL levels (Schaefer & Asztalos, 2006; Barter *et al*, 2007).

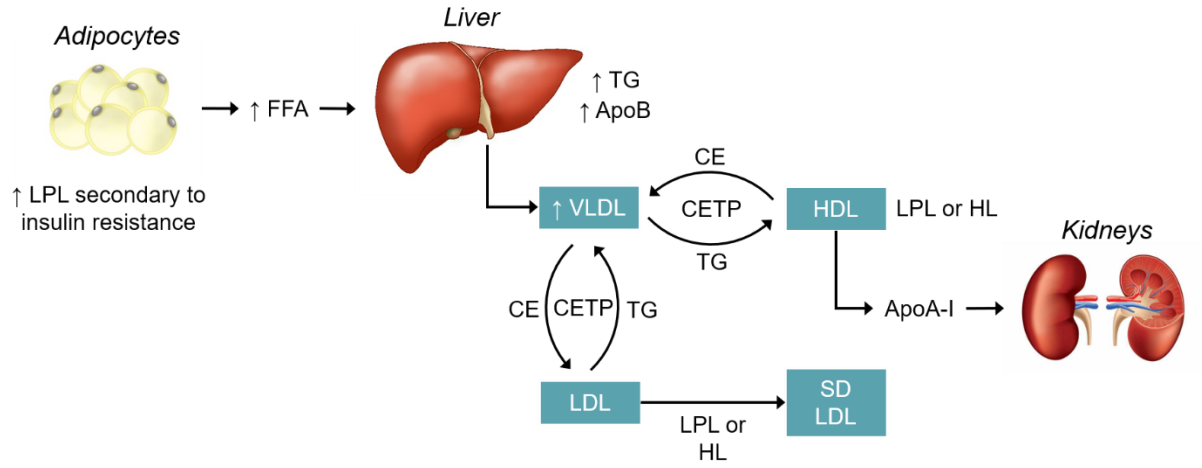

Figure 2.5.1: The role of insulin resistance in diabetic dyslipidaemia. *Insulin resistance initiates the characteristic triad of high triglyceride, low HDL cholesterol and high small dense LDL levels. If the concentration of VLDL- transported triglyceride is high, CETP promotes the transfer of LDL cholesteryl ester or HDL cholesteryl ester in exchange for triglyceride. Triglyceride-rich HDL cholesterol or LDL cholesterol can undergo hydrolysis by hepatic lipase or lipoprotein lipase. Abbreviations: ↑, increased level; ApoA-1, apolipoprotein A-1; ApoB, apolipoprotein B; CE, cholesteryl ester; CETP, cholesteryl ester transfer protein; FFA, free fatty acid; HL, hepatic lipase; LPL, lipoprotein lipase; SD LDL, small dense LDL cholesterol; TG, triglyceride. (Adapted from Mooradian, A. G., 2008).*

2.5.1 3D Culture

In vitro primary hepatocyte cultures lose important hepatic functionality during culture. In order to overcome this, modified primary liver tumour cells or immortalised cell lines have been created which have the advantage of long-term stability, rapid growth, and liver functionality (Baquerizo *et al*, 2015).

In terms of research, it has been a concern that hepatocytes – both primary and secondary cultures, traditionally used as 2D cultures – do not accurately reflect liver function (Wrzesinki *et al*, 2013; Edmondson *et al*, 2014; Anton *et al*, 2015). Passaging cells by trypsinisation is particularly strenuous to cultured cells as trypsin is a proteolytic enzyme used to dissociate adherent cells from the growth surface. Consequently, Wrzesinki *et al* (2013) showed that in 3D culture, hepatocytes, specifically C3A cells, recover fully from trypsinisation after 15 to 18 days and thereafter remain stable for at least 24 days, indicating their transition from exponential growth typical of 2D culture to stable dynamic equilibrium (Wrzesinki *et al*, 2013; Wrzesinki *et al*, 2014). In dynamic equilibrium, advanced liver functions (such as urea and cholesterol synthesis, P450 expression, and cellular organization) are re-established in the 3D spheroids and they remain stable models for mid- to long-term assessment of compounds (Wrzesinki *et al*, 2013). Liver spheroids produced by 3D culture allow for the evaluation of pharmacodynamics and/or mechanistic biomarkers, which is useful for understanding the compounds' mode of action (Wrzesinki *et al*, 2013; Edmondson *et al*, 2014; Anton *et al*, 2015).

3 Aims of Investigation

This study aims to investigate the potential hepatoprotective effects of Rooibos against atorvastatin (ATV)-induced hepatotoxicity using an *in vitro* C3A liver cell model.

Hypothesis

Hypothesis (H_a): Aspalathin-enriched Rooibos extract ameliorates ATV-induced hepatotoxicity in a normal or hyperlipidaemic condition

Null hypothesis (H_0): Aspalathin-enriched Rooibos extract does not ameliorate ATV-induced hepatotoxicity in a normal or hyperlipidaemic condition

Objectives

- To induce acute hepatotoxicity using atorvastatin in C3A liver cells using time- and concentration-dependent assays, in a normal and hyperlipidaemic condition
- To measure the extent of hepatotoxic damage by assessing apoptosis using flow cytometry probing for annexin V as well as a propidium iodide staining, further confirmed by a caspase 3/7 assay in 2D culture
- To determine ATV-induced cellular ROS and mitochondrial integrity changes with and without GRT co-treatment using a DCF assay, as well as a JC-1 stain, measured with flow cytometry, in 2D culture
- To determine the hepatoprotective effects of GRT against chronic ATV-induced hepatotoxicity using a 3D culture system

4 Methodology & Materials

A more detailed description of the preparation of reagents as well as experimental methods can be found in *Chapter 11: Appendices*.

4.1 *In vitro* culturing of C3A cells in 2D culture

The human-derived hepatocarcinoma cell line C3A (ATCC® HB8065™) was purchased from the American Type Culture Collection (ATCC). In order to create a large reserve of cryopreserved cells, the cells were passaged and sub-cultured. C3A cells were seeded at a density of $11x10^4$ cells per millilitre in 75 cm^2 tissue culture flasks and supplemented with Eagle's Modified Essential Medium (EMEM; Lonza, MD, USA), 10% v/v foetal bovine serum (FBS; Gibco, catalogue no.: 10500064; ThermoFisher Scientific, Johannesburg, South Africa) and 1% v/v L-glutamine (Lonza, MD, USA), the combination thereof hereafter referred to as growth medium. Cells were incubated in a RS Biotech Galaxy R CO_2 Incubator in humidified air at 37°C with 5% CO_2 and the culture media was replaced every 2 – 3 days. Cells were sub-cultured at 70 – 80% confluence. For all experiments, cells were subject to the same culturing conditions and reagent concentrations pertaining to cell maintenance.

Palmitate was prepared in ethanol, thereafter palmitate treatment was prepared in growth medium with 2 mg/mL BSA (bovine serum albumin; fraction V, BSAV-RO, Roche, Sigma-Aldrich, Johannesburg, South Africa) and 4.7 g/L sodium bicarbonate ($NaHCO_3$; catalogue no.: S3817, Sigma, Stanheim, Germany) and left to conjugate in a water-bath at 37°C for two hours (Mazibuko *et al*, 2013; Mazibuko *et al*, 2015).

Afriplex GRT™ (*Aspalathus linearis* (Brum.f) R.Dahlgren) extract was obtained from Afriplex, ATV was obtained from Sigma-Aldrich (catalogue no.: PHR1422), and palmitate was obtained from Sigma-Aldrich (catalogue no.: P0500). These, and all other chemicals for experimental use were of cell culture grade. Stock solutions were prepared in dimethyl sulfoxide (DMSO) and final working concentrations of treatments were not more than 0.25% v/v DMSO.

4.2 Acute ATV and GRT cytotoxicity assessment in 2D culture (MTT)

See *Chapter 11: Appendices: 11.2*.

Measuring the activity of various mitochondrial dehydrogenase enzymes allows for the assessment of mitochondrial viability as an indication of cell viability. The tetrazolium salt, 3-(4, 5-dimethylthiazol-2-yl)-2, 5-diphenyl tetrazolium bromide (MTT), is reduced in active mitochondria from a soluble yellow salt to insoluble purple formazan crystals which can be measured spectrophotometrically (Mosmann, 1983).

In order to assess cellular metabolic activity, an MTT cell viability assay (catalogue no.: M5655; Sigma, Stanheim, Germany) was used. C3A (ATCC® HB8065™) cells were seeded in four 96-well plates (0.32 cm^2) (Nest Biotech; Whitehead Scientific, Cape Town, South Africa) at a density of $11x10^4$ cells per millilitre in 200 µL growth medium per well. Seventy-two hours after seeding, the media was refreshed. One hundred and twenty hours after seeding, culture media was aspirated and cells were exposed to a vehicle control (media with 0.25% DMSO for palmitate positive and palmitate negative controls), ATV (0.5 µM, 1 µM, 2.5 µM, 5 µM, 10 µM, 12.5 µM, 25 µM, 50 µM, and 100 µM), or GRT (0.01 mg/mL, 0.02 mg/mL, 0.05 mg/mL, 0.1 mg/mL, 0.2 mg/mL, 0.25 mg/mL, 0.5 mg/mL, 1 mg/mL, and 2 mg/mL) for 3, 6, 12, and 24 hours. Treatments were added to EMEM with 0.25% DMSO. Three replicates per concentration of ATV and GRT were assessed in three independent experiments.

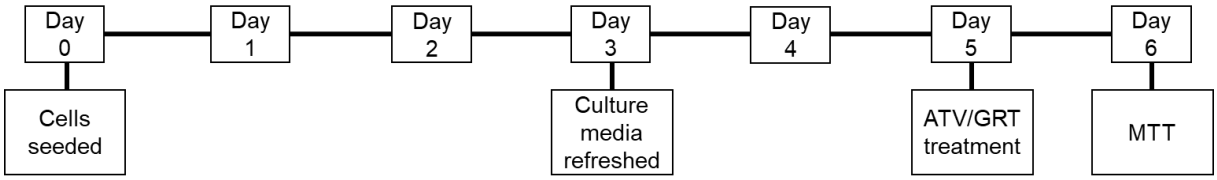

Figure 4.2.1: Schematic representation of the timeline of the MTT experiments for the optimisation of the ATV and GRT concentrations.

For the assay, culture media was aspirated and cells were washed with pre-warmed PBS before being incubated with 50 µL 2 mg/mL MTT for 30 minutes at 37°C. Following incubation, the MTT was aspirated, 200 µL DMSO and 25 µL Sorenson's Buffer was added (DMSO lyses cells, effectively stopping cellular respiration, while Sorenson's Buffer is a fixation buffer). Spectrophotometric measurements were recorded using a BioTek EL*x*800 absorbance microplate reader at OD_{570}. Cytotoxicity was calculated as a percentage relative to the untreated vehicle control group. Results were generated using Gen5 version 1.05 (BioTek Instruments, Inc., Winooski, VT, USA).

Similarly, an MTT assay was used to assess palmitate cytotoxicity. C3A (ATCC® HB8065™) cells were seeded at a density of 11x10^4 cells per millilitre in a 96-well plate (0.32 cm^2) (Nest Biotech; Whitehead Scientific, Cape Town, South Africa) in 200 µL growth medium per well. Seventy-two hours after seeding, culture media was aspirated and the cells were exposed to varying concentrations of palmitate (0 µM, 200 µM, 500 µM, 750 µM) for 24 hours. One hundred and twenty hours after seeding, pre-treatment was aspirated and replaced with vehicle control (media with 0.25% DMSO for palmitate positive and palmitate negative controls), ATV (10 µM or 25 µM), or GRT (0.01 mg/mL or 0.1 mg/mL) for a further 24 hours. Treatments were made up in EMEM with 0.25% DMSO. Three replicates per concentration of palmitate, ATV, and GRT were assessed in three independent experiments. Cell viability was expressed normalised to the vehicle control at 100%.

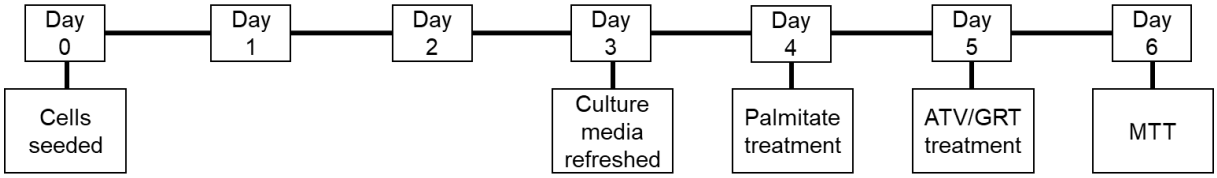

Figure 4.2.2: Schematic representation of the timeline of the MTT experiments for the optimisation of the palmitate concentration.

4.3 Assessment of induction of the disease condition

See *Chapter 11: Appendices: 11.3*.

CYP3A4 is responsible for the majority of human drug metabolism, including ATV and, interestingly, GRT notwithstanding (Patel *et al*, 2016). Moreover, it has been shown that the hyperlipidaemic disease state results in the upregulation of CYP3A4 (Shu *et al*, 2016b).

Assessment of the modulation of CYP3A4 enzyme activity was assessed using Western Blot analysis. C3A (ATCC® HB8065™) cells were seeded in a clear 6-well plate (9.5 cm^2) (catalogue no.: CLS3516; Corning® Costar®, Sigma, Stanheim, Germany) at a density of 11x10^4 cells per millilitre in 3 mL growth medium per well. Seventy-two hours after seeding, culture media was refreshed. Ninety-six hours after seeding, culture medium was aspirated and cells were exposed to culture medium, 500 µM palmitate, culture medium and 10 µM rifampicin (catalogue no.: R3501, Sigma, Stanheim, Germany), or a combination of 500 µM palmitate and 10 µM rifampicin for 24 hours.

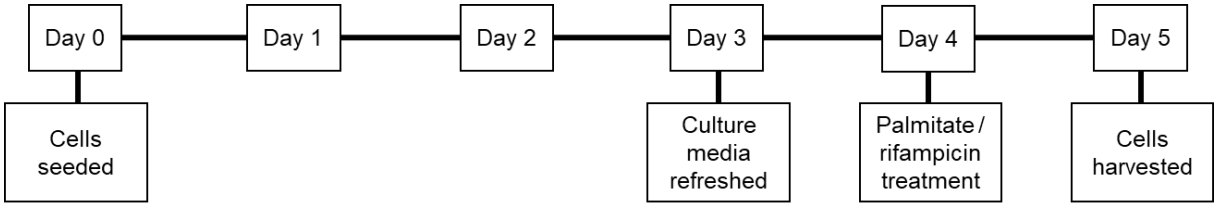

Figure 4.3.1: Schematic representation of the timeline for CYP3A4 Western blot assessment.

For cell harvesting, 300 µL radioimmunoprecipitation assay (RIPA) lysis buffer supplemented with phenylmethylsulfonyl fluoride (PMSF; catalogue no.: 78830; Fluka, Bucharest, Romania) was used to lyse the cells. Lysed cells were further homogenised with a Qiagen TissueLyser II (Qiagen, Hilden, Germany) before being centrifuged and the supernatant collected and stored at -80 °C until further use. A reducing agent compatible and detergent compatible (RC DC) protein assay kit (RC DC™ Protein Assay Kit II; catalogue no.: 5000122; Bio-Rad, California, United States) was used to determine the protein concentrations of diluted (1:10) samples, compared to a BSA standard curve of 0.0 mg/mL, 0.125 mg/mL, 0.25 mg/mL, 0.5 mg/mL, 0.75 mg/mL, 1.0 mg/mL, 1.5 mg/mL, and 2.0 mg/mL. Absorbance readings were recorded using a SpectraMax i3x multi-mode microplate reader (Molecular Devices, LLC, Sunnyvale, CA, USA) at OD_{630}. Results were generated on SoftMax Pro 7 software, version 7.0.2 (Molecular Devices, LLC, Sunnyvale, CA, USA).

Sample buffer (4X SDS Sample Buffer, catalogue no.: 70607; Sigma, Stanheim, Germany) mixed with β-mercaptoethanol (Fluka, Bucharest, Romania) was prepared and mixed with 60 µg protein lysate in a 1:4 ratio. Mini-PROTEAN® TGX™ 12% Precast Gels (catalogue no.: 4561044; Bio-Rad, California, United States) were placed in a gel electrophoresis tank, filled with 1x Tris/Glycine/SDS running buffer (catalogue no.: 1610732; Bio-Rad, California, United States). Precision Plus Protein™ WesternC™ marker (catalogue no.: 1610376; Bio-Rad, California, United States) and 60 µg protein sample was loaded onto the gel. A PowerPac™ Basic (catalogue no.: 1645050; Bio-Rad, California, United States) was set at 150 V for protein gel electrophoresis. Thereafter, proteins were transferred to a nitrocellulose membrane using a Trans-Blot® Turbo™ RTA Mini Nitrocellulose Transfer Kit (catalogue no.: 1704270; Bio-Rad, California, United States). The transfer sandwich was assembled in a Trans-Blot® Turbo™ transfer cassette (catalogue no.: 1704150; Bio-Rad, California, United States) and run as a Bio-Rad mixed molecular weight transfer for 10 min at 25 V and 2.5 A. Following transfer, the success of the protein transfer was assessed with a Ponceau S stain (Ponceau S solution; catalogue no.: P7170; Sigma-Aldrich, Missouri, United States), before being counterstained with 1 x Tris-buffered saline with 0.1% Tween 20 (TBS-T). The membrane was then blocked

in 5% (w/v) skim milk powder/TBS-T at room temperature, before three washes with TBS-T followed by overnight incubation in primary antibody (1:500 dilution; CYP3A4 (D9U6N) Rabbit monoclonal Ab #13384; Cell Signaling Technology, Anatech Instruments (Pty) Limited, Olivedale, South Africa) in 5% (w/v) BSA and TBS-T at 4°C on an orbital shaker. The following day, the membrane was washed three times with TBS-T. Thereafter, the membrane was incubated in StrepTactin® HRP Conjugate (catalogue no.: 161-0381; Bio-Rad, California, United States) and horseradish peroxidase (HRP) conjugated secondary antibody in 2.5% (w/v) skim milk powder in TBS-T. The membrane was then washed another three times in TBS-T before chemiluminescent detection. The membrane was saturated in Clarity™ Western enhanced chemiluminescence (ECL) Substrate (catalogue no.: 1705061; Bio-Rad, California, United States) and incubated in the dark before imaging on the Bio-Rad ChemiDoc™ MP System (catalogue no.: 12003154; Bio-Rad, California, United States). Image Lab™ Software (catalogue no.: 1709691; Bio-Rad, California, United States) was used to quantify the protein bands and protein expression was normalised to the housekeeping gene, GAPDH, which served as the loading control.

4.4 Oxidative stress assessment in 2D culture

See *Chapter 11: Appendices: 11.4*.

The production of reactive oxygen species (ROS) is considered an integral component of the development of statin-induced hepatotoxicity. 2', 7'-dichlorofluorescin diacetate (DCFDA) is a fluorogenic dye that measures ROS production – such as hydroxyls and peroxyls – within the cells. DCFDA is initially deacetylated by cellular esterases before undergoing oxidation by ROS, resulting in the generation of highly fluorescent 2', 7'-dichlorofluorescein (DCF) which can be determined by means of fluorescence spectroscopy (Kalyanaraman *et al*, 2012).

Oxidative stress was assessed by means of a DCF stain (catalogue no.: D6883; Sigma, Stanheim, Germany). C3A (ATCC® HB8065™) cells were seeded in a black 96-well clear bottom plate (0.32 cm^2) (Nest Biotech; Whitehead Scientific, Cape Town, South Africa) at a density of $11x10^4$ cells per millilitre in 200 µL growth medium. Seventy-two hours after seeding, culture media was aspirated and the cells were exposed to 500 µM palmitate treatment medium for 24 hours. One hundred and twenty hours after seeding, culture media was aspirated and cells were exposed to a vehicle control (media with 0.25% DMSO for palmitate positive and palmitate negative controls), ATV (10 µM and 25 µM), GRT (0.01 mg/mL and 0.1 mg/mL), or a combination thereof (10 µM ATV + 0.01 mg/mL GRT, 10 µM ATV + 0.1

mg/mL GRT, or 25 µM ATV + 0.1 mg/mL GRT) for 24 hours. All treatments were added to vehicle control medium. ROS production was determined using an end-point fluorogenic DCF assay incubated for 30 minutes. Treatments were made up in EMEM with 0.25% DMSO. Fluorescent readings were recorded using a SpectraMax i3x multi-mode microplate reader (Molecular Devices, LLC, Sunnyvale, CA, USA) at an excitation wavelength of 485 nm and an emission wavelength of 535 nm. Results were generated on SoftMax Pro 7 software, version 7.0.2 (Molecular Devices, LLC, Sunnyvale, CA, USA). Three replicates per treatment were assessed in three independent experiments. Reactive oxygen species production was calculated relative to cell viability assessed by an MTT assay (catalogue no.: M5655; Sigma, Stanheim, Germany), previously described in section *4.2*.

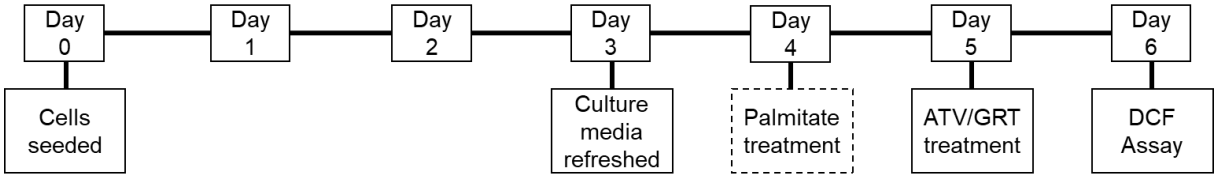

Figure 4.4.1: Schematic representation of the timeline of the DCF experiments.

4.5 Mitochondrial membrane potential assessment in 2D culture

See *Chapter 11: Appendices: 11.5.1*.

5, 5', 6, 6'-Tetrachloro-1, 1', 3, 3'-tetraethylbenzimidazolylcarbocyanine iodide (JC-1) is a dual-emission cationic dye that accumulates in polarized mitochondria. JC-1 is either a green fluorescent (λ_{ex} 520 nm) monomer, as a result of low concentrations entering the mitochondria due to a low membrane potential, or a red fluorescent (λ_{em} 596 nm) aggregate, as a result of high concentrations in the mitochondrial matrix due to a high membrane potential. As such, mitochondrial membrane depolarization is indicated by decreased aggregate fluorescence, and is dependent only on the membrane potential (Reers *et al.*, 1991; Di Lisa *et al.,* 1995).

Mitochondrial membrane integrity was assessed by means of a JC-1 stain (catalogue no.: T3168; Sigma, Stanheim, Germany). C3A (ATCC® HB8065™) cells were seeded in a 24-well plate (1.9 cm^2) (catalogue no.: M8812; Greiner CELLSTAR®, Sigma, Stanheim, Germany) at a density of $11x10^4$ cells per millilitre in 1 mL growth medium per well. Seventy-two hours after seeding, culture media was refreshed. Ninety-six hours after seeding, 500 µM palmitate was used to treat the cells for 24 hours. One hundred and twenty hours after seeding, cells were

exposed to a vehicle control (media with 0.25% DMSO for palmitate positive and palmitate negative controls), ATV (10 µM and 25 µM), GRT (0.01 mg/mL and 0.1 mg/mL), or a combination thereof (10 µM ATV + 0.01 mg/mL GRT, 10 µM ATV + 0.1 mg/mL GRT, or 25 µM ATV + 0.1 mg/mL GRT) for a further 24 hours. All treatments were added to vehicle control medium. Post treatment, treatment media was aspirated, replaced with 500 µL of 2 µM JC-1 stain, and incubated at 37°C for half an hour. Mitochondrial membrane potential was assessed with flow cytometry, using a BD Accuri™ C6 (BD Biosciences, Johannesburg, South Africa). Results were generated using Accuri C6 software (BD Biosciences, Johannesburg, South Africa). Two replicates per treatment were assessed in three independent experiments.

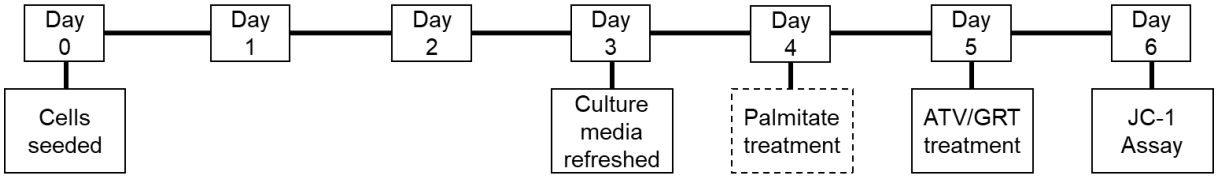

Figure 4.5.1: Schematic representation of the timeline of the JC-1 experiments.

The forward scatter and fluorescent 1 (area) (FL1-A) of the cells was plotted for each population of each treatment group. Polygonal gating (P6; *Figure 4.5.1*) was applied to the unstained, untreated control cells as an indication of the dispersion of viable cells.

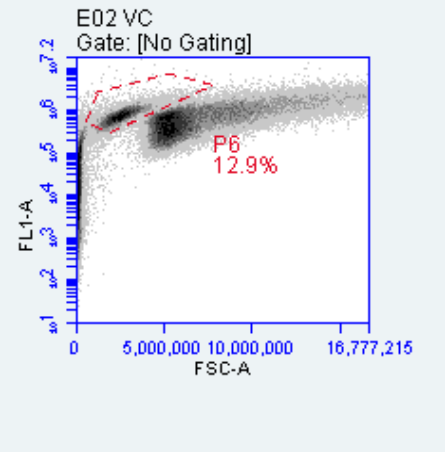

Figure 4.5.2: Representative image of gating applied to forward scatter/fluorescent 1 channel plots. *Polygonal gating was set around the unstained untreated cell population (P6) as an indication of the dispersion of the cell populations.*

The colour of the FL-1 and FL-2 channels was compensated accordingly, and quadrant gating was applied to the stained untreated cell population, gated in P6. A second, rectangular gate (R1) was set around the entire population so as to correct for the inaccuracy of the

percentages displayed in the quadrants as a result of the application of appropriate colour compensation (*Figure 4.5.2*).

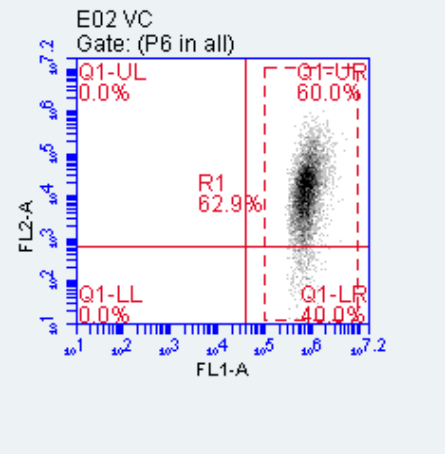

Figure 4.5.3: Representative image of gating for JC-1 stain. *Quadrant gating was applied to the stained untreated cell population. A second gate was applied, R1, to isolate the region of interest for analysis.*

The FL-1 and FL-2 channels were compared to each other and the population was set to include the population gated in R1, which was already gated to include the population gated in P6 (*Figure 4.5.3*). Quadrant gating was applied around the population. With each treatment, there was a shift in the percentage of the total population of JC-1 inactive cells falling in the lower right quadrant, which was averaged for three experimental repeats. Further, the mean red (FL-2) fluorescence intensity was measured and calculated as a percentage relative to the appropriate control and tabulated (*Supplementary Data: Table 10-1 and Table 10-2*).

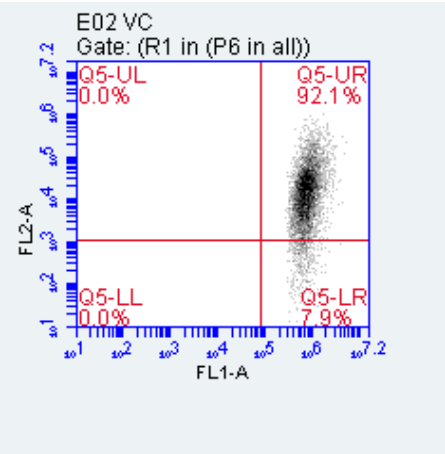

Figure 4.5.4: Representative image of plot for analysis, following a JC-1 stain. *Quadrant gating was set around the stained untreated cell population. The percentage of cells in the lower right quadrant was indicative of JC-1inactive cells as a result of decreased mitochondrial membrane potential.*

To generate representative images (*Chapter 10: Supplementary Data: Figure 10.1.1*), palmitate pre-treated cells were imaged on the Nikon Eclipse Ti-S with PRIOR ProScan III (NIS Elements AR4.40; Nikon Instruments Inc. Johannesburg, South Africa).

4.6 Viability and apoptosis assessment in 2D culture

See *Chapter 11: Appendices: 11.5.2*.

One of the earliest indicators of apoptosis is the loss of plasma membrane asymmetry, allowing for the translocation of the membrane phospholipid phosphatidylserine (PS) to outside the plasma membrane, exposed to the external cellular environment. Annexin V is a protein that can be conjugated to fluorochromes while maintaining its high affinity for PS, making it a sensitive probe for the assessment of apoptosis by flow cytometry. The translocation of PS allows for the distinction of early apoptotic cells as it precedes the loss of plasma membrane integrity – a key element of apoptotic cell death. This calls for the concurrent use of a vital dye. As such, damaged plasma membranes are permeable and allow propidium iodide, a DNA-intercalating agent, into the cells. Therefore, annexin V positive, PI negative cells are in early apoptosis, whereas annexin V positive, PI positive cells have undergone cell death (Vermes *et al.*, 1995; van Engeland *et al.*, 1996). As such, early and late apoptosis were assessed with dual staining of annexin V/propidium iodide (PI) (annexin V: catalogue no.: A13199; ThermoFisher Scientific, Johannesburg, South Africa; PI: catalogue no.: P4170; Sigma, Stanheim, Germany stain. C3A (ATCC® HB8065™) cells were seeded in a 24-well plate (1.9 cm^2) (Greiner CELLSTAR®, Sigma, Stanheim, Germany) at a density of $11x10^4$ cells per millilitre in 1 mL growth medium per well.

Seventy-two hours after seeding, culture media was refreshed. Ninety-six hours after seeding, culture media was aspirated, and the cells were exposed to 500 µM palmitate for 24 hours. One hundred and twenty hours after seeding, culture media was aspirated and cells were exposed to a vehicle control (media with 0.25% DMSO for palmitate positive and palmitate negative controls), ATV (10 µM and 25 µM), GRT (0.01 mg/mL and 0.1 mg/mL), or a combination thereof (10 µM ATV + 0.01 mg/mL GRT, 10 µM ATV + 0.1 mg/mL GRT, or 25 µM ATV + 0.1 mg/mL GRT) for 24 hours. All treatments were added to vehicle control medium. Apoptosis status was assessed with dual staining of annexin V and PI, incubated at 37°C for thirty minutes. Flow cytometry was performed using a BD Accuri™ C6 (BD Biosciences, Johannesburg, South Africa). Results were generated using Accuri C6 software (BD Biosciences, Johannesburg, South Africa). Two replicates per treatment were assessed

in three independent experiments. A comparison of the percentages in each viability state was tabulated for the normal condition (*Supplementary Data: Table 10-3*) and the hyperlipidaemic condition (*Chapter 10: Supplementary Data: Table 10-4*).

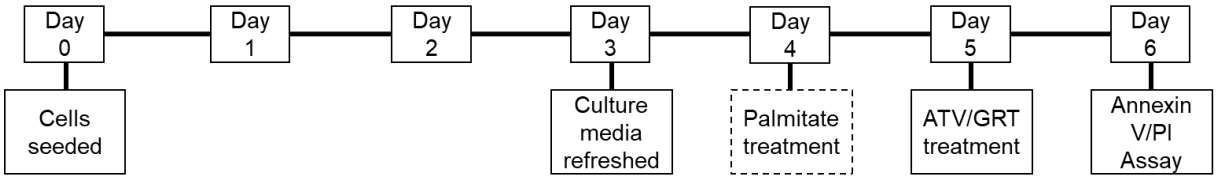

Figure 4.6.1: Schematic representation of the timeline of the annexin V/PI experiments.

Gating was applied on the forward scatter/side scatter plots to demarcate the dispersion of the healthy population (P1; *Figure 4.6.1*).

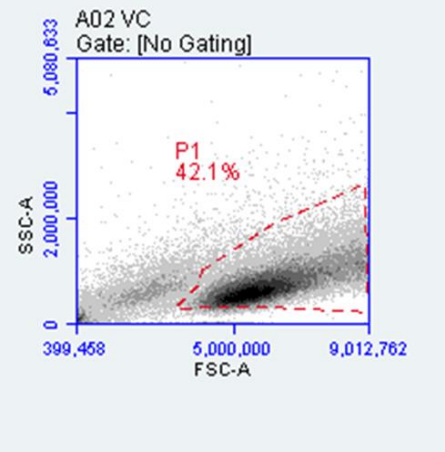

Figure 4.6.2: Representative images of gating applied to forward and side scatter plots. *Polygonal gating was set around the unstained untreated cell population (P1) as an indication of the dispersion of the healthy cell population.*

Quadrant gating was applied to the stained untreated population, gated in P1. A rectangular gate (R1) was set around the entire plot so as to correct for the inaccuracy of the percentages displayed in each quadrant as a result of the application of appropriate colour compensation (*Figure 4.6.2*).

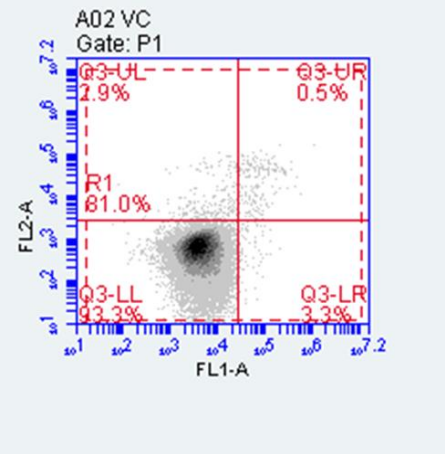

Figure 4.6.3: Representative image of gating for annexin V/propidium iodide stain. *Quadrant gating was set around the stained untreated cell population, gated in P1. A rectangular gate (R1) was set around the entire plot, correcting for inconsistencies due to colour compensation.*

Thereafter, the FL-1 and FL-2 channels were compared and the population was set to include the previously R1-gated population, in P1 (*Figure 4.6.3*). Quadrant gating was applied around the population to establish the percentage of cells in each quadrant.

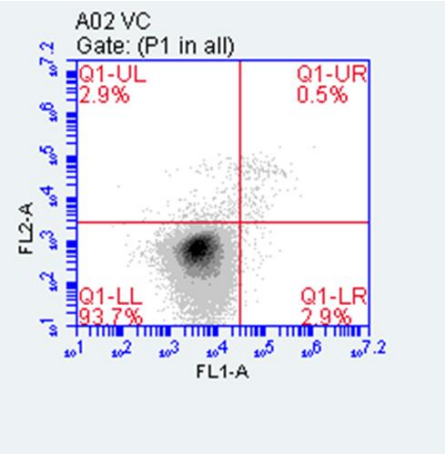

Figure 4.6.4: Representative image of gating for annexin V/propidium iodide stain. *The percentage of cells in each quadrant was indicative of viable cells (lower left quadrant), early apoptosis (upper and lower right quadrant), and late apoptosis (upper left quadrant).*

The percentage of each population landing in the various quadrants was an indication of the following: the lower left (LL) quadrant was an indication of viable cells; the upper and lower right (UR and LR) quadrants were an indication of early apoptosis, and the upper left (UL) quadrant was an indication of late apoptosis.

4.7 Apoptosis assessment in 2D culture

See *Chapter 11: Appendices: 11.6*.

Caspase 3 and caspase 7 are executioner caspases in the pathway of apoptotic cell death. Despite having unique roles to play within the cascade, it has been shown that they are indistinguishable in the cleavage of certain fluorogenic peptides. This allows for the fluorescent measurement of apoptosis (Walsh *et al.*, 2008).

Late apoptosis was assessed by means of a caspase 3/7 stain (catalogue no.: C10423; ThermoFisher Scientific, Johannesburg, South Africa). C3A (ATCC® HB8065™) cells were seeded in a black 96-well clear bottom plate (0.32 cm^2) (Nest Biotech; Whitehead Scientific, Cape Town, South Africa) at a density of $11x10^4$ cells per millilitre in 200 µL growth medium per well. Seventy-two hours after seeding, culture media was refreshed. Ninety-six hours after seeding, culture media was aspirated, and the cells were exposed to 500 µM palmitate for 24 hours. One hundred and twenty hours after seeding, culture media was aspirated and cells were exposed to a vehicle control (media with 0.25% DMSO for palmitate positive and palmitate negative controls), ATV (10 µM and 25 µM), GRT (0.01 mg/mL and 0.1 mg/mL), or a combination thereof (10 µM ATV + 0.01 mg/mL GRT, 10 µM ATV + 0.1 mg/mL GRT, or 25 µM ATV + 0.1 mg/mL GRT) for 24 hours. All treatments were added to vehicle control medium. Apoptosis was assessed using a 10 µM caspase 3/7 stain, incubated at 37°C for an hour. Fluorescent readings were recorded on a SpectraMax i3x multi-mode microplate reader (Molecular Devices, LLC, Sunnyvale, CA, USA) at an excitation wavelength of 502nm and an emission wavelength of 530nm every 15 minutes for 60 minutes. Results were generated on SoftMax Pro 7 software, version 7.2 (Molecular Devices, LLC, Sunnyvale, CA, USA). Three replicates per treatment were assessed in three independent experiments.

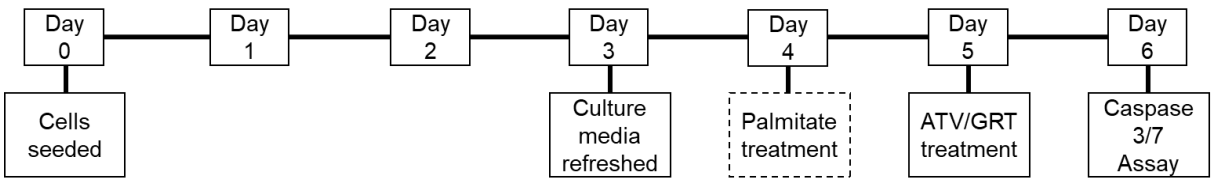

Figure 4.7.1: Schematic representation of the timeline of the caspase 3/7 experiments.

4.8 *In vitro* culturing of C3A cells in 3D culture

See *Chapter 11: Appendices: 11.7*

For 3D culturing of C3A cells, a protocol described by Wrzesinki *et al* (2013) was optimized. Two 3D bioreactors were assembled and prepared 24 hours before use (Day 0). Briefly, an AggreWell™ 800 plate (catalogue no.: 34811, STEMCELL Technologies, Cape Town, South Africa) was prepared and stored in an incubator until needed. Cells at 85 – 90% confluence were added to the prepared AggreWell™ plate at a density of $4.8x10^6$ cells per millilitre, topped up with complete growth medium, and incubated overnight (± 20 hours). On Day 1, the cell aggregates/clusters were gently dislodged from the AggreWell™ plate using a plastic Pasteur pipette and transferred to the growth chamber of the bioreactor to produce spheroids. The bioreactor was then returned to the incubator and rotated on the lowest speed (approximately 14.5 rpm). The speed was adjusted to create a microgravitational environment, whereby the spheroids remain in the same position without colliding with the sides of the vessel, or each other. Incubators for bioreactors were set at 5% CO_2, 95% air, and 37ºC for a minimum of 18 days, with growth media being exchanged every 2 days, and the speed being adjusted according to growth of the spheroids. Once treatment began, treatment media was replaced daily.

Eighteen-day-old spheroids were exposed to a 500 µM palmitate pre-treatment for 96 hours. Thereafter, treatment with 0.1 mg/mL GRT, 10 µM ATV, or a combination thereof, began for a further 14 days. Treatment concentrations were extrapolated from 2D culture. An untreated control bioreactor served as the negative control and was exposed only to complete growth medium, while the palmitate-only bioreactor served as the positive control. Three other bioreactors were used and treated with palmitate and 0.01 mg/mL GRT, palmitate and 10 µM ATV, or a combination of palmitate, 0.01 mg/mL GRT, and 10 µM ATV.

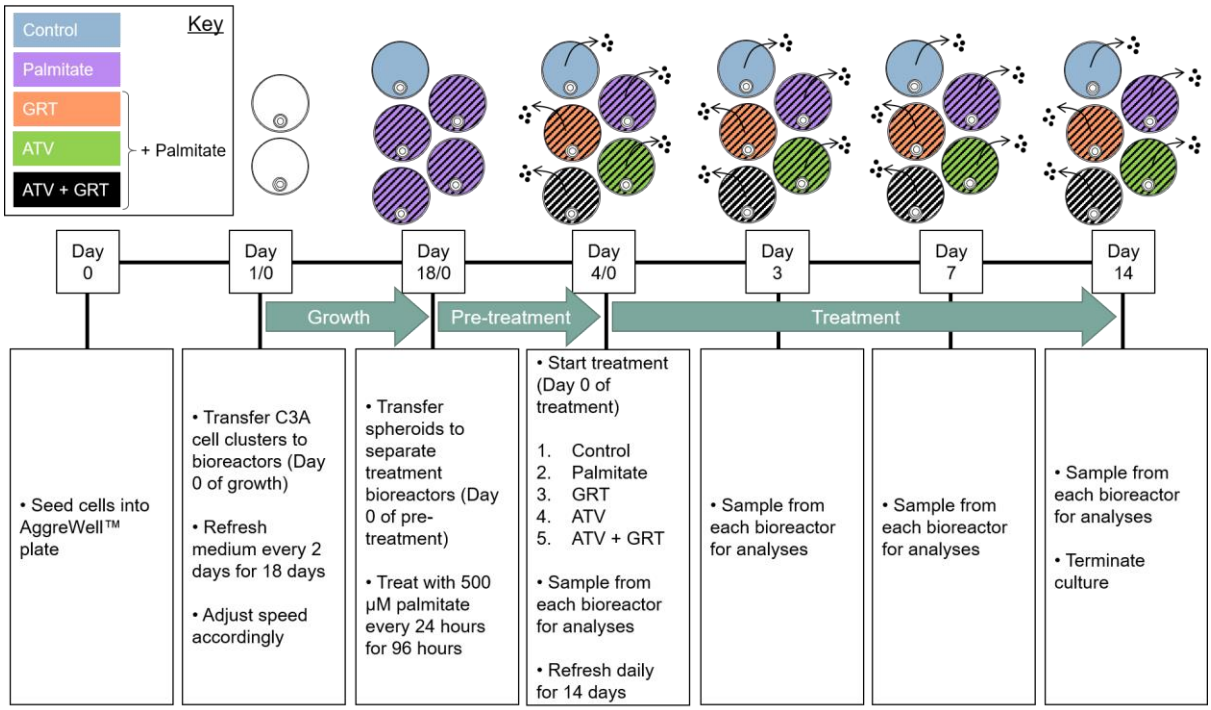

Figure 4.8.1: Schematic representation of 3D culturing timeline.

4.9 Glucose utilisation

As an indication of cellular respiration, glucose levels in the growth media was measured using a One Touch® Select® glucometer (Roche Diabetes Care South Africa). Media and treatment media was aspirated from the bioreactors with a 10 mL syringe. A sample (5 µL) of fresh and aspirated media was tested on a glucose test strip and measured in mmol/L. Glucose remaining in the media was calculated as a percentage relative to the fresh media added, set at 100%.

4.10 Electron microscopy

4.10.1 Tissue preparation

(Method: NHLS Department of Electron Microscopy Laboratory, Department of Anatomical Pathology, Tygerberg Hospital – Mrs. N Muller)

Harvested C3A spheroids were fixed in 2.5% glutaraldehyde in 0.1M phosphate buffer pH 7.2 at 4°C for 8 - 12 hours. After a 5 min wash in phosphate buffer, spheroids were post-fixed in 3% osmium tetroxide in Palade's buffer for 1 hour. Thereafter, the osmium tetroxide was

removed and the spheroids washed in distilled water and processed in processing vials according to an established protocol (*Table 4-1*).

Table 4-1: Tissue processing schedule.

Reagent	Time (min)
10% uranyl acetate	15
70% alcohol	10
70% alcohol	10
10% uranyl nitrate	20
100% alcohol	15
100% alcohol	20
100% alcohol	30
100% alcohol: Spurr's resin	90
Spurr's resin	60
Spurr's resin	60

Spheroids were then embedded with Spurr's resin into gelatin capsules and allowed to polymerize overnight at 60°C.

4.10.2 Ultra-thin sectioning

Ultra-thin (100 nm) sections of the spheroids were cut from the resin blocks using a glass knife fitted with a water-trough using a Leica EM UC7 ultramicrotome (Vienna, Austria). The ultra-thin ribbon sections were collected from the water surface onto 200G grids, and allowed to dry on filter paper before staining. The grids were first stained with 2% uranyl acetate in 70% alcohol for 10 minutes, rinsed in 70% alcohol and distilled water. Thereafter the grids were stained with Reynold's lead acetate for 5 minutes, washed in distilled water and allowed to dry on filter paper. The spheroid sections were imaged using a Joel JEM 1011 (Akishima, Tokyo) transmission microscope.

4.11 Spheroid viability assessment

See *Chapter 11: Appendices: 11.8*

The luminescent assessment of ATP allows for luciferin, adenosine triphosphate (ATP) and co-factor Mg^{2+} to be metabolised by luciferase to produce oxyluciferin and energy in the form

of luminescence. ATP is a co-factor for the reaction, and the luminescence produced is proportional to the amount of ATP present, representative of metabolically active cells (Hannah *et al*, 2015).

Spheroid viability was assessed using a CellTiter-Glo® Luminescent Cell Viability Assay (Catalogue no.: G7571; Promega, Anatech Instruments Pty. Ltd, Johannesburg, South Africa). Spheroids from each treatment group were sampled at Day 0, 3, 7, and 14 in a white-walled 96-well clear bottom plate (0.32 cm^2) (catalogue no.: M1062; Greiner CELLSTAR®, Sigma, Stanheim, Germany). The CellTiter-Glo® lysis buffer was added to each well and incubated at 37°C for 1 hour on a microtiter plate shaker. Luminescence readings were measured with a SpectraMax i3x multi-mode microplate reader (Molecular Devices, LLC, Sunnyvale, CA, USA) Results were generated on SoftMax Pro 7 software, version 7.2 (Molecular Devices, LLC, Sunnyvale, CA, USA). Three technical replicates were performed with three spheroids per repeat. ATP production was normalised to average spheroid volume (μm^3) and expressed as luminescence (arbitrary units; AU) per μm^3.

4.12 Adenylate kinase assessment

See *Chapter 11: Appendices: 11.9*

Damage to the mitochondrial membrane causes a loss of cellular integrity and allows for the leakage of mitochondrial proteins and enzymes into the cytosol and culture media. Compromised mitochondria have been shown to non-selectively release mitochondrial proteins into the cytosol, such as cytochrome *c*. Adenylate kinase has been shown to be concomitantly released with cytochrome *c* (Single *et al*, 1998; Köhler *et al*, 1999). Adenylate kinase is present in all mitochondria and can be measured bioluminescently to sensitively and accurately determine cytolysis and cytotoxicity. A luciferase reaction occurs due to the enzymatic production of ATP by adenylate kinase substrate and ADP, allowing for a directly proportional luminescent measurement of the presence of adenylate kinase (Olsson *et al*, 1983).

Culture and treatment medium were sampled upon refreshing the bioreactors and stored at -20°C until required. Using the ToxiLight™ bioassay kit (catalogue no.: LT07-217; Lonza, MD, USA), the presence of adenylate kinase in the medium was measured. All reagents were thawed to room temperature and 5 µL of sampled medium was transferred into a clean white-walled 96-well clear bottom plate (0.32 cm^2) (catalogue no.: M1062; Greiner CELLSTAR®,

Sigma, Stanheim, Germany), followed by the addition of 100 µL of reconstituted adenylate kinase detection reagent, incubated at room temperature for 5 minutes. Luminescence readings were taken on a SpectraMax i3x multi-mode microplate reader (Molecular Devices, LLC, Sunnyvale, CA, USA). Results were generated on SoftMax Pro 7 software, version 7.2 (Molecular Devices, LLC, Sunnyvale, CA, USA). Three technical replicates were performed per sample medium per time point. Adenylate kinase production was measured as luminescence (RLU), normalised to average spheroid volume per treatment (μm^3), and calculated as a percentage relative to the first sample, set at 100%.

4.13 Statistical analysis

Statistical analysis was performed using GraphPad Prism 8.0.0 (GraphPad Software, La Jolla, California, United States of America) and data were compared using a one-way or two-way (where appropriate) Analysis of Variance (ANOVA), followed by a Tukey post hoc test. Data are presented as mean ± standard deviation (SD) and p-values of ≤ 0.05 were considered statistically significant.

5 Results

5.1 Acute GRT, ATV, and palmitate cytotoxicity assessment in 2D culture (MTT)

By assessing the activity of mitochondria in live cells with an MTT assay, the concentration- and time-dependent assessment of ATV and Afriplex GRT (hereafter referred to as GRT) on cytotoxicity was determined.

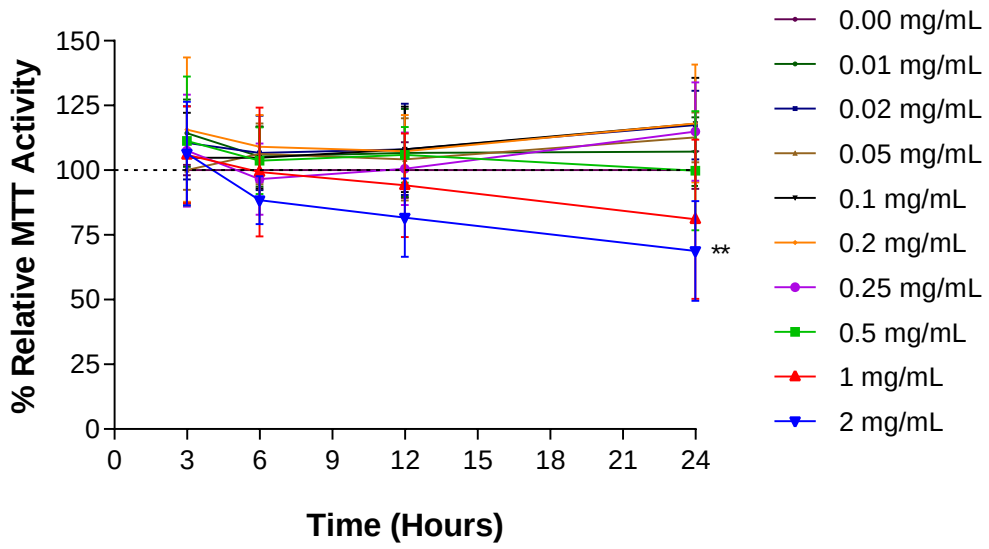

Figure 5.1.1: MTT assay for the assessment of cell viability in GRT-treated cells. *Cells were exposed to ten different concentrations of GRT (0.0 mg/mL, 0.01 mg/mL, 0.02 mg/mL, 0.05 mg/mL, 0.1 mg/mL, 0.2 mg/mL, 0.25 mg/mL, 0.5 mg/mL, 1 mg/mL, and 2 mg/mL) and assessed at 4 different time points, namely 3, 6, 12, and 24 hours. Data is normalised against the relevant control for each time point set at 100%. Data are mean ± SD derived from four independent experiments each with three technical repeats (n = 4). A Two-way Analysis of Variance was performed with a Tukey post hoc test. ** = p<0.01.*

An MTT assay was used to assess cell viability based on mitochondrial dehydrogenase activity in a time- and concentration-dependent fashion. Ten concentrations of GRT (0.0 mg/mL, 0.01 mg/mL, 0.02 mg/mL, 0.05 mg/mL, 0.1 mg/mL, 0.2 mg/mL, 0.25 mg/mL, 0.5 mg/mL, 1 mg/mL, and 2 mg/mL) were tested at 4 time points, namely: 3 hours, 6 hours, 12 hours, and 24 hours, as shown in *Figure 5.1.1*. Cytotoxicity was observed only at 24 hours for the highest concentration of GRT.

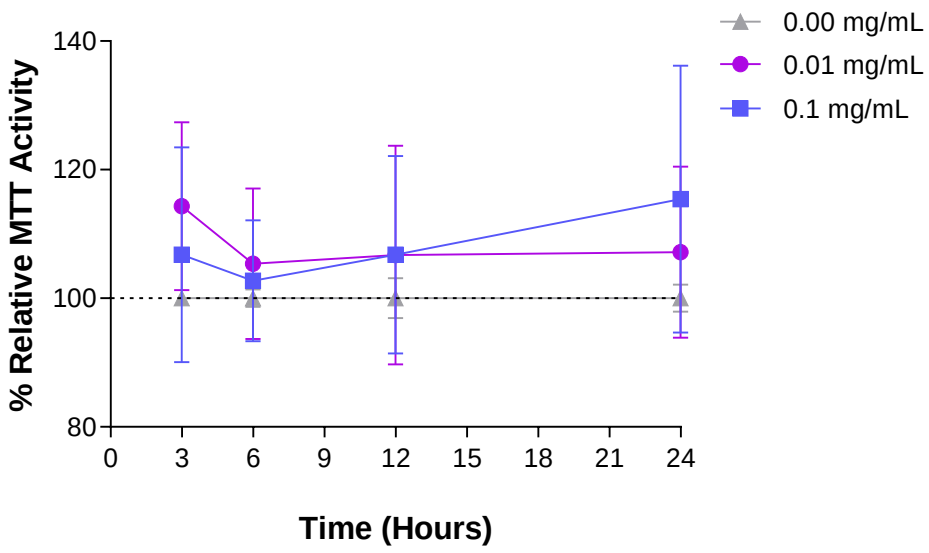

Figure 5.1.2: Selection of GRT concentrations and time points based on an MTT assay. *Based on the concentration curves in Figure 5.1.1, two concentrations of GRT (0.01 and 0.1 mg/mL) showing the most positive effect on mitochondrial dehydrogenase activity at 24 hours were selected as the optimal GRT treatment concentrations in the C3A cells. Data is normalised against the relevant control for each time point set at 100%. Data are mean ± SD derived from four independent experiments each with three technical repeats (n = 4). A Two-way Analysis of Variance was performed with a Tukey post hoc test.*

Figure 5.1.2 shows the MTT activity effect of GRT on C3A cells, concentrations of 0.01 mg/mL and 0.1 mg/mL of GRT for the 24 hours treatment period was selected based on their positive effect on mitochondrial dehydrogenase activity of the C3A cells. Afriplex GRT™ is formulated to contain 12% aspalathin.

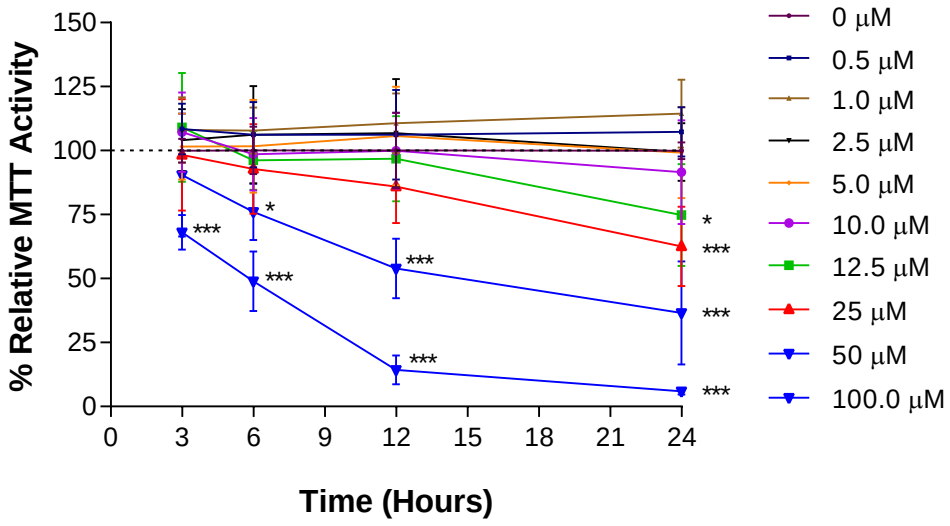

Figure 5.1.3: MTT assay for the assessment of cytotoxicity and cell growth inhibition by ATV-treated C3A cells. *Cells were exposed to 10 concentrations of ATV (0 µM, 0.5 µM, 1 µM, 2.5 µM, 5 µM, 10 µM, 12.5 µM, 25 µM, 50 µM, and 100 µM) and assessed at 4 different time points, namely 3, 6, 12, and 24 hours (Figure 5.1.3). Data is normalised against the relevant control for each time point set at 100%. Data are mean ± SD derived from*

*four independent experiments each with three technical repeats (n = 4). A Two-way Analysis of Variance was performed with a Tukey post hoc test. * = p<0.05; *** = p<0.001.*

Figure 5.1.3 shows that ATV was cytotoxic to the cells from a concentration of 25 µM over the 24 hour period tested. At the higher concentrations of 50 µM and 100 µM ATV, significant cytotoxicity was apparent from 6 hours (*p<0.001*) at 76.02% ± 11.09 and 48.92% ± 11.61 respectively.

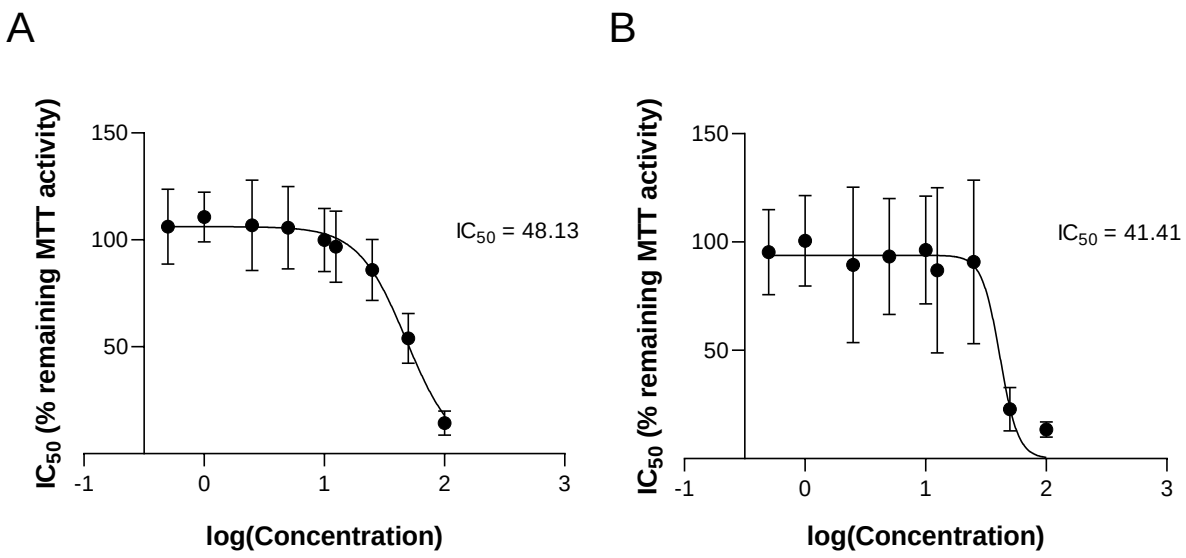

Figure 5.1.4: Semi Log concentration response curves and calculated IC_{50} values of ATV in C3A cells. *Remaining MTT activity was determined at 12 (Figure 5.1.4.A) and 24 hours (Figure 5.1.5.B). Error bars: ± SD. Data from four independent experiments each with three technical repeats (n = 4).*

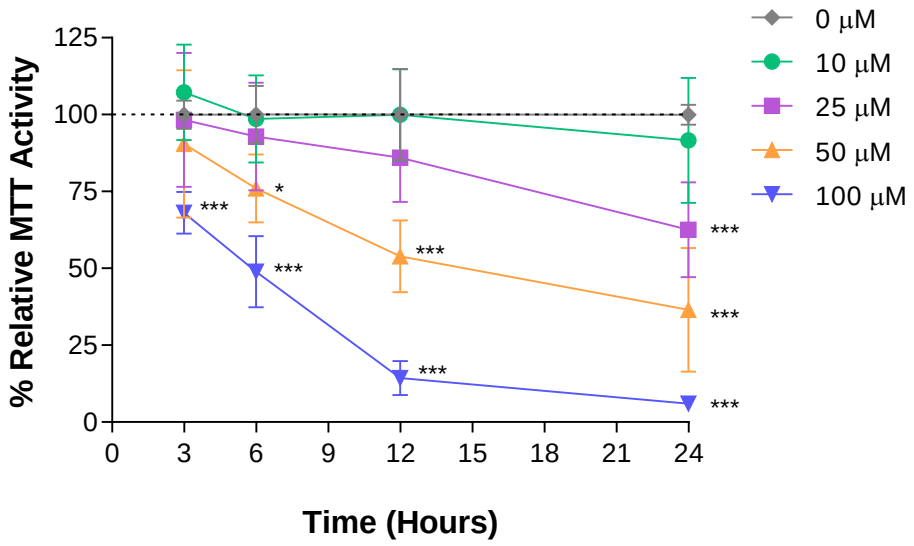

Figure 5.1.5: Selection of ATV concentrations and time points based on MTT assay. *Comparison of four selected ATV concentrations to illustrate the rationale for selection of 10 and 25 µM ATV for 24 hours as optimal treatment options. Data is normalised against the relevant control for each time point set at 100%. Data from four independent experiments each with three technical repeats (n = 4), presented as mean ± SD. A two-way Analysis of Variance was performed with a Tukey post hoc test. * = p<0.05; *** = p<0.001.*

As seen in *Figures 5.1.3* and *5.1.5*, the two highest concentrations tested (50 µM and 100 µM) of ATV induced noticeable toxicity in C3A cells after 12 hours (53.88% ± 11.71 and 14.28% ± 5.60 respectively) and 24 hours (36.53% ± 20.14 and 5.96% ± 1.24 respectively) and were thus deemed too toxic to fit the model being used, which called for the induction of hepatic injury. Based on the 12- and 24-hour MTT IC_{50} values (48.13 µM ± 2.08 and 41.41 µM ± 3.67 respectively), two lower concentrations of 10 µM and 25 µM, were considered the more intermediate, physiologically and literature-relevant concentrations for further experiments.

Palmitate treatment was used to mimic a hyperlipidaemic physiological state *in vitro* as previously described by Hu *et al* (2014). This was verified by assessing the CYP3A4 activity as Shu *et al* (2016b) showed that CYP3A4 activity is increased in the hyperlipidaemic state. Cells were expected to react differently to the statin treatment as a result of the varying metabolic status of the cells. The introduction of a palmitate pre-treatment noticeably decreased cell viability, as shown in *Figure 5.1.6*. Hu *et al* (2014) made use of 200 µM palmitate treatment for 24 hours.

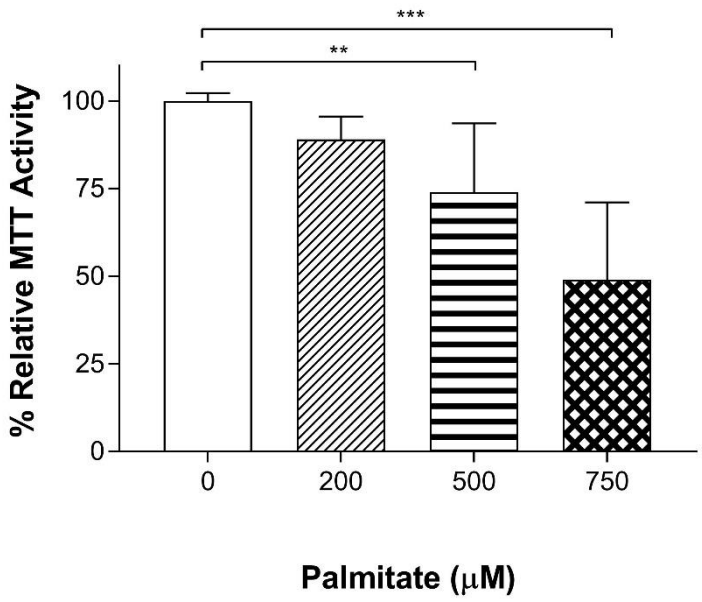

Figure 5.1.6: MTT assay for the assessment of cell viability in palmitate-treated C3A cells. *Cells were exposed to three different concentrations of palmitate (200µM, 500µM, and 750µM) for 24 hours, as this was the pre-treatment period before 24 hours of ATV and/or GRT treatment. Data are mean ± SD derived from three independent experiments each with three technical repeats (n = 3). A Two-way Analysis of Variance was performed with a Tukey post hoc test. Comparative statistics were between each concentration of palmitate in each treatment group and the respective palmitate negative control. ** = p<0.01; *** = p<0.001.*

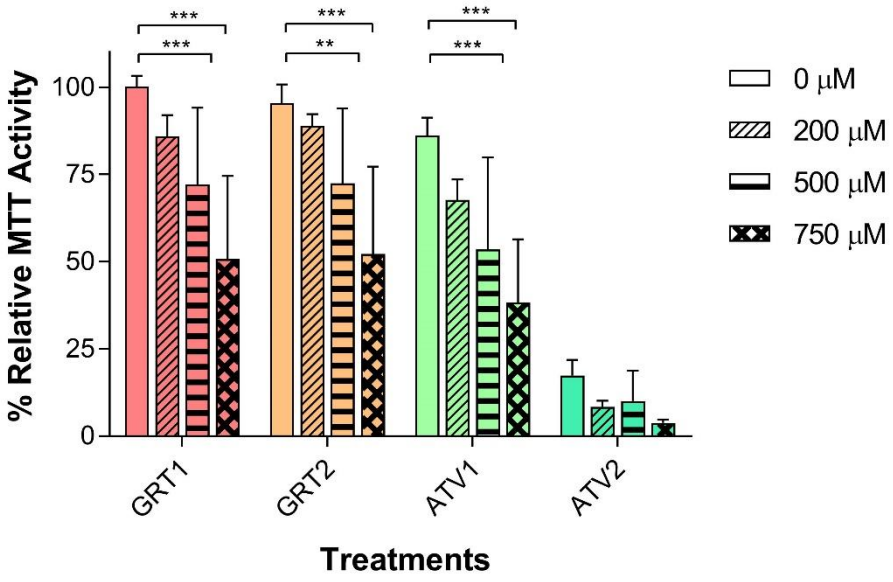

Figure 5.1.7: MTT assay for the assessment of GRT and atorvastatin (ATV) treatment on C3A cell viability in palmitate pre-treated cells. *C3A cells were exposed to three different concentrations of palmitate (200µM, 500µM, and 750µM) for 24 hours before 24 hours of ATV and GRT treatment. Data are mean ± SD derived from three independent experiments each with three technical repeats (n = 3). Data are normalised against the relevant control set at 100%. Data are mean ± SD. A Two-way Analysis of Variance was performed with a Tukey post hoc test. Comparative statistics were between each concentration of palmitate in each treatment group and the respective palmitate negative control. ** = p<0.01; *** = p<0.001. GRT1 = 0.01 mg/mL; GRT2 = 0.1 mg/mL; ATV1 = 10 µM and ATV2 = 25 µM.*

C3A cells were exposed to three different concentrations of palmitate pre-treatment, followed by a 24 hour treatment with GRT or ATV. Pre-treatment of C3A cells with 200 µM palmitate did not significantly reduce cell viability when compared to the cells not treated with palmitate in each treatment group (*Figure 5.1.7*). Treatment with 750 µM palmitate showed a significant decrease ($p<0.001$) in cell viability in all treatment groups as compared to their respective controls, with viability decreasing by approximately half in each treatment group. Viability was significantly decreased ($p<0.01$ and $p<0.001$) compared to the control in the treatment groups when cells were treated 500 µM palmitate, however, being an intermediate and literature-relevant concentration, it was chosen as an appropriate concentration for an *in vitro* model of hepatic injury.

5.2 Assessment of CYP3A4 induction by palmitate

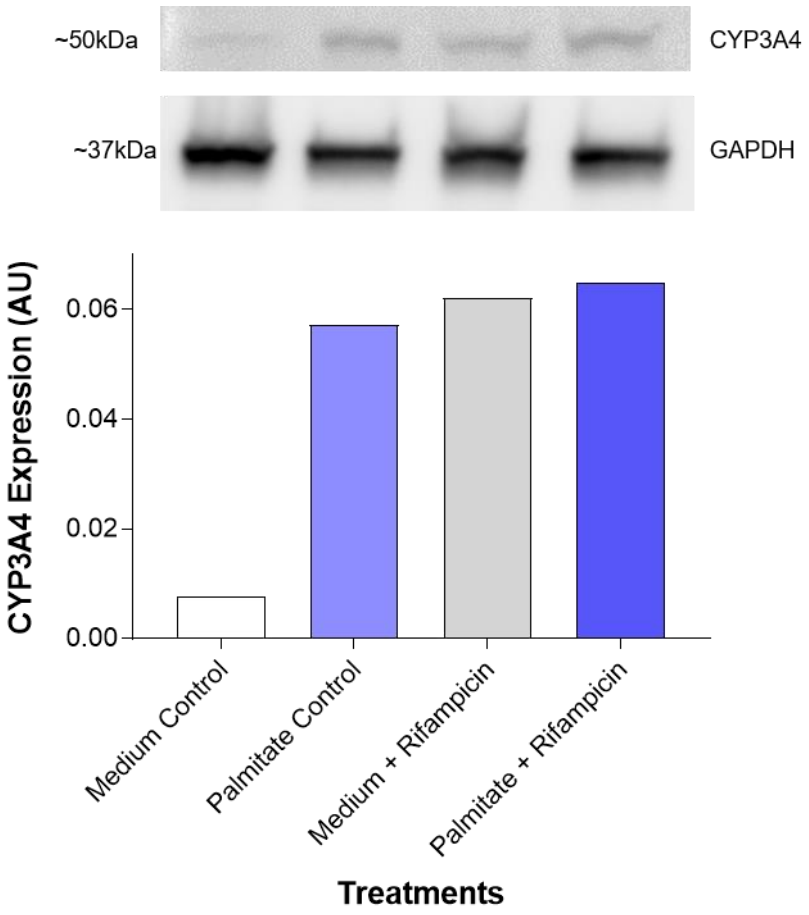

Figure 5.2.1: Western blot analysis assessing the modulation of CYP3A4 activity in palmitate-treated C3A cells. *Cells were exposed to different treatments (24 hours) and the protein expression of CYP3A4 (~52 kDa) and GAPDH (~37 kDa) was quantified by Western blot gel electrophoresis: Medium Control = culture medium; Palmitate Control = 500 µM palmitate; Medium + Rifampicin = culture medium + 10 µM Rifampicin; Palmitate + Rifampicin = 500 µM palmitate + 10 µM Rifampicin. CYP3A4 protein expression was normalised to the housekeeping gene, GAPDH, and expressed in arbitrary units (AU). n = 1. Statistical analysis not performed.*

Literature shows that the hyperlipidaemic state increases CYP3A4 activity when compared to the healthy condition. Rifampicin is used as a positive control as it is an inducer of CYP3A4 activity. As seen in *Figure 5.2.1*, the Medium Control showed the lowest CYP3A4 expression (0.008 AU). Palmitate treatment showed increased CYP3A4 expression (0.057 AU) compared to the Medium Control, and the Rifampicin-treated combination cells both showed further increased protein expression (0.062 AU for the Medium + Rifampicin group, and 0.065 AU for the Palmitate + Rifampicin group).

5.3 Viability assessment in C3A cells not exposed to palmitate (normal condition) and exposed to palmitate pre-treatment (hyperlipidaemic condition).

An MTT assay was used to assess mitochondrial function as an indication of cell viability in C3A cells not exposed to palmitate (normal condition), as well as pre-treated with palmitate (hyperlipidaemic condition), and subsequently treated with the previously selected concentrations of GRT or ATV or combination treatment.

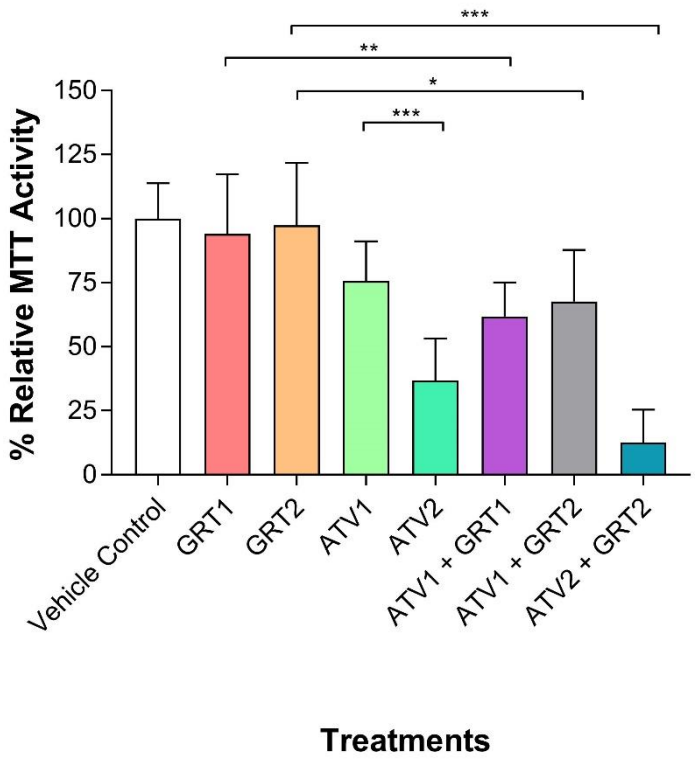

Figure 5.3.1: MTT assay assessment of cell viability in C3A cells not exposed to palmitate (normal condition) treated with GRT, atorvastatin, and combinations thereof. *C3A cells were exposed to the following treatments and combinations (24 hours). Vehicle control = media with 0.25% DMSO; ATV1 = 10 µM; ATV2 = 25 µM; GRT1 = 0.01 mg/mL; GRT2 = and 0.1 mg/mL; ATV1 + GRT1 = 10 µM ATV + 0.01 mg/mL GRT; ATV1 + GRT2 = 10 µM ATV + 0.1 mg/mL GRT; ATV2 + GRT2 = 25 µM ATV + 0.1 mg/mL GRT. Data are mean ± SD derived from three independent experiments each with three technical repeats (n = 3). A One-way Analysis of Variance was performed with a Tukey post hoc test. All results were calculated as percentage relative absorbance normalised to the vehicle control at 100%. * = p<0.05; ** = p<0.01; *** = p<0.001.*

Figure 5.3.1 shows that GRT treatment at the concentrations tested (GRT1 = 0.01 mg/mL and GRT2 = 0.1 mg/mL) had no significant effect on cell viability in C3A cells not exposed to palmitate (normal condition). In contrast, ATV reduced C3A cell viability in a concentration dependent manner. A significant decline in C3A cell viability was demonstrated between 10 µM versus a 25 µM 24 hour treatments (75.66% ± 15.52 vs 36.77% ± 16.45; *p<0.001*).

Combination treatment of ATV (10 µM and 25 µM) with GRT (0.01 mg/mL and 0.1 mg/mL) did not ameliorate ATV-induced cytotoxicity.

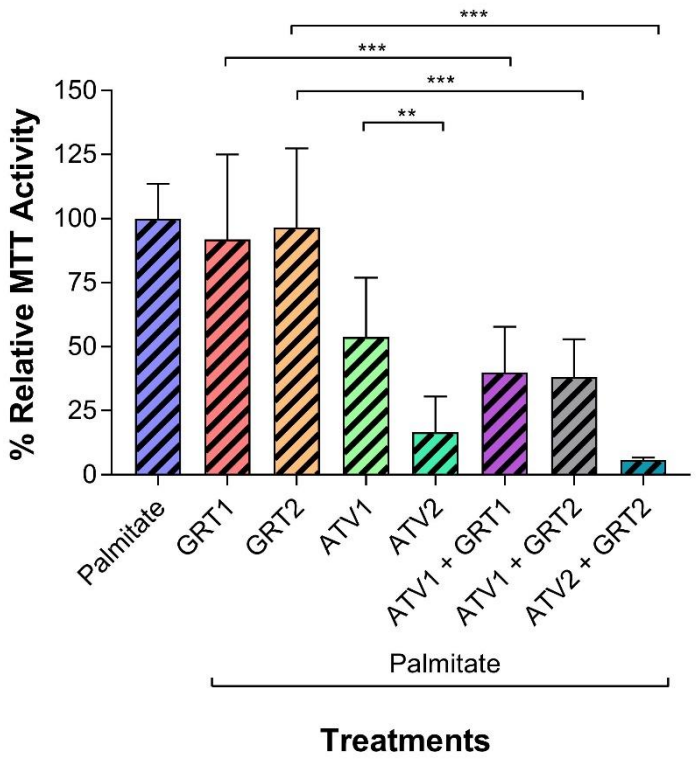

Figure 5.3.2: MTT assay assessment of cell viability in C3A cells pre-treated with 500 µM palmitate for 24 hours (hyperlipidaemic condition), treated with GRT, atorvastatin and combinations thereof. *Cells exposed to 500 µM palmitate pre-treatment were subsequently treated with the following treatments and combinations (24 hours). Palmitate control = palmitate pre-treated cells exposed to media with 0.25% DMSO for 24 hours; ATV1 = 10 µM; ATV2 = 25 µM; GRT1 = 0.01 mg/mL; GRT2 = and 0.1 mg/mL; ATV1 + GRT1 = 10 µM ATV + 0.01 mg/mL GRT; ATV1 + GRT2 = 10 µM ATV + 0.1 mg/mL GRT; ATV2 + GRT2 = 25 µM ATV + 0.1 mg/mL GRT. %. Data are mean ± SD derived from three independent experiments each with three technical repeats (n = 3). A one-way Analysis of Variance was performed with a Tukey post hoc test. All results were calculated as percentage relative absorbance normalised to the palmitate control at 100%. ** = p<0.01; *** = p<0.001.*

In C3A cells treated with 500 µM palmitate for 24 hours, used to simulate a hyperlipidaemic condition, GRT did not significantly reduce cell viability. As was seen in the normal condition, atorvastatin induced cytotoxicity in C3A cells in a concentration-dependent manner. A significant decline in C3A cell viability was demonstrated between 10 µM versus 25 µM treatments for 24 hour (53.78% ± 23.20 vs 16.58% ± 13.99; *p<0.001*). The adverse effect of atorvastatin was not improved by the combination treatment with GRT at either concentration.

5.4 Oxidative stress assessment in 2D culture

Reactive oxygen species (ROS) production, relative to cell viability was assessed to elucidate the effect of oxidative stress. This was analysed in the normal condition as well as the hyperlipidaemic condition.

5.4.1 Intracellular ROS production in the normal condition

Determination of cellular ROS production was assessed by the DCF assay that determined the rate of deacetylation of DCFDA by cellular esterases, and by its oxidation by intracellular ROS, generating a highly fluorescent DCF product.

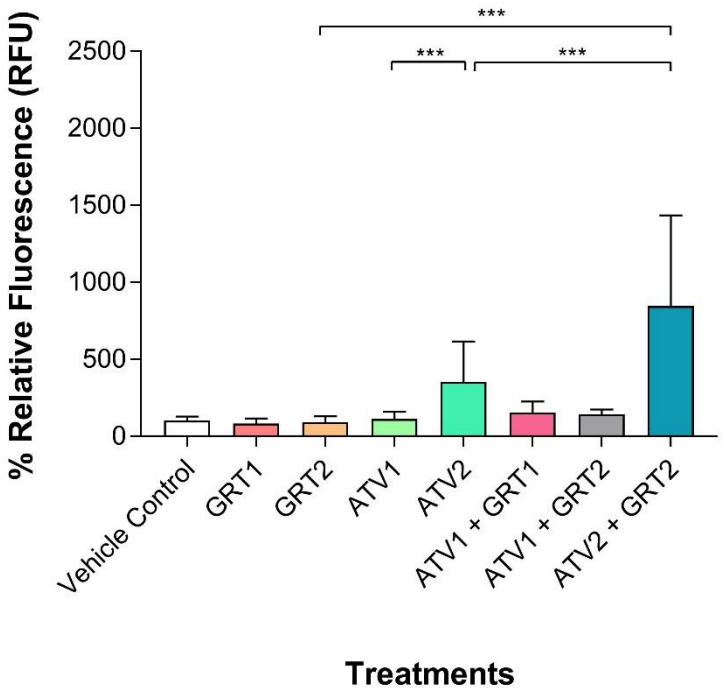

Figure 5.4.1: DCF assay assessment of oxidative stress in C3A cells not exposed to palmitate (normal condition) treated with GRT, atorvastatin and combinations thereof. *C3A cells were treated with GRT, atorvastatin and combinations (24 hours). Vehicle control = media with 0.25% DMSO; ATV1 = 10 µM; ATV2 = 25 µM; GRT1 = 0.01 mg/mL; GRT2 = and 0.1 mg/mL; ATV1 + GRT1 = 10 µM ATV + 0.01 mg/mL GRT; ATV1 + GRT2 = 10 µM ATV + 0.1 mg/mL GRT; ATV2 + GRT2 = 25 µM ATV + 0.1 mg/mL GRT. %. Data are mean ± SD derived from three independent experiments each with three technical repeats (n = 3). A one-way Analysis of Variance was performed with a Tukey post hoc test. All results were calculated as percentage relative fluorescence normalised to the vehicle control at 100%. *** = p<0.001.*

In the normal condition as shown in *Figure 5.4.1*, GRT had no significant effect on intracellular ROS production; whist ATV increased intracellular ROS in a concentration related manner. Co-treatment with GRT has a significant (*p<0.001*) additive effect on ATV-induced intracellular ROS production compared to ATV2 monotherapy.

5.4.2 Intracellular ROS production in the hyperlipidaemic condition

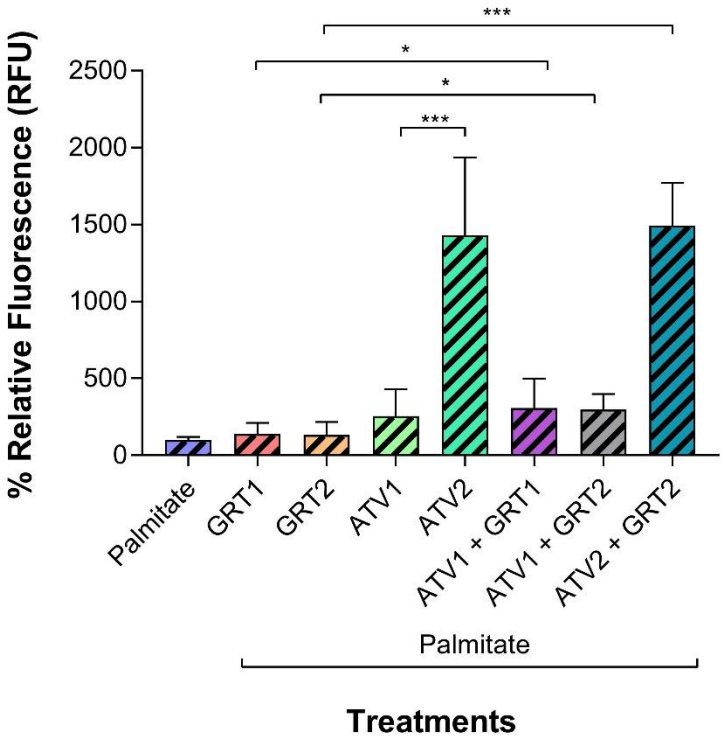

Figure 5.4.2: DCF assay assessment of oxidative stress in C3A cells exposed to 500 µM palmitate for 24 hours to simulate hyperlipidaemia, treated with GRT, atorvastatin and combinations thereof. *Palmitate-treated C3A cells were exposed to the following treatments and combinations (24 hours): Palmitate control = palmitate pre-treated cells exposed to media with 0.25% DMSO for 24 hours; ATV1 = 10 µM; ATV2 = 25 µM; GRT1 = 0.01 mg/mL; GRT2 = and 0.1 mg/mL; ATV1 + GRT1 = 10 µM ATV + 0.01 mg/mL GRT; ATV1 + GRT2 = 10 µM ATV + 0.1 mg/mL GRT; ATV2 + GRT2 = 25 µM ATV + 0.1 mg/mL GRT. Data are mean ± SD derived from three independent experiments each with three technical repeats (n = 3). A one-way Analysis of Variance was performed with a Tukey post hoc test. All results were calculated as percentage relative fluorescence normalised to the palmitate control at 100%. * = p<0.05; *** = p<0.001.*

Under the simulated hyperlipidaemic condition (*Figure 5.4.2*) ATV showed a concentration dependent increase in intracellular ROS, with 25 µM ATV greatly increasing (>10-fold) intracellular ROS production (1431.00% ± 504.20). The increase in intracellular ROS induced by the higher concentration of ATV was more than double than what was induced under the normal condition. In combination, GRT at the concentrations used did not moderate an ATV-induced increase in ROS production.

5.5 Mitochondrial membrane potential assessment

Mitochondrial membrane potential was assessed for the accumulation of JC-1 J-aggregates by active mitochondria, represented by red fluorescence, derived from a green fluorescent monomer of the JC-1 dye. Red J-aggregates accumulate in the mitochondria due to higher mitochondrial membrane integrity, whereas green monomers are present when there is decreased mitochondrial membrane potential. Increased red fluorescence signal is due to higher mitochondrial membrane potential, while the presence of the green fluorescence is due to decreased mitochondrial membrane potential. This dual-emission JC-1 dye allows for the fluorescent determination of mitochondrial integrity changes. Cell populations were measured in terms of mean fluorescence (FL2-A) intensity, where increased fluorescence intensity is indicative of increased presence of red aggregates as an indication of mitochondrial membrane integrity, and in terms of JC-1 inactive cells, where “inactive” cells represents the percentage of the cell population that fall beneath the minimum red fluorescence threshold of the measurement of J-aggregates.

5.5.1 JC-1 fluorescence in the normal condition

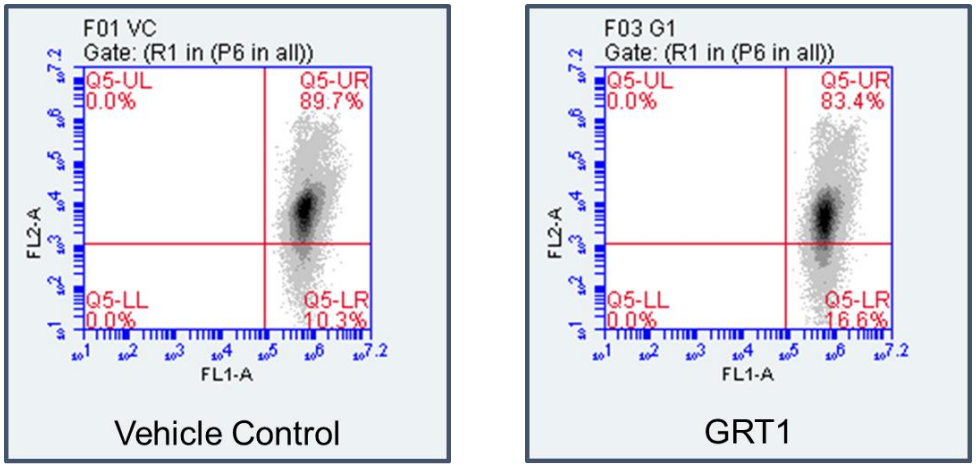

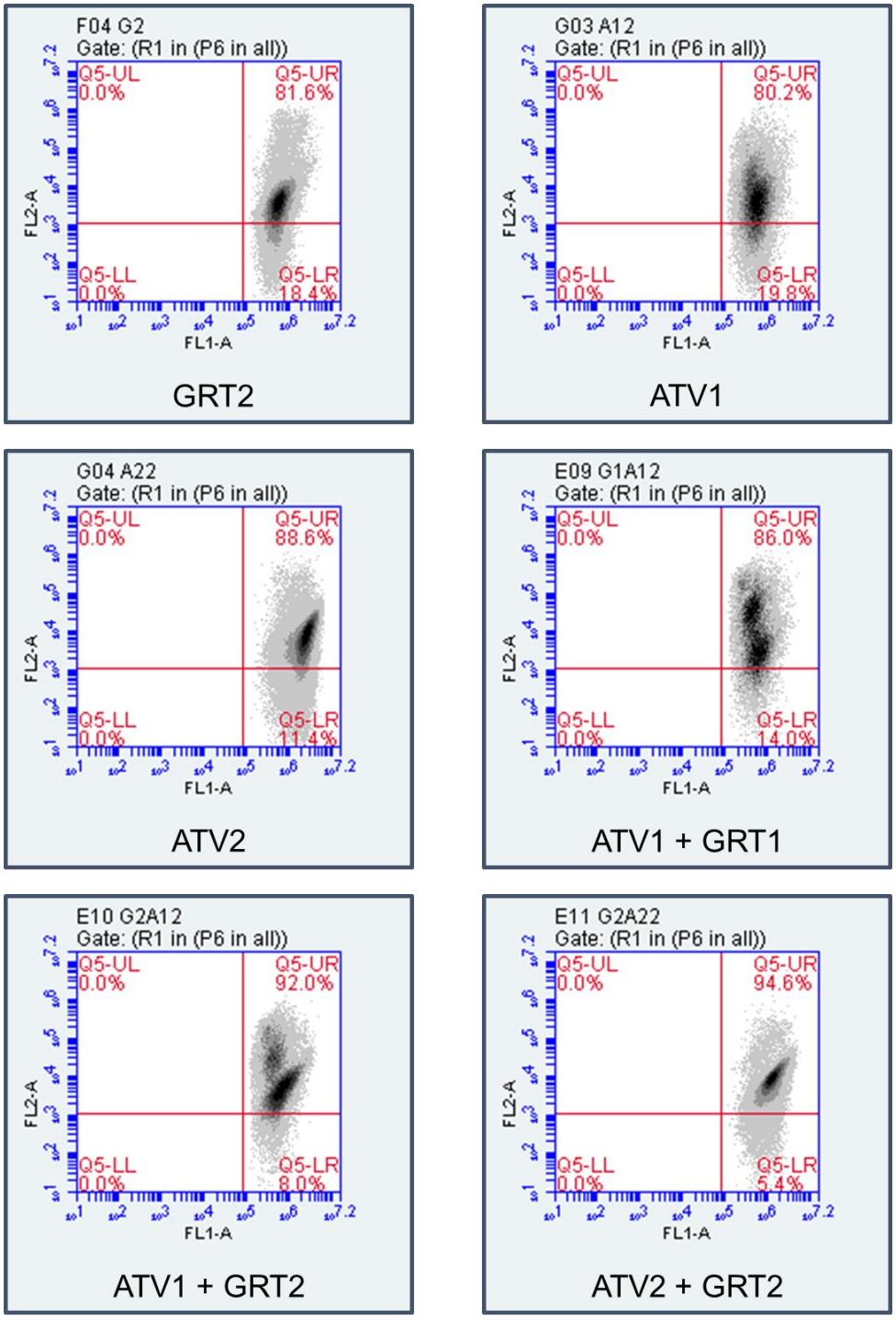

Figure 5.5.1: JC-1 flow cytometric assessment of mitochondrial polarisation (activity) in C3A cells not exposed to palmitate (normal condition) treated with GRT, atorvastatin and combinations thereof. *Representative flow cytometry dot plots of JC-1 J-aggregates (FL2-A; red fluorescence) versus JC-1 monomers (FL1-A; green fluorescence). C3A cells were treated with GRT, atorvastatin and combinations (24 hours). Vehicle control = media with 0.25% DMSO; ATV1 = 10 µM; ATV2 = 25 µM; GRT1 = 0.01 mg/mL; GRT2 = and 0.1 mg/mL; ATV1 + GRT1 = 10 µM ATV + 0.01 mg/mL GRT; ATV1 + GRT2 = 10 µM ATV + 0.1 mg/mL GRT; ATV2 + GRT2 = 25 µM ATV + 0.1 mg/mL GRT.*

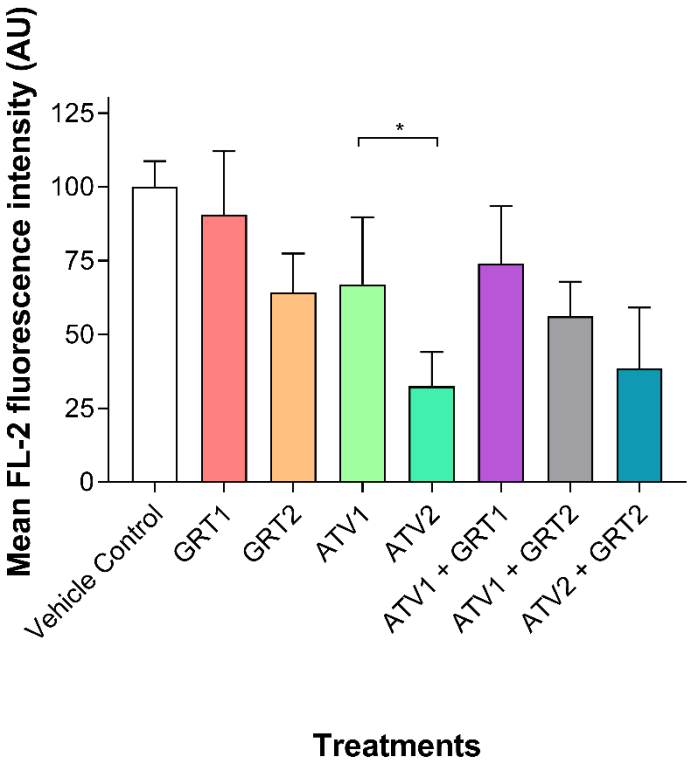

Figure 5.5.2: Mean FL-2 (red) fluorescence intensity in C3A cells not exposed to palmitate (normal condition) as an indication of mitochondrial membrane potential. *C3A cells were treated with GRT, atorvastatin and combinations (24 hours). Vehicle control = media with 0.25% DMSO; ATV1 = 10 µM; ATV2 = 25 µM; GRT1 = 0.01 mg/mL; GRT2 = and 0.1 mg/mL; ATV1 + GRT1 = 10 µM ATV + 0.01 mg/mL GRT; ATV1 + GRT2 = 10 µM ATV + 0.1 mg/mL GRT; ATV2 + GRT2 = 25 µM ATV + 0.1 mg/mL GRT. Data are mean ± SD derived from three independent experiments each with three technical repeats (n = 3). A one-way Analysis of Variance was used with a Tukey post hoc test. All results were expressed as a percentage relative fluorescence intensity normalised to the vehicle control at 100%. * = p<0.05.*

In terms of mitochondrial function in the normal condition, *Figure 5.5.2* shows the effect of 24 hours' treatment on mitochondrial membrane potential (Δψm). There was a difference in the mean fluorescence intensity measured between GRT1 (90.62% ± 21.45) and GRT2 (64.28% ± 13.16), however this was not significant. The ATV1 group (66.99% ± 22.73) showed a significantly greater (*p<0.05*) mean fluorescence intensity compared to the ATV2 group (32.48% ± 11.55).

5.5.2 JC-1 fluorescence in the hyperlipidaemic condition

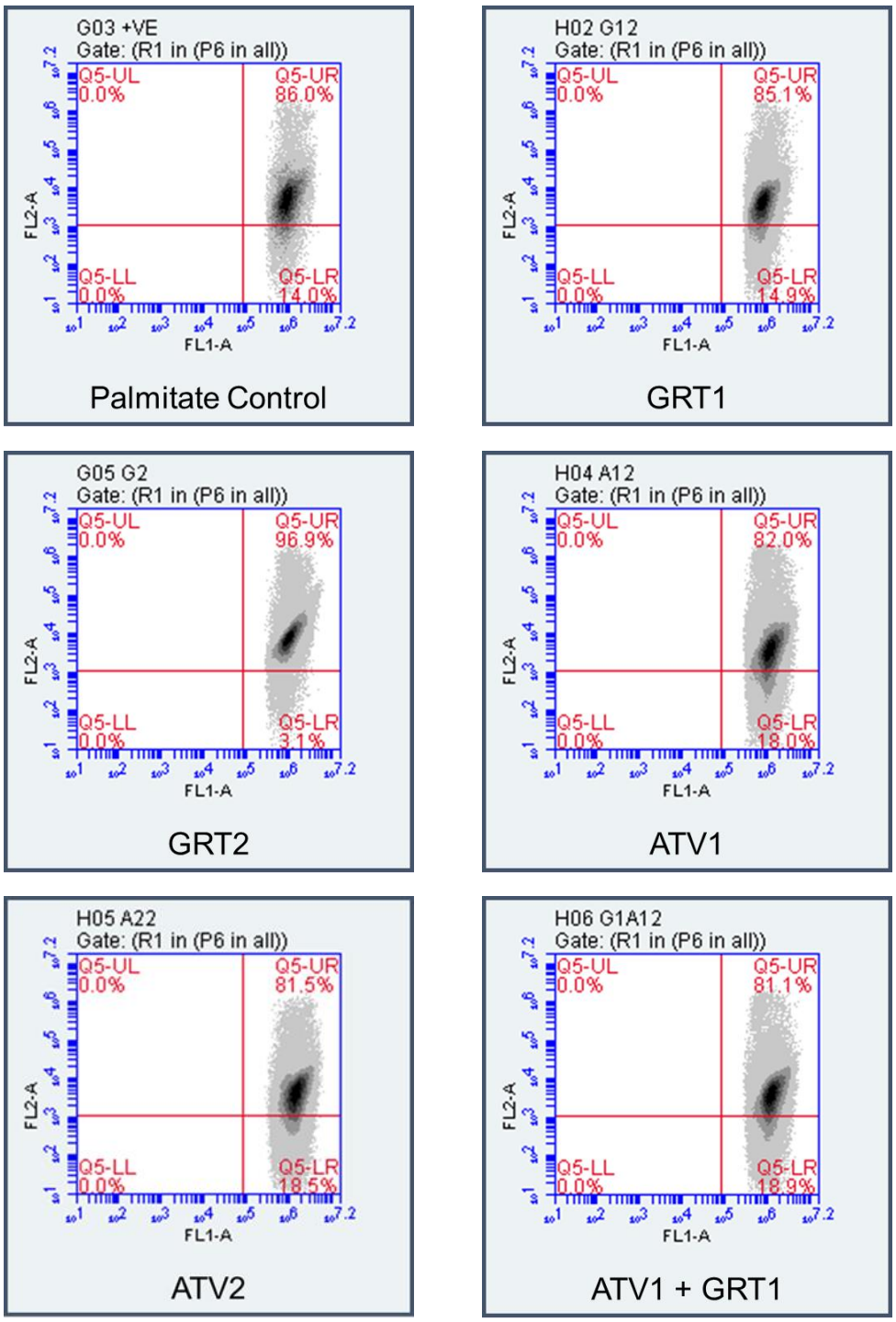

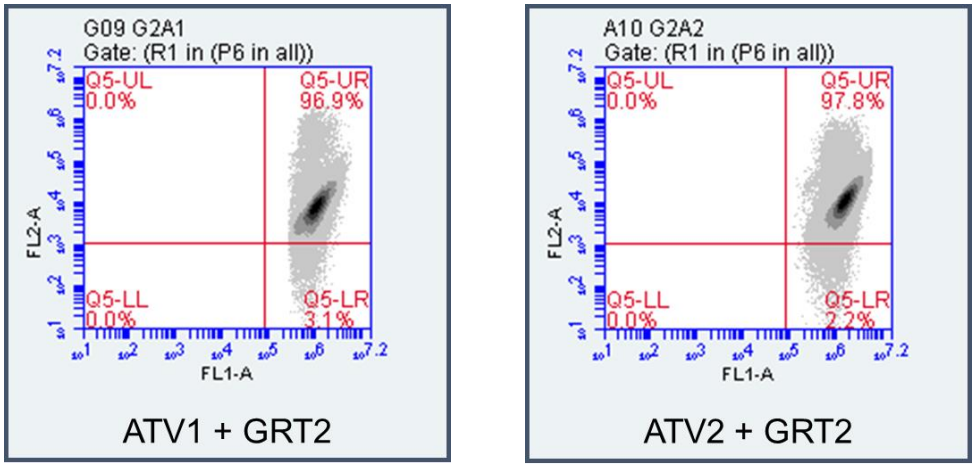

Figure 5.5.3: Percentage of JC-1 J-aggregate formation in the hyperlipidaemic condition as an indication of mitochondrial membrane potential. *Representative flow cytometry dot plots of JC-1 J-aggregates (FL2-A; red fluorescence) versus JC-1 monomers (FL1-A; green fluorescence). C3A cells were treated with GRT, ATV and combinations (24 hours) after a 500 µM palmitate pre-treatment for 24 hours. Palmitate control = palmitate pre-treated cells with media with 0.25% DMSO; ATV1 = 10 µM; ATV2 = 25 µM; GRT1 = 0.01 mg/mL; GRT2 = 0.1 mg/mL; ATV1 + GRT1 = 10 µM ATV + 0.01 mg/mL GRT; ATV1 + GRT2 = 10 µM ATV + 0.1 mg/mL GRT; ATV2 + GRT2 = 25 µM ATV + 0.1 mg/mL GRT.*

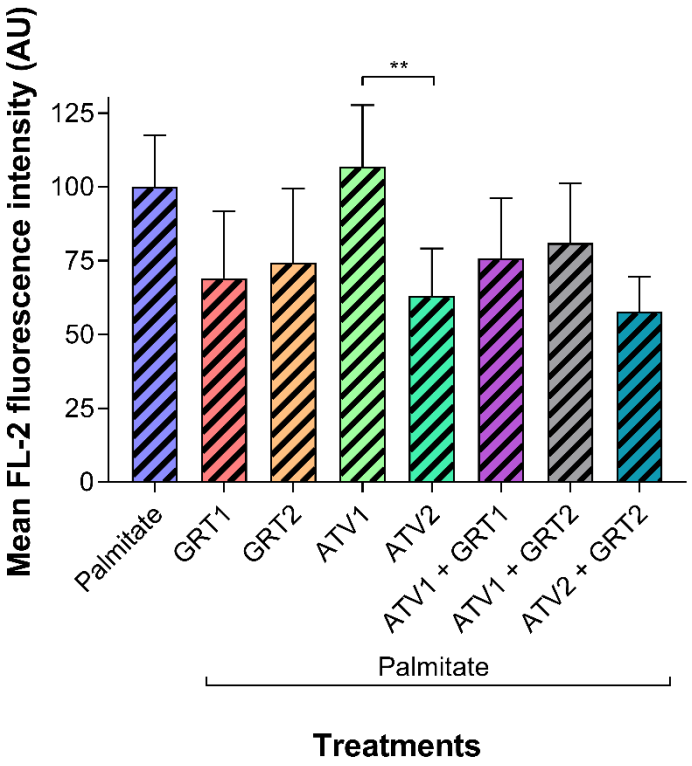

Figure 5.5.4: Mean FL-2 (red) fluorescence intensity in the hyperlipidaemic condition as an indication of mitochondrial membrane potential. *C3A cells were treated with GRT, ATV and combinations (24 hours) after a 24 hour 500 µM palmitate pre-treatment. Palmitate control = palmitate pre-treated cells with media with 0.25% DMSO; ATV1 = 10 µM; ATV2 = 25 µM; GRT1 = 0.01 mg/mL; GRT2 = 0.1 mg/mL; ATV1 + GRT1 = 10 µM ATV + 0.01 mg/mL GRT; ATV1 + GRT2 = 10 µM ATV + 0.1 mg/mL GRT; ATV2 + GRT2 = 25 µM ATV + 0.1 mg/mL GRT. Data are mean ± SD derived from three independent experiments each with three technical repeats (n = 3). A one-way Analysis of Variance was used with a Tukey post hoc test. All results were expressed as a percentage relative fluorescence intensity normalised to the palmitate control at 100%. ** = p<0.01.*

Figure 5.5.4 shows that, in the hyperlipidaemic condition, ATV1 (106.90% ± 20.81) showed a significantly greater (*p<0.01*) mean fluorescence intensity ATV2 (63.02% ± 16.17). No other significant differences were noted between any other groups.

5.6 Apoptosis assessment

The extent of apoptosis related hepatotoxic damage was measured using an annexin V and a propidium iodide stain. Annexin V is a protein, conjugated to fluorochromes, that has a high affinity for phosphatidylserine (PS). Phosphatidylserine is translocated outside the membrane due to the loss of plasma membrane asymmetry. This translocation precedes the loss of plasma membrane integrity which is a crucial part of apoptotic and necrotic cell death. The loss of plasma membrane integrity causes the membrane to be permeable, allowing for vital dyes, such as propidium iodide, to enter the cell. Therefore, annexin V positive, PI negative cells indicate cells in early apoptosis, whereas annexin V positive, PI positive cells have undergone cell death (late apoptotic/necrotic).

5.6.1 Annexin V/PI apoptosis assessment in the normal condition

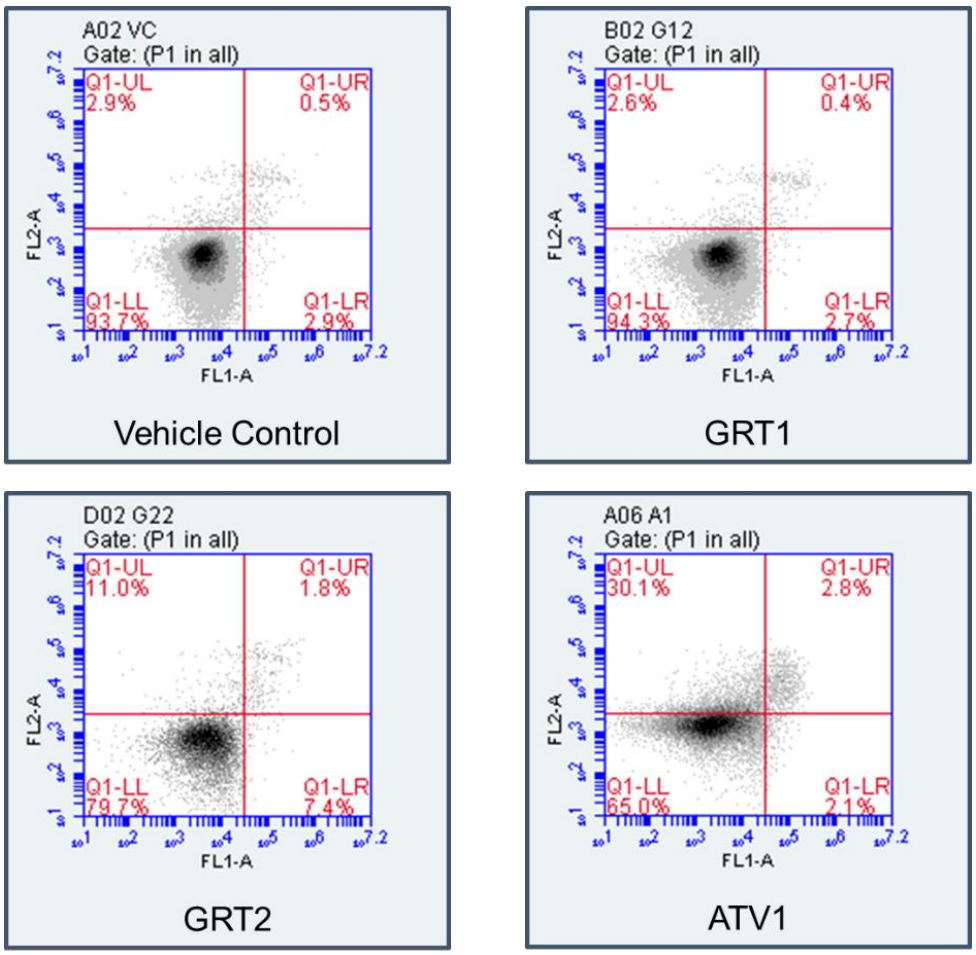

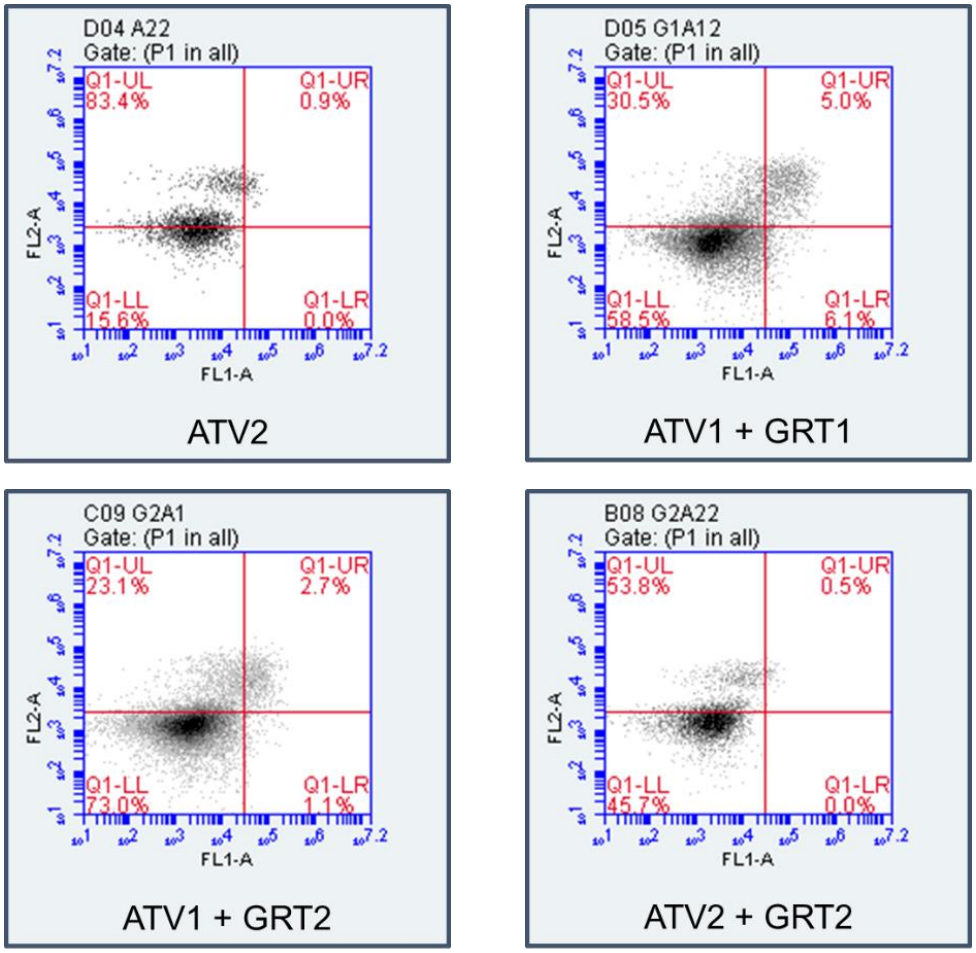

Figure 5.6.1: Representative scatter plots of annexin V/PI flow cytometry assessment in the normal condition. *Representative flow cytometry scatter plots of C3A cells were treated with GRT, atorvastatin and combinations (24 hours). Vehicle control = media with 0.25% DMSO; ATV1 = 10 µM; ATV2 = 25 µM; GRT1 = 0.01 mg/mL; GRT2 = and 0.1 mg/mL; ATV1 + GRT1 = 10 µM ATV + 0.01 mg/mL GRT; ATV1 + GRT2 = 10 µM ATV + 0.1 mg/mL GRT; ATV2 + GRT2 = 25 µM ATV + 0.1 mg/mL GRT.*

5.6.2 Viable

Annexin V negative, propidium iodide negative cells were considered viable cells. All results were calculated as a percentage of the cell population in the lower left quadrant, averaged over three experiments.

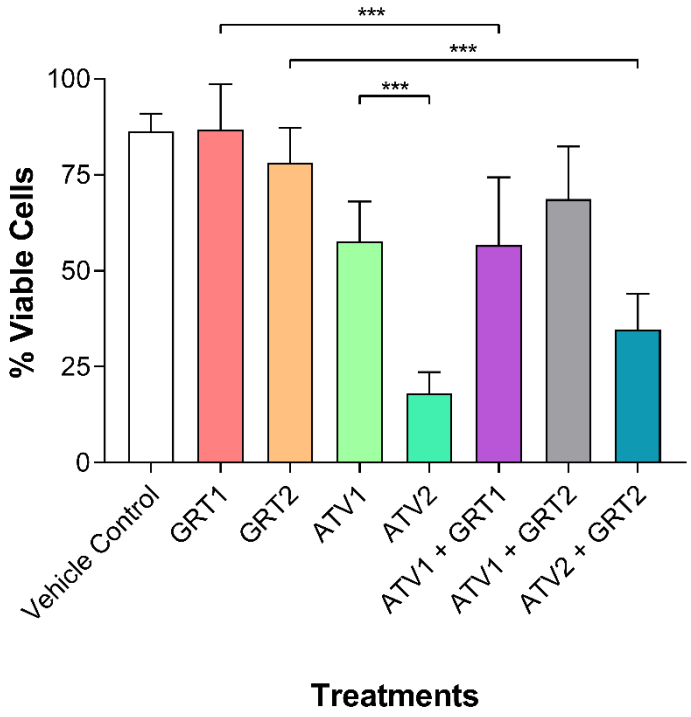

Figure 5.6.2: Quantification of the percentage of viable cells in the normal condition. *C3A cells were treated with GRT, atorvastatin and combinations (24 hours). Vehicle control = media with 0.25% DMSO; ATV1 = 10 µM; ATV2 = 25 µM; GRT1 = 0.01 mg/mL; GRT2 = and 0.1 mg/mL; ATV1 + GRT1 = 10 µM ATV + 0.01 mg/mL GRT; ATV1 + GRT2 = 10 µM ATV + 0.1 mg/mL GRT; ATV2 + GRT2 = 25 µM ATV + 0.1 mg/mL GRT. Data are mean ± SD derived from three independent experiments each with two technical repeats (n = 3). A one-way Analysis of Variance was used with a Tukey post hoc test. All results were expressed as a percentage of the cell population falling in the lower left quadrant. *** = p<0.001.*

Figure 5.6.2 shows that, in the normal condition, there was a significant difference (*p<0.001*) in viable cells between GRT1 (86.83% ± 11.81) and ATV1 + GRT1 (56.67% ± 17.68). The combination of ATV2 + GRT2 (34.67% ± 9.4) compared to GRT2 (78.17% ± 9.09) showed a significant (*p<0.001*) decrease in the percentage of viable cells. There was a significant (*p<0.001*) decrease in the percentage of viable cells when ATV1 and ATV2 were compared (57.67% ± 10.41 and 18.00% ± 5.62 respectively). The combination ATV2 + GRT2 showed almost twice the percentage of viable cells compared to ATV2 alone (34.67% ± 9.4 vs 18.00% ± 5.62) although this was not significant.

5.6.3 Early apoptosis

Apoptotic cells were annexin V positive, PI negative cells. All results were calculated as a percentage of the cell population in the upper and lower right quadrants, averaged over three experiments.

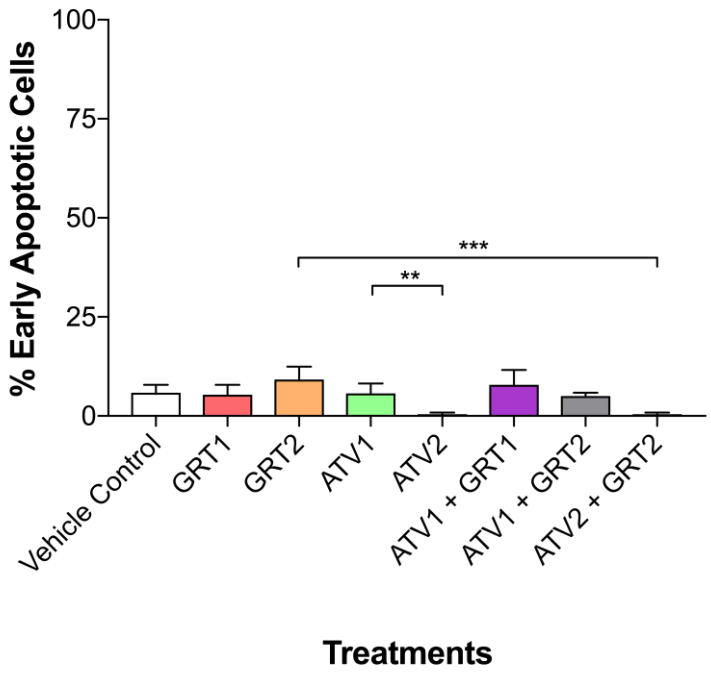

Figure 5.6.3: Quantification of the percentage of early apoptotic cells in the normal condition. *C3A cells were treated with GRT, atorvastatin and combinations (24 hours). Vehicle control = media with 0.25% DMSO; ATV1 = 10 µM; ATV2 = 25 µM; GRT1 = 0.01 mg/mL; GRT2 = and 0.1 mg/mL; ATV1 + GRT1 = 10 µM ATV + 0.01 mg/mL GRT; ATV1 + GRT2 = 10 µM ATV + 0.1 mg/mL GRT; ATV2 + GRT2 = 25 µM ATV + 0.1 mg/mL GRT. Data are mean ± SD derived from three independent experiments each with two technical repeats (n = 3). A one-way Analysis of Variance was used with a Tukey post hoc test All results were expressed as a percentage of the cell population falling in the upper and lower right quadrants. ** = p<0.01; *** = p<0.001.*

There was a significant difference (*p<0.001*) in the percentage of early apoptotic cells when GRT2 (9.17% ± 3.25) and ATV2 + GRT2 (0.33% ± 0.52) were compared. The ATV1 group (5.67% ± 2.50) showed significantly greater (*p<0.01*) prevalence of early apoptosis as compared to ATV2 (0.33% ± 0.52). The ATV1 + GRT1 combination group (4.17% ± 0.41) showed a slightly decreased percentage of early apoptotic cells compared to ATV1 alone, while ATV1 + GRT2 (3.67% ± 0.52) showed a more than 1-fold decrease compared to ATV1. The ATV2 group showed only a marginally greater prevalence of early apoptotic cells as compared to ATV2 + GRT2 (0.33% ± 0.52). The combination of GRT1 and GRT2 did not significantly improve ATV1 or ATV2-induced apoptosis.

5.6.4 Late apoptosis

Late apoptotic cells were defined as annexin V dim, PI positive cells, where the proportion of PI positive fluorescence greatly overshadowed the annexin V fluorescence. All results were calculated as a percentage of the cell population in the upper left quadrant, averaged over three experiments.

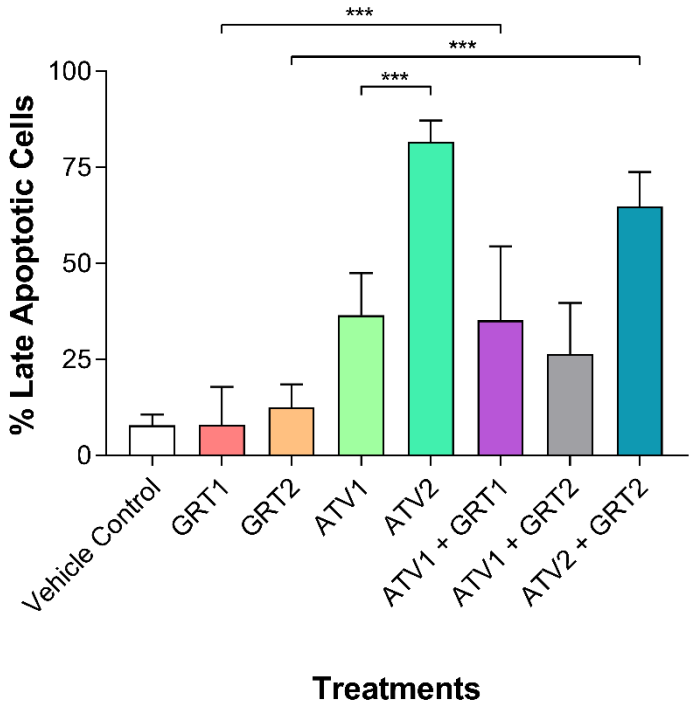

Figure 5.6.4: Quantification of the percentage of late apoptotic cells in the normal condition. *C3A cells were treated with GRT, atorvastatin and combinations (24 hours). Vehicle control = media with 0.25% DMSO; ATV1 = 10 µM; ATV2 = 25 µM; GRT1 = 0.01 mg/mL; GRT2 = and 0.1 mg/mL; ATV1 + GRT1 = 10 µM ATV + 0.01 mg/mL GRT; ATV1 + GRT2 = 10 µM ATV + 0.1 mg/mL GRT; ATV2 + GRT2 = 25 µM ATV + 0.1 mg/mL GRT. Data are mean ± SD derived from three independent experiments each with two technical repeats (n = 3). A one-way Analysis of Variance was used with a Tukey post hoc test. All results were expressed as a percentage of the cell population falling in the upper left quadrant. *** = p<0.001.*

Compared to ATV1 + GRT1 (35.17% ± 19.28), GRT1 (8.00% ± 9.90) showed a significant (*p<0.01*) decrease in the prevalence of late apoptotic cells. The GRT2 group (12.50% ± 6.06) showed an insignificant decrease in the percentage of late apoptotic cells compared to ATV1 + GRT2 (26.33% ± 13.40), and a significant (*p<0.001*) decrease compared to ATV2 + GRT2 (64.83% ± 8.98). The ATV1 group (36.50% ± 10.93) showed significantly (*p<0.001*) less late apoptotic cells compared to ATV2 (81.67% ± 5.57), which showed the greatest percentage of late apoptotic of all the treatment groups in the normal condition.

5.6.5 Annexin V/PI apoptosis assessment in the hyperlipidaemic condition

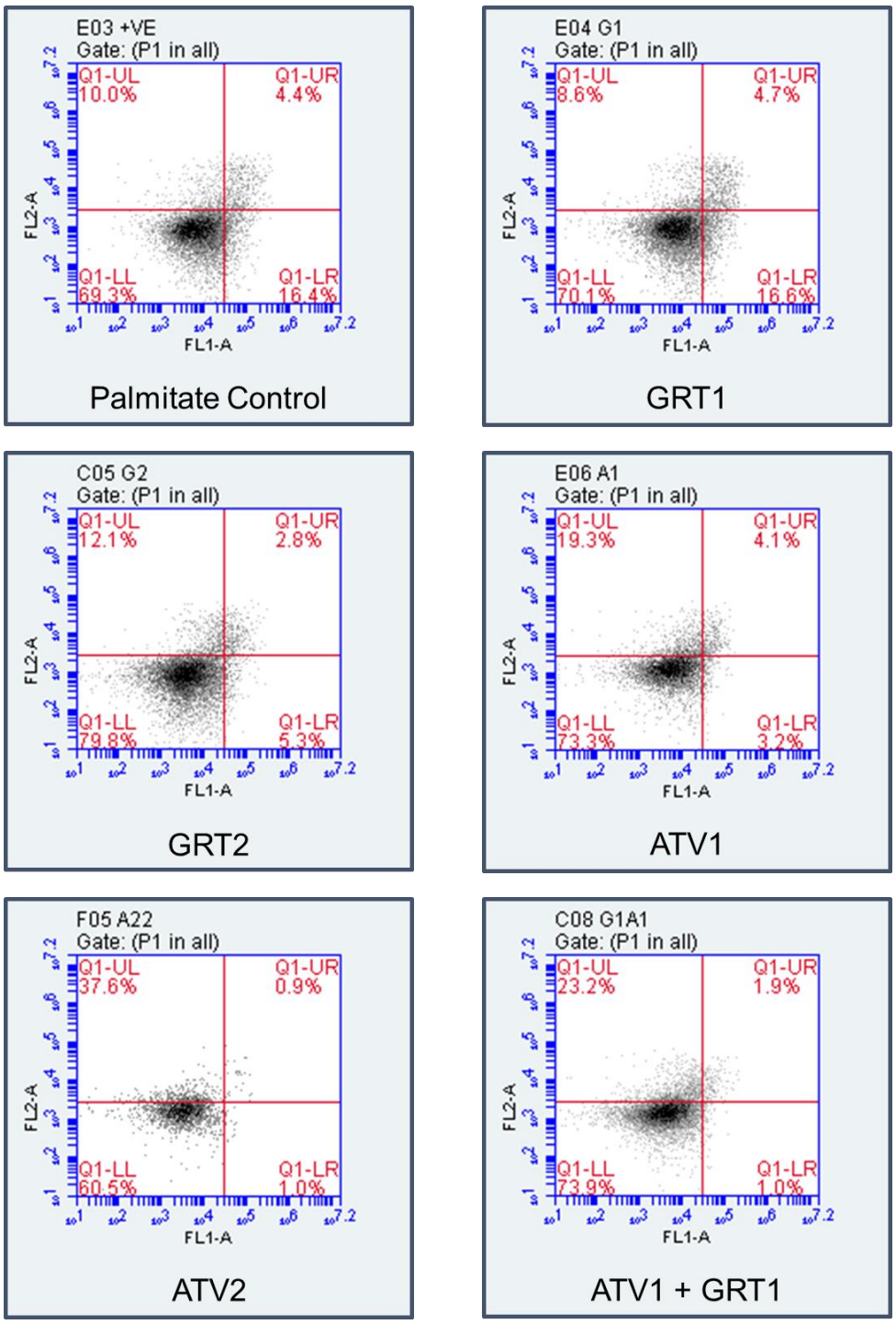

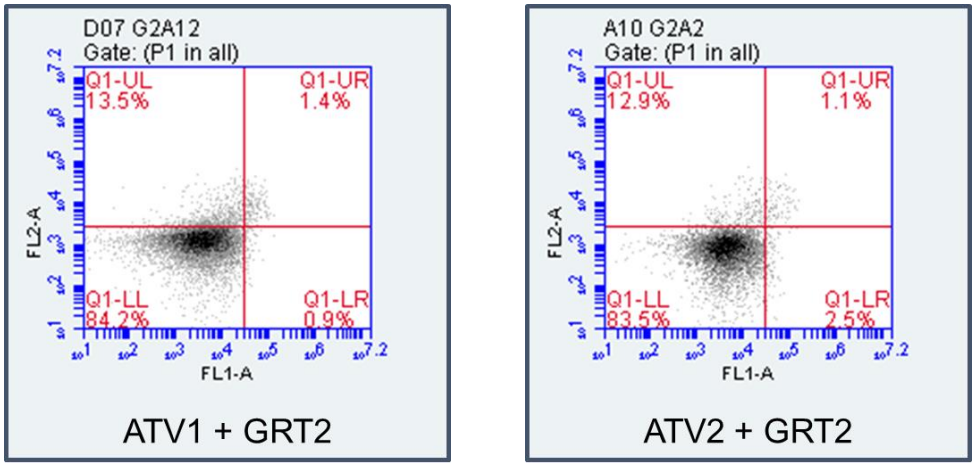

Figure 5.6.5: Representative scatter plots of annexin V/PI flow cytometry assessment in the hyperlipidaemic condition. *Scatter plots subjected to the appropriate gating and colour compensation were used for analysis and comparison.*

5.6.6 Viable

Annexin V negative, propidium iodide negative cells were considered viable cells. All results were calculated as a percentage of the cell population in the lower left quadrant, averaged over three experiments.

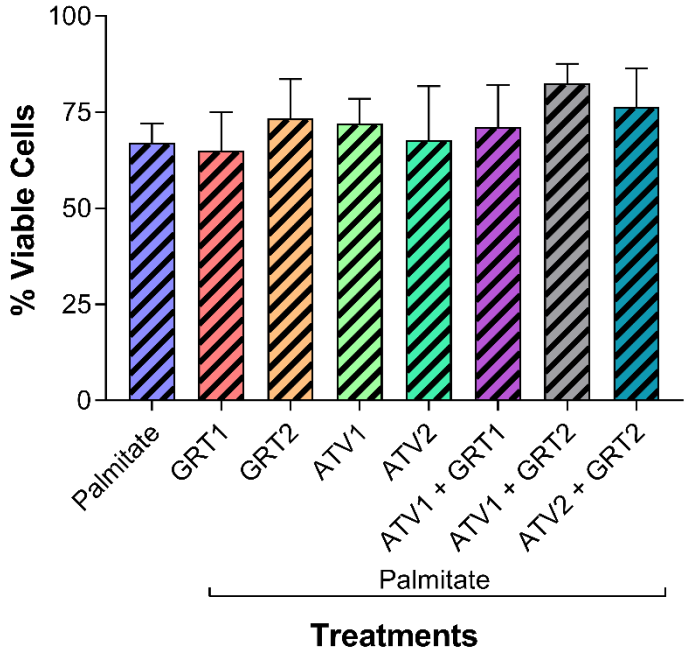

Figure 5.6.6: Quantification of the percentage of viable cells in the hyperlipidaemic condition. *C3A cells were treated with GRT, ATV and combinations (24 hours) after a 24 hour 500 µM palmitate pre-treatment. Palmitate control = palmitate pre-treated cells with media with 0.25% DMSO; ATV1 = 10 µM; ATV2 = 25 µM; GRT1 = 0.01 mg/mL; GRT2 = 0.1 mg/mL; ATV1 + GRT1 = 10 µM ATV + 0.01 mg/mL GRT; ATV1 + GRT2 = 10 µM ATV + 0.1 mg/mL GRT; ATV2 + GRT2 = 25 µM ATV + 0.1 mg/mL GRT. Data are mean ± SD derived from three independent experiments each with two technical repeats (n = 3). A one-way Analysis of Variance was used with a Tukey post hoc test. All results were expressed as a percentage of the cell population falling in the upper left quadrant.*

In terms of the percentage of viable cells, there was no statistical differences between any of the different treatment groups. Although insignificant, GRT1 showed the lowest percentage of viable cells (65.00% ± 10.04) while ATV1 + GRT2 showed the greatest percentage of viable cells (82.50% ± 5.09).

5.6.7 Early apoptosis

Early apoptotic cells were annexin V positive, PI negative cells. All results were calculated as a percentage of the cell population in the upper and lower right quadrants, averaged over three experiments.

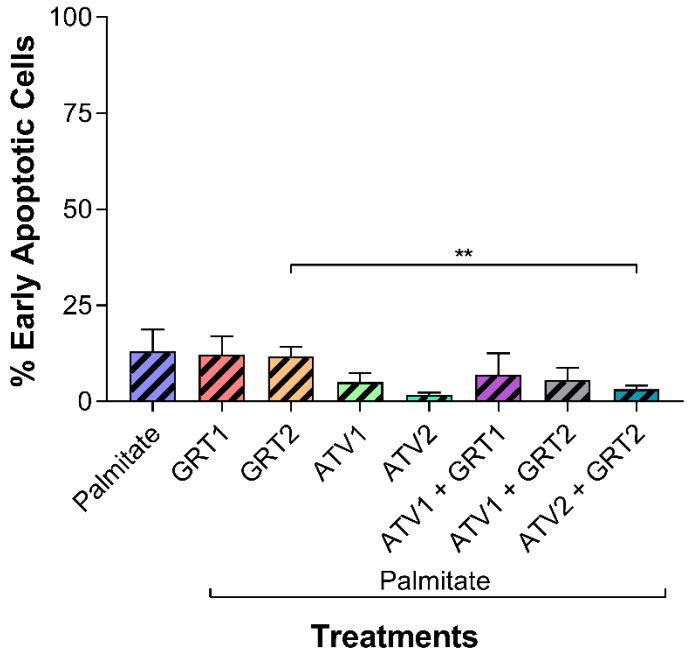

Figure 5.6.7: Quantification of the percentage of early apoptotic cells in the hyperlipidaemic condition. *C3A cells were treated with GRT, ATV and combinations (24 hours) after a 24 hour 500 µM palmitate pre-treatment. Palmitate control = palmitate pre-treated cells with media with 0.25% DMSO; ATV1 = 10 µM; ATV2 = 25 µM; GRT1 = 0.01 mg/mL; GRT2 = 0.1 mg/mL; ATV1 + GRT1 = 10 µM ATV + 0.01 mg/mL GRT; ATV1 + GRT2 = 10 µM ATV + 0.1 mg/mL GRT; ATV2 + GRT2 = 25 µM ATV + 0.1 mg/mL GRT. Data are mean ± SD derived from three independent experiments each with two technical repeats (n = 3). A one-way Analysis of Variance was used with a Tukey post hoc test. All results were expressed as a percentage of the cell population falling in the upper and lower right quadrants. ** = p<0.01.*

In terms of early apoptosis in the hyperlipidaemic condition, only GRT2 (11.67% ± 2.58) and ATV2 + GRT2 (3.17% ±0.98) showed significantly different results (*p<0.01*). The Palmitate Control treatment group showed the greatest percentage of early apoptotic cells (13.00% ± 5.73) while ATV2 showed the least early apoptotic cells (1.75% ± 0.50), although this was insignificant.

5.6.8 Late apoptosis

Late apoptotic cells were annexin V positive, PI positive cells, where the proportion of PI positive fluorescence greatly overshadowed the annexin V fluorescence.

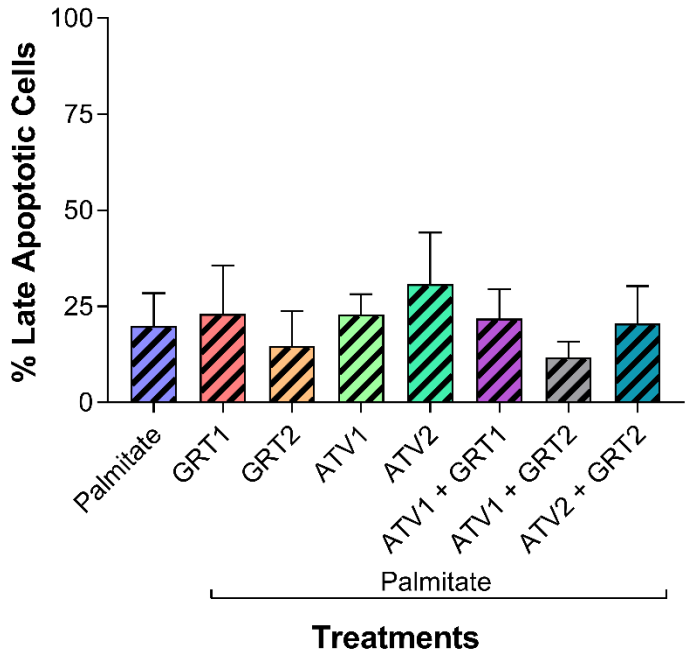

Figure 5.6.8: Quantification of the percentage of late apoptotic cells in the hyperlipidaemic condition. *C3A cells were treated with GRT, ATV and combinations (24 hours) after a 24 hour 500 µM palmitate pre-treatment. Palmitate control = palmitate pre-treated cells with media with 0.25% DMSO; ATV1 = 10 µM; ATV2 = 25 µM; GRT1 = 0.01 mg/mL; GRT2 = 0.1 mg/mL; ATV1 + GRT1 = 10 µM ATV + 0.01 mg/mL GRT; ATV1 + GRT2 = 10 µM ATV + 0.1 mg/mL GRT; ATV2 + GRT2 = 25 µM ATV + 0.1 mg/mL GRT. Data are mean ± SD derived from three independent experiments each with two technical repeats (n = 3). A one-way Analysis of Variance was used with a Tukey post hoc test. All results were expressed as a percentage of the cell population falling in the upper left quadrant.*

The ATV1 + GRT2 group showed the least number of late apoptotic cells (11.67% ± 4.13) while the ATV2 group showed the greatest percentage of late apoptotic cells (30.75% ± 13.45). None of the differences between any of the groups was significant.

5.7 Caspase activation assessment

The cleavage of fluorogenic peptides allowed for the fluorescent measurement of the executioner caspases 3 and 7, confirming the extent of apoptosis-induced hepatotoxic damage.

5.7.1 Caspase 3/7 assessment in the normal condition

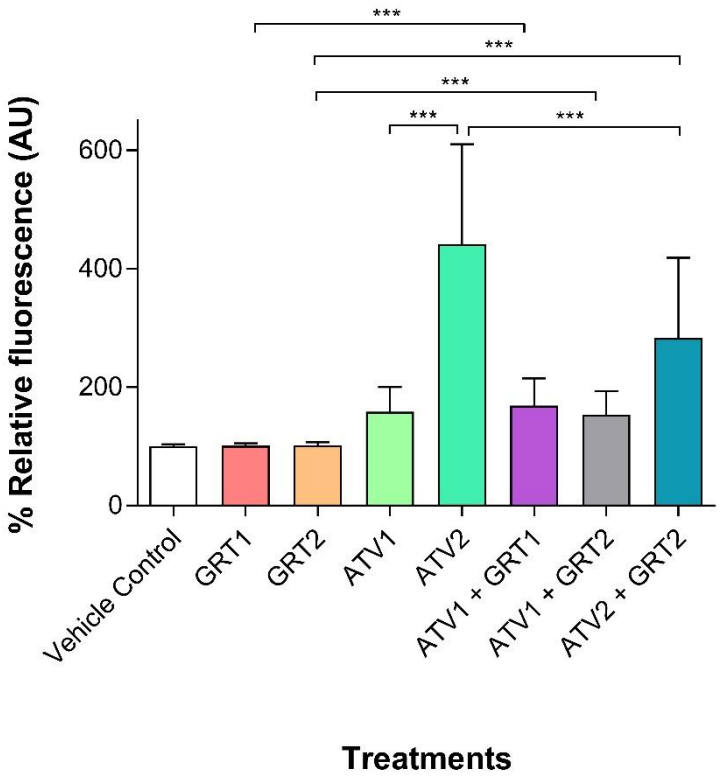

Figure 5.7.1: Caspase 3/7 activity as a marker of apoptosis in the normal condition. *Cells were exposed to various treatments and combinations (24 hours). Vehicle control = media with 0.25% DMSO for 24 hours; GRT1 = 0.01 mg/mL; GRT2 = and 0.1 mg/mL; ATV1 = 10 µM; ATV2 = 25 µM; ATV1 + GRT1 = 10 µM ATV + 0.01 mg/mL GRT; ATV1 + GRT2 = 10 µM ATV + 0.1 mg/mL GRT; ATV2 + GRT2 = 25 µM ATV + 0.1 mg/mL GRT. Data are mean ± SD derived from three independent experiments each with three technical repeats (n = 3). A one-way Analysis of Variance was used with a Tukey post hoc test. All results were expressed as a percentage relative fluorescence normalised to the vehicle control at 100%. *** = p<0.001.*

Figure 5.7.1 shows that, in the normal condition, there was a negligible difference in caspase 3/7 activity of GRT1 (100.90% ± 4.44) and GRT2 (101.80% ±5.32). The ATV1 (158.50% ± 41.78) group alone showed significantly less caspase 3/7 activity compared to ATV2 (441.00% ± 169.20; *p<0.001*). The difference between ATV1 and ATV1 + GRT1 (168.70% ± 45.81) was slight, but insignificant, as was the difference between ATV1 and ATV1 + GRT2 (153.50% ± 39.40). There was a significant (*p<0.001*) difference between ATV2 and ATV2 + GRT2 (283.20% ± 135.00).

5.7.2 Caspase 3/7 assessment in the hyperlipidaemic condition

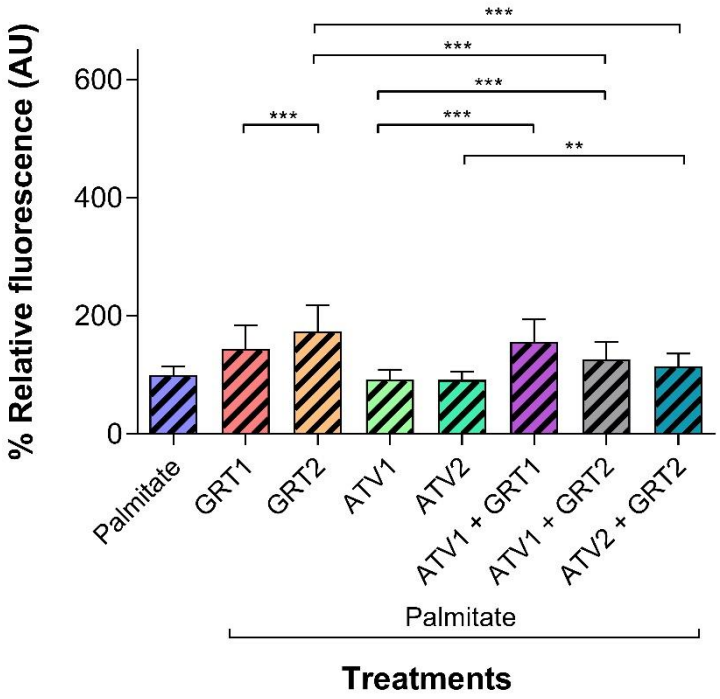

Figure 5.7.2: Caspase 3/7 activity as an indication of late apoptosis in the hyperlipidaemic condition. *Cells were exposed to various treatments and combinations (24 hours) subsequent to a 500µM palmitate pre-treatment for 24 hour. Palmitate control = palmitate pre-treated cells exposed to media with 0.25% DMSO for 24 hours; GRT1 = 0.01 mg/mL; GRT2 = and 0.1 mg/mL; ATV1 = 10 µM; ATV2 = 25 µM; ATV1 + GRT1 = 10 µM ATV + 0.01 mg/mL GRT; ATV1 + GRT2 = 10 µM ATV + 0.1 mg/mL GRT; ATV2 + GRT2 = 25 µM ATV + 0.1 mg/mL GRT. Data are mean ± SD derived from three independent experiments each with three technical repeats (n = 3). A one-way Analysis of Variance was used with a Tukey post hoc test. All results were expressed as a percentage relative fluorescence normalised to the palmitate control at 100%. ** = p<0.01; *** = p<0.001.*

Figure 5.7.2 shows that the GRT1 group showed significantly less caspase 3/7 activity compared to the GRT2 group (144.20% ± 40.45 and 174.20% ± 43.65 respectively; *p<0.001*) in the hyperlipidaemic condition. The ATV1 and ATV2 groups showed similar values (92.24% ± 16.85 and 91.85% ± 13.82 respectively). The ATV1 + GRT2 combination group showed greater activity (126.20% ± 29.90), while the ATV1 + GRT1 combination group showed significantly greater caspase 3/7 activity (*p<0.001*) when compared to ATV1. The ATV2 + GRT2 combination group (114.70% ± 21.82) showed significantly greater activity than the ATV2 group (*p<0.01*).

5.8 *In vitro* culturing of C3A spheroids

Three-dimensional culturing allows for long-term culturing and, as such, the assessment of the implications of exposure to chronic treatment. Further, it has been shown that cultured spheroids regain a degree of hepatic functionality (Wrzesinki *et al*, 2013). This allows for a more in-depth analysis of the effects of chronic treatment in a model that is truer to *in vivo* models than traditional culturing methods.

5.9 Transmission electron micrographs

Transmission electron microscopy is a technique that contributes to the field of molecular microscopy as it allows for the visualisation and identification of cellular components on a subcellular level. Further, this contributes to the understanding of the specialisation of cells and tissue in order to sense the extracellular environment and adjust functionality accordingly (Hayat, 1986). Untreated control spheroids were sampled for transmission electron microscopy in order to assess the cellular changes on a structural and molecular level, demonstrating ultrastructural features of the cells.

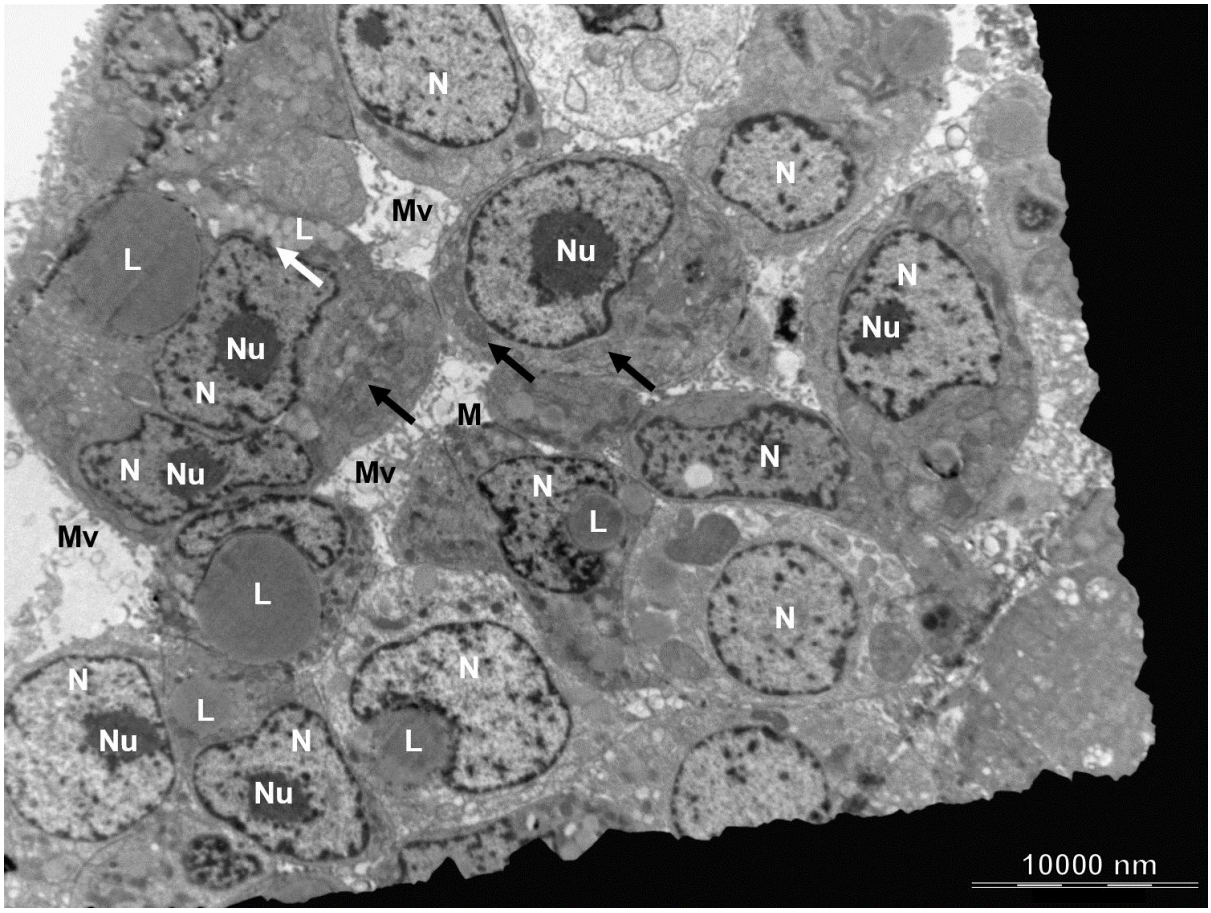

Figure 5.9.1: Transmission electron micrograph of C3A liver spheroids. *N = nucleus; Nu = nucleolus; M = mitochondria (black arrows); Mv = microvilli; L = lipid droplets (white arrow). Scale bar = 10 000 nm.*

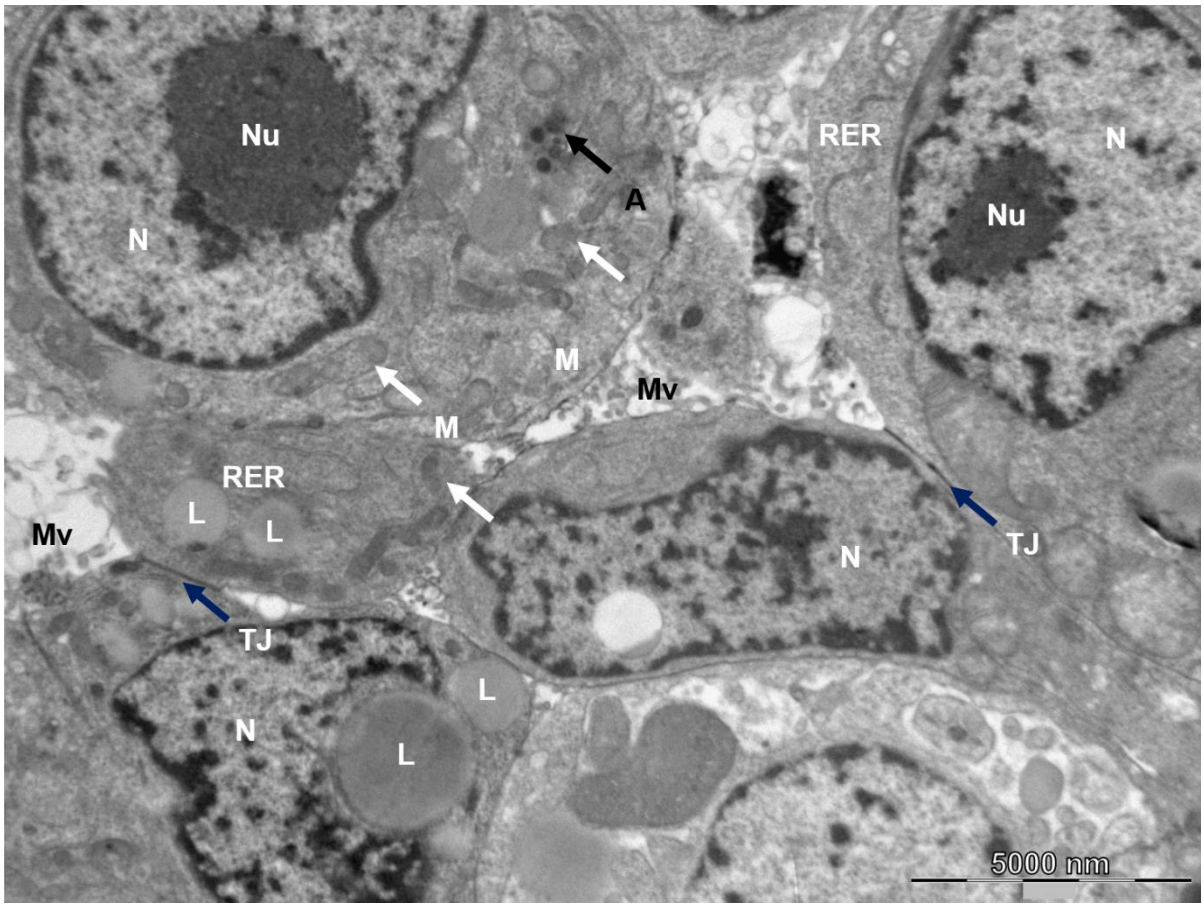

Figure 5.9.2: Transmission electron micrograph of C3A liver spheroids showing the cellular specialisation of the hepatocytes. *N = nucleus; Nu = nucleolus; M = mitochondria (white arrows); Mv = microvilli; L = lipid droplets; RER = rough endoplasmic reticulum; TJ = tight junction (blue arrows); A = autophagosome (black arrow). Scale bar = 5 000 nm.*

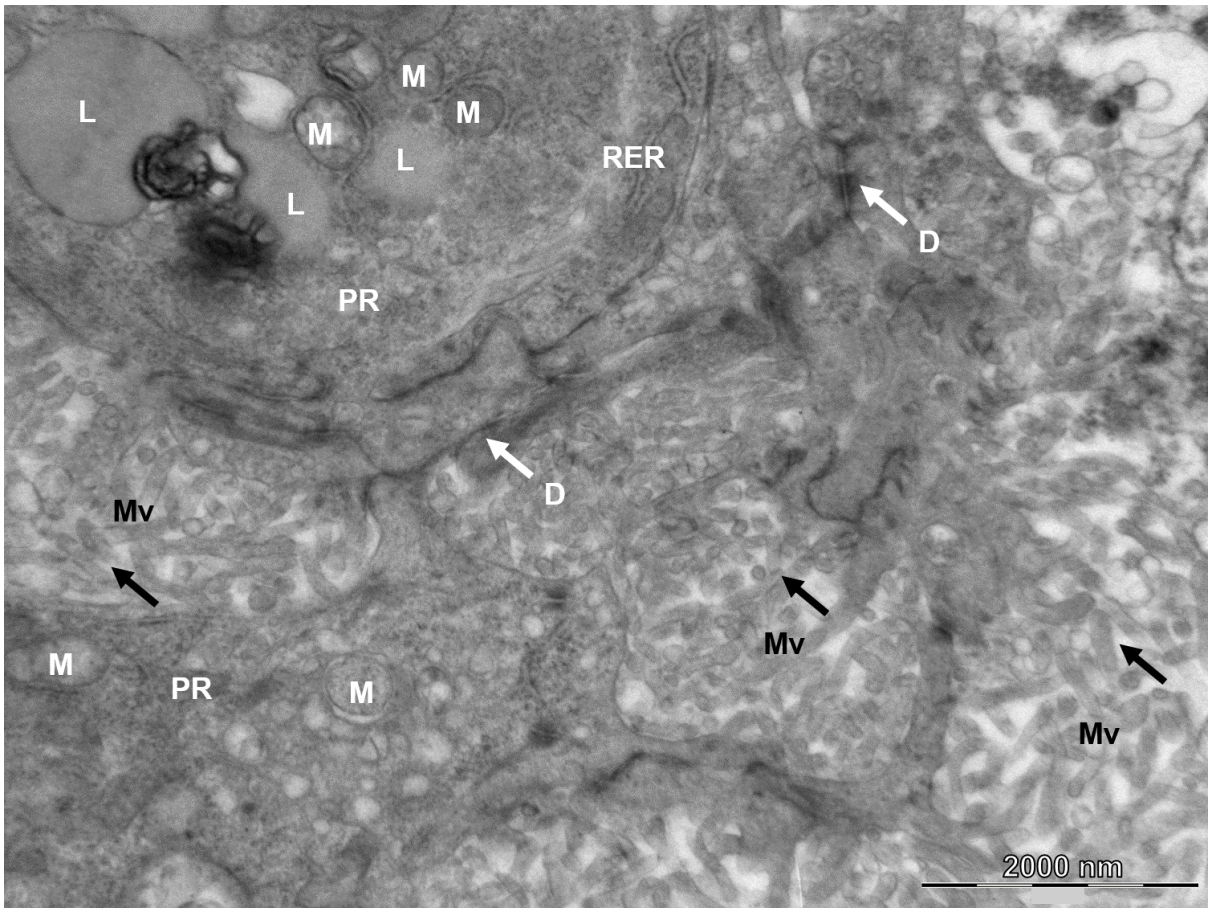

Figure 5.9.3: Transmission electron micrograph of C3A liver spheroids showing the cellular specialisation of the hepatocytes. *N = nucleus; Nu = nucleolus; M = mitochondria; Mv = microvilli (black arrows); L = lipid droplets; RER = rough endoplasmic reticulum; PR = polyribosomes; D = desmosome (white arrows). Scale bar = 2 000 nm.*

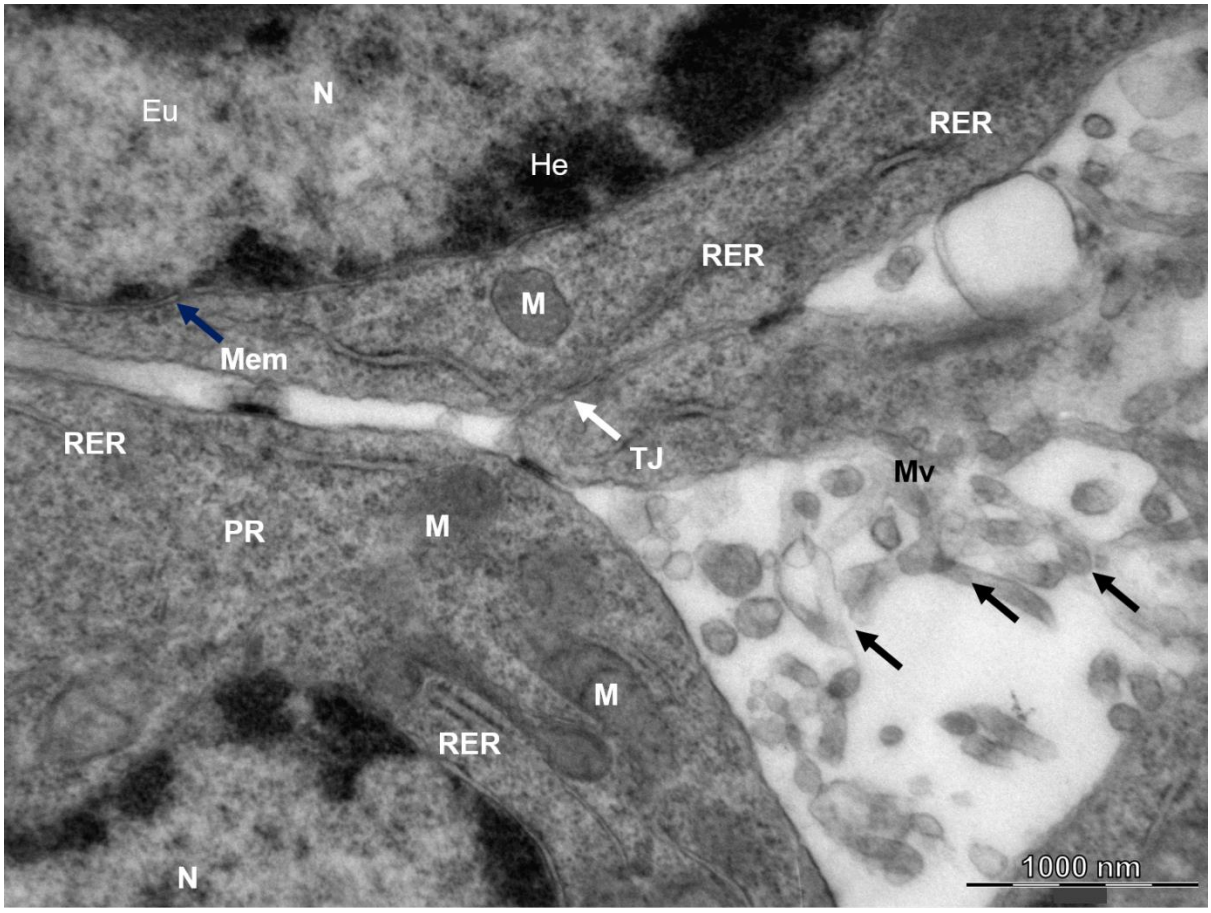

Figure 5.9.4: Transmission electron micrograph of C3A liver spheroids showing the cellular specialisation of the hepatocytes. *N = nucleus; Nu = nucleolus; M = mitochondria; Mv = microvilli (black arrows); RER = rough endoplasmic reticulum; TJ = tight junction (white arrows); PR = polyribosomes; Mem = nuclear membrane (blue arrow); Eu = euchromatic DNA; He = heterochromatic DNA. Scale bar = 1 000 nm.*

Structural hepatic-specific changes were evident in all micrographs. Extracellularly, microvilli were present, increasing the cellular surface area for the transfer of nutrients. Further, tight junctions were present, preventing the intercellular exchange of fluids, as well as the presence of desmosomes, contributing to the cellular strength. Intracellularly, lipid droplets were found in the hepatocytes due to active lipid synthesis. The presence of autophagosomes, polyribosomes, and rough endoplasmic reticulum showed the functionality of normal cell and protein turnover mechanisms. Further evidence of active protein synthesis is shown by the presence of euchromatic nuclei.

An untreated control spheroid was sampled for electron microscopy. As such, the above micrographs serve as representative images of this form of 3D culture, and the structural differences in the cells as a result of the culturing method, as compared to 2D-cultured C3A cells.

5.10 Spheroid size

Sampled spheroid diameter length was measured in micrometres (µm) longitudinally and latitudinally and the values were averaged. The time points selected for measurement were as follows: Day 0, the day the spheroids were dislodged from the AggreWell™ plate and introduced to the bioreactors; Day 7, a week after being introduced to the bioreactors; Day 14, two weeks of culturing in the bioreactors; Day 18, the literature-determined time that spheroids were considered mature enough to survive the introduction of treatment and, as such, became Day 0 of treatment; Day 36, the day of termination of the culturing, post treatment.

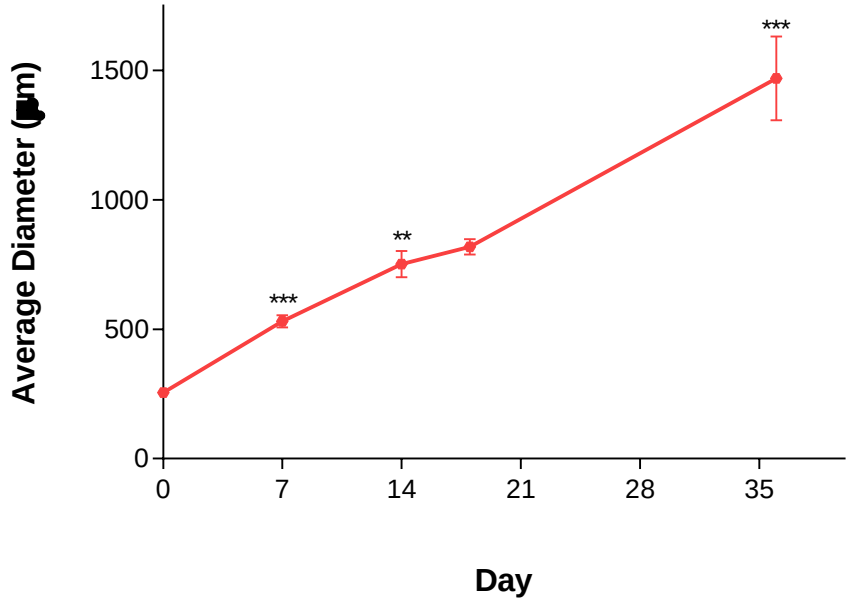

Figure 5.10.1: Average spheroid size. *Sampled spheroid diameters were measured longitudinally and latitudinally in micrometres at Day 0, 7, 14, 18, and 36 and measurements were averaged. Data are mean ± SD derived from five time points each with three sampled spheroids (n = 3). A two-way Analysis of Variance was used with a Tukey post hoc test. ** = p< 0.01; ** = p<0.001 compared to Day 0.*

Figure 5.10.1 shows that the average spheroid size at Day 7 (530.80 µm ± 23.63) was significantly (*p<0.001*) greater than Day 0 (255.30 µm ± 16.69), and Day 14 (751.20 µm ± 50.44) was significantly (*p<0.01*) greater than Day 7. Day 14 and Day 18 (818.80 µm ± 30.69) showed similar results, and Day 36 (1470.00 µm ± 162.40) was signficantly (*p<0.001*) greater than both Day 14 and Day 18.

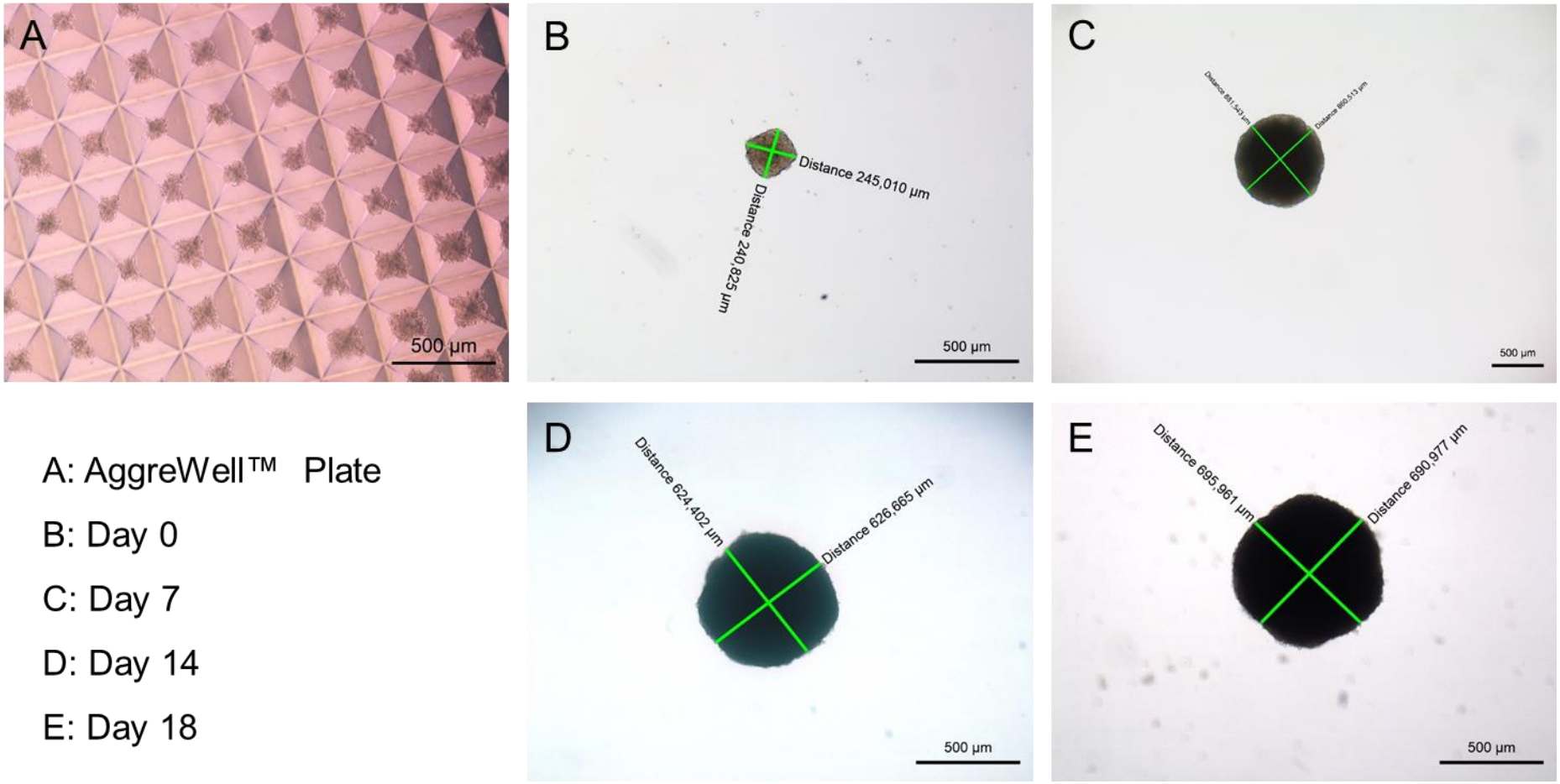

Figure 5.10.2: Representative images of spheroids sampled for measurement. *Spheroids were sampled at Day 0, 7, 14, and 18 of the growth period. Spheroid diameters were measured longitudinally and latitudinally in micrometres at 40X magnification. Scale bar = 500 µm.*

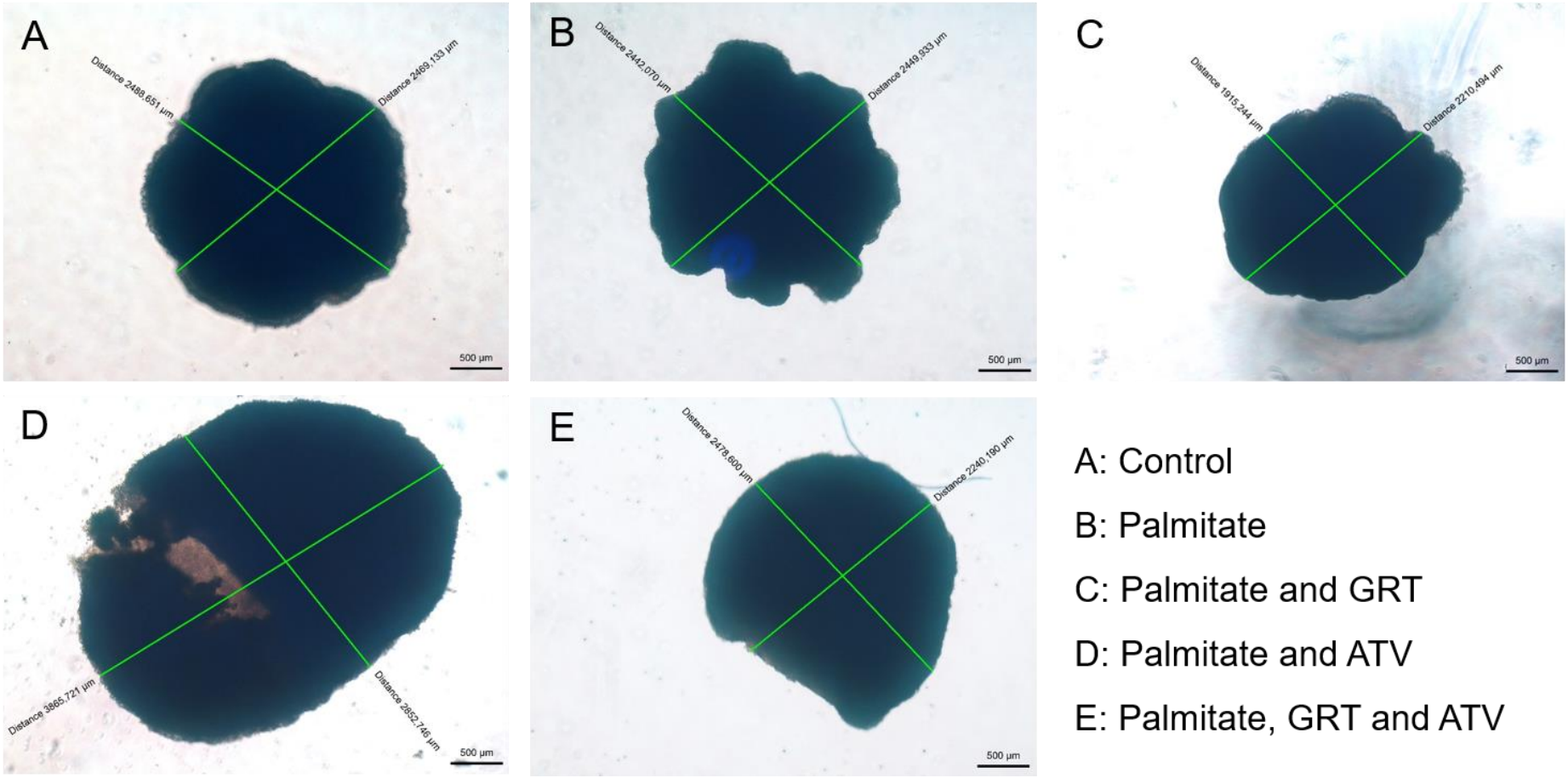

Figure 5.10.3: Representative images of treated spheroids sampled for measurement. *Spheroids were sampled from each treatment group at Day 36. Spheroid diameters were measured longitudinally and latitudinally in micrometres at 40X magnification. Scale bar = 500 µm.*

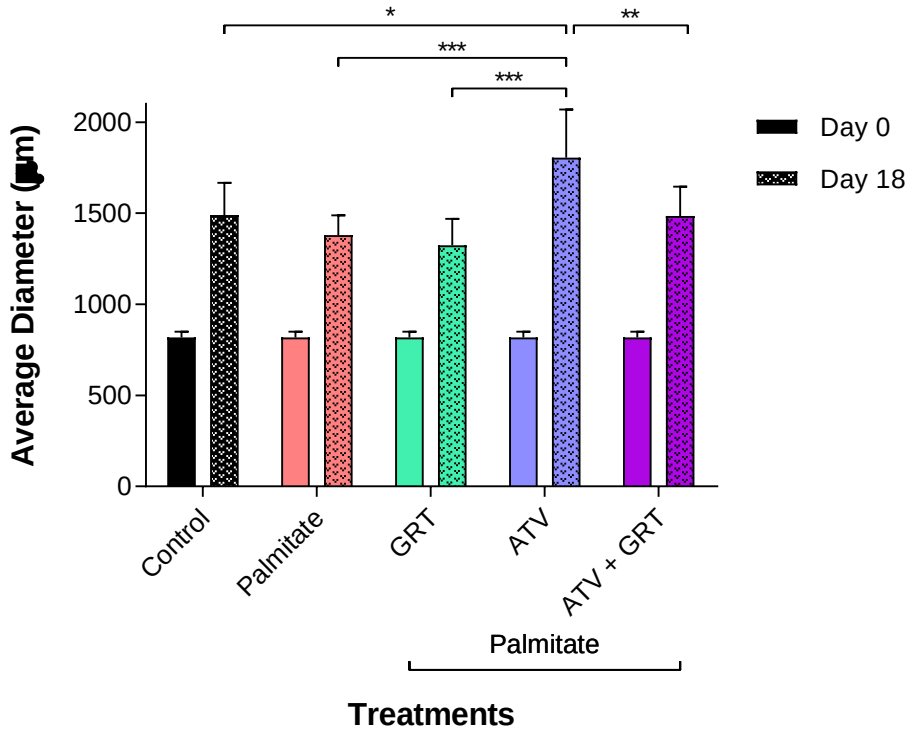

Figure 5.10.4: Comparison of average spheroid size between start and end of treatment. *Sampled spheroid diameters were measured longitudinally and latitudinally in micrometres at Day 0 and Day 18 of treatment and measurements in µm were averaged. GRT = 0.01 mg/mL; ATV = 10 µM; ATV+GRT = 10 µM ATV + 0.01 mg/mL GRT. Data are mean ± SD derived from two time points each with three sampled spheroids (n = 3). A two-way Analysis of Variance was used with a Tukey post hoc test. * = p<0.05; ** = p<0.01; *** = p<0.001 compared to ATV at Day 18.*

Before treatment, varying numbers of spheroids were grown in individual bioreactors. For treatment purposes, all spheroids were removed from all bioreactors and placed in a Petri dish. From there, a calculated number of spheroids were individually counted and re-introduced into a bioreactor. As such, the average size of the spheroids at Day 0 of treatment was the same (818.80 µm ± 30.69), however the average size of the spheroids significantly (*p<0.001*) increased between Day 0 and Day 18 in each treatment group. The average size of the Control and ATV+GRT groups were almost identical (1491 µm ± 175.50 and 1486 µm ± 160.80, respectively), while the palmitate group showed a decrease in average spheroid size (1380 µm ± 108.70), as did the GRT group (1324 µm ± 144.10), although neither of these decreases were significant. The ATV group, however, showed a significant (*p<0.001*) increase in average spheroid size (1805 µm ± 264.40) compared to all the other treatment groups.

5.11 Glucose utilisation

The measurement of glucose concentration in the growth media acts as an indication of cellular respiration of the spheroids. Refreshing of growth and treatment media was performed using a 10 mL syringe, from which 5 µL of the aspirated media was tested using a One Touch® Select® glucometer. The glucose concentration of a sample of the fresh media was also tested. Increased cellular respiration resulted in decreased glucose concentration values. The concentration of the fresh media was taken as 100% and the glucose concentration of the sampled aspirated media was calculated as a percentage relative to the fresh media.

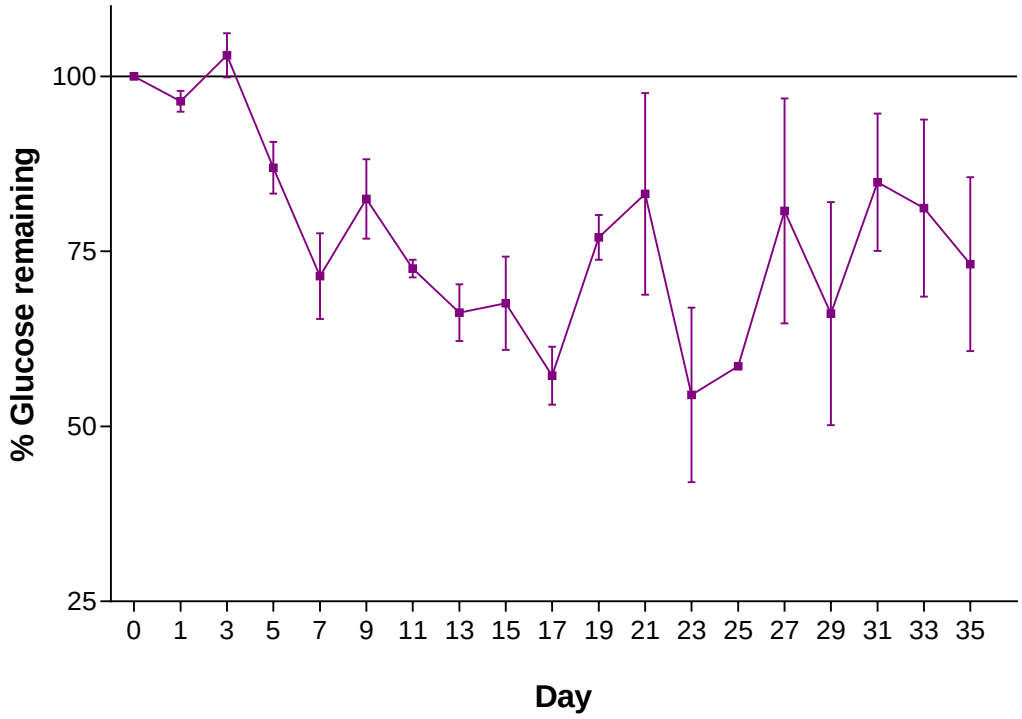

Figure 5.11.1: Average glucose utilisation for all bioreactors monitored for 36 days of culturing. *Glucose concentration was measured in mmol/L when growth media was refreshed and calculated as a percentage relative to the freshly added media at 100%. Data are mean ± SD.*

Initially, growth media was refreshed every two days and the average concentration of glucose in the media was measured concurrently. *Figure 5.11.1* gives an indication in the continuation of cellular respiration of the spheroids over 36 days of culturing. From Day 18, growth or treatment media was refreshed daily and the average glucose concentration was therefore also measured daily.

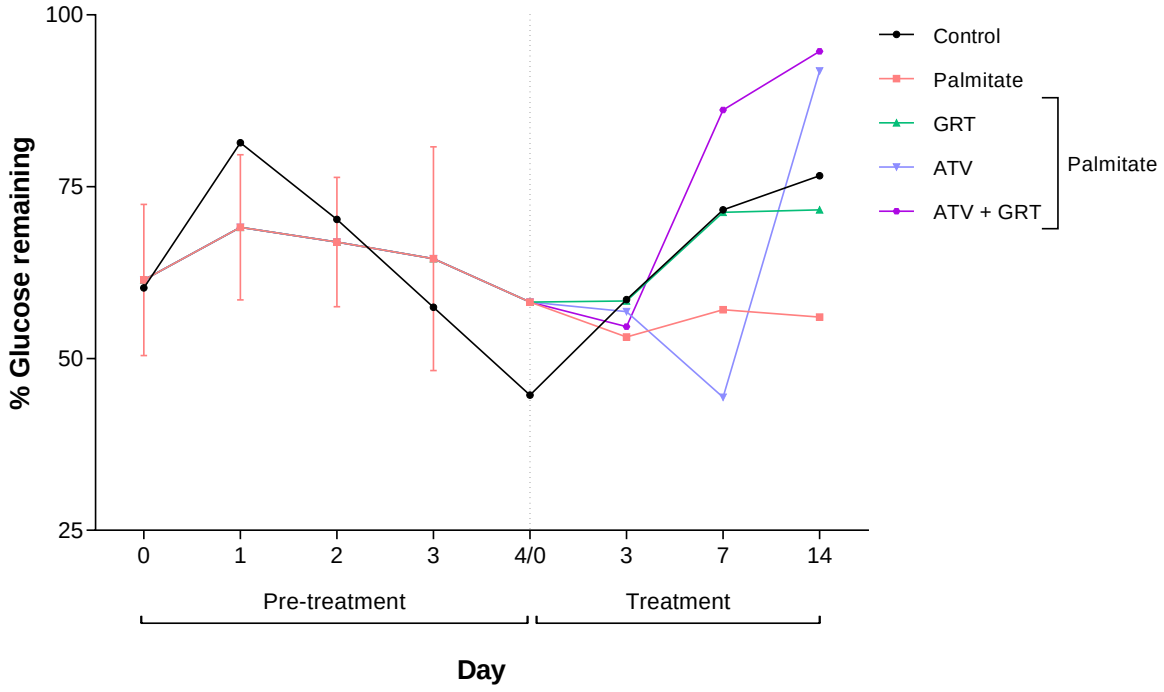

Figure 5.11.2: Average glucose utilisation for all spheroids monitored for 18 days of treatment. *Glucose concentration was measured in mmol/L when growth or treatment media was refreshed and calculated as a percentage relative to the fresh medium, in which the treatments were made up daily, at 100%. Data are mean ± SD. A two-way Analysis of Variance was used with a Tukey post hoc test.*

Day 18 of culturing was Day 0 of treatment. On Day 0, spheroids were exposed to a palmitate pre-treatment which was refreshed with fresh palmitate treatment every day, for four days. As such, glucose utilisation in old media, relative to the fresh media added, was measured daily as treatment medium was replenished. *Figure 5.11.2* shows that spheroids were treated for 4 days with palmitate, and then a further 14 days with various treatments, and shows the glucose utilisation of the spheroids over the total 18 day treatment period. The pre-treatment and treatment periods are two different phases. The last day of pre-treatment, Day 4, was considered the first day of treatment, Day 0.

In terms of the effect of individual treatments on the spheroids, the control, palmitate, and GRT treated spheroids showed a similar trend in terms of glucose utilisation over the 14 day treatment period. By Day 7, ATV noticeably increased glucose utilisation, whereas ATV+GRT noticeably decreased glucose utilisation. By Day 14, however, there was a steep decrease in glucose utilisation in the ATV treated group, although this was insignificant. The ATV and ATV+GRT (91.83% and 94.68% respectively) groups showed decreased glucose utilisation

at Day 14, with results approaching the glucose concentration of the fresh media. However, none of these changes in glucose utilisation were significant.

5.12 Spheroid viability assessment

The luminescent intensity measured, indicative of the production of ATP, is directly proportional to the number of viable and active cells. The normalisation of this luminescence to the average volume of the spheroid allows for quantification of the viability of treated spheroids.

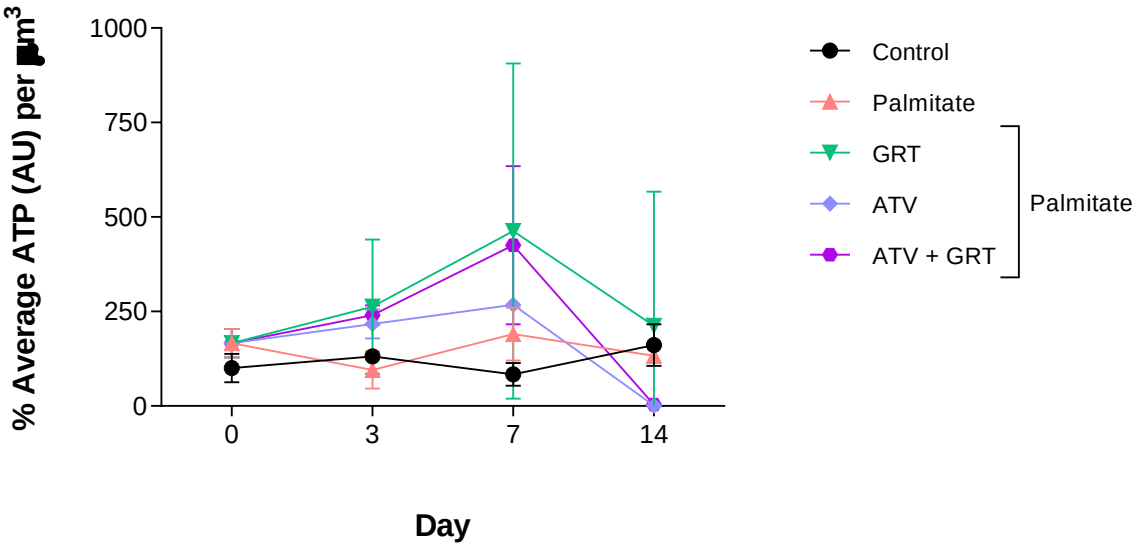

Figure 5.12.1: Comparison of average ATP production in treated spheroids at Day 0, 3, 7, and 14 of treatment. *Average ATP production of spheroids was luminescently measured in arbitrary units (AU) and normalised to average spheroid volume (µm^3) at each time point. GRT = 0.01 mg/mL; ATV = 10 µM; ATV+GRT = 10 µM ATV + 0.01 mg/mL GRT. Data are mean ± SD derived from five treatments at four time points each with three sampled spheroids (n = 3). A two-way Analysis of Variance was used with a Tukey post hoc test.*

Changes in ATP production started as early as Day 3 after treatment, however none of the differences between the treatment groups was significant. Throughout the treatment period, the control and palmitate-treated spheroids showed similar ATP fluorescence which stayed relatively constant. By Day 14, the ATV, and ATV+GRT groups' ATP production plummeted to almost non-existent (1.45 AU/µm^3 ± 1.00, and 3.79 AU/µm^3 ± 2.32 respectively).

5.13 Adenylate kinase production

Adenylate kinase is an enzyme present in the inter-mitochondrial membrane space and leaks into the cytosol and culture media when the cellular and mitochondrial membranes are compromised. The presence of adenylate kinase in treatment or culture medium can be luminescently tagged and measured. Expressed luminescence is proportional to the number of compromised cells. The normalisation of the luminescent readings to the average spheroid volume at the relevant time points allows for the quantification of damage done to the integrity of the cells.

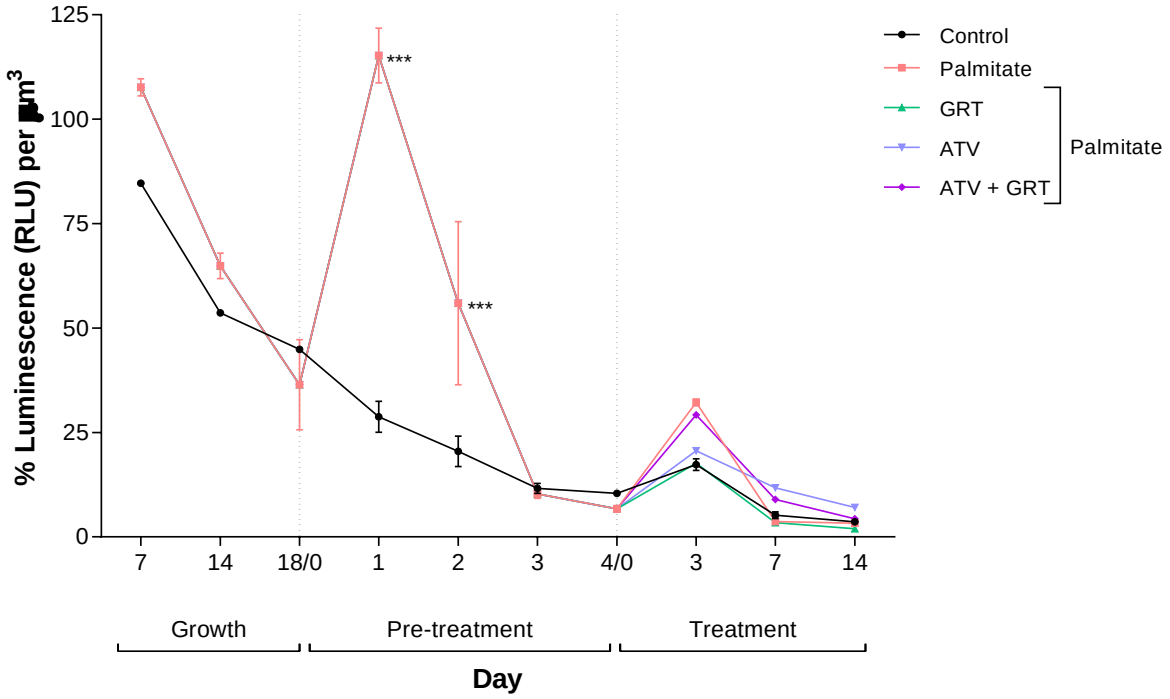

Figure 5.13.1: Adenylate kinase luminescence relative to average spheroid volume at different time points. *Media collected as various time points were assessed for the presence of adenylate kinase. GRT = 0.01 mg/mL; ATV = 10 µM; ATV + GRT = 10 µM ATV + 0.01 mg/mL GRT. Data are mean ± SD derived from five treatments at ten time points each with three technical repeats (n = 3). Results are expressed as percentage luminescence per average spheroid volume, normalised to the control at the first time point set at 100%. A two-way Analysis of Variance was used with a Tukey post hoc test. *** = p<0.001.*

Adenylate kinase levels decreased steadily in the control group for the duration of the study. The addition of palmitate significantly (*p<0.001*) damaged the spheroids as was seen by an increase in adenylate kinase at Day 1 of pre-treatment with palmitate compared to the control (28.72% ± 3.72 vs 115.27% ± 6.60). Similarly, as shown in *Figure 5.13.1*, Day 2 of pre-treatment also showed a significant increase (*p<0.001*) in luminescence in the palmitate group

(55.92% ± 19.55) compared to the control group (20.48% ± 3.64). Thereafter, the adenylate kinase levels were similar in both treatment groups until the end of pre-treatment. There was an increase in the adenylate kinase levels in all treatment groups, however this was insignificant ($p>0.05$), followed by a steady decrease in the levels in all treatment groups from Day 3 to Day 14.

6 Discussion

6.1 Background

Statins are one of the most frequently prescribed therapeutic drugs for the treatment of dyslipidaemia and hypercholesterolaemia. Through competitive inhibition of hydroxymethylglutaryl coenzyme-A (HMG-CoA), statins inhibit cholesterol synthesis at a rate-limiting step of the mevalonate pathway. Statins are prescribed to patients who have dyslipidaemia, hypercholesterolaemia (familial, acquired, or combined), or patients who are at risk of cardiovascular disease, such as patients with an unfavourable LDL/HDL ratio. The need for such therapeutic interventions is increasing due to the rising prevalence of a sedentary lifestyle, Westernised diet, and its consequent metabolic perturbations (Metabolic Syndrome) and Type 2 Diabetes Mellitus. The reduction in plasma lipid levels of cholesterol allows for a decrease in potential cardiovascular disease and associated complications. For example, a decrease in the progression of atherosclerosis, the formation of atherosclerotic plaques, and the potential for myocardial infarction.

Approximately 38.6 million Americans were using statins in 2016 (Adedinswo *et al*, 2016). A retrospective cohort study published in 2016 showed that, in the United Kingdom between 1997 and 2006, moderate to severe hepatotoxicity occurred in 0.44% of patients on high dose (40 – 80 mg per day) atorvastatin, compared to 0.07% of patients on low dose (10 – 20 mg per day) atorvastatin. By comparison, 0.09% of high dose (40 – 80 mg per day) simvastatin patients and 0.05% of low dose (10 – 20 mg per day) simvastatin patients exhibited moderate to severe hepatotoxicity (Clarke *et al*, 2016).

Statin associated side-effects cannot be ignored, specifically the potential for statin-induced hepatotoxicity. Typically, statin-related adverse effects include an increased incidence of diabetes, myopathy, and an increase in serum transaminases. Save for the possibility of new onset diabetes mellitus, cessation of statin treatment has shown to rectify these side-effects. However, in the majority of cases, continued and prolonged use of statins has been shown to reduce the severity of the side-effects (Zhang *et al*, 2013).

Statin-induced hepatotoxicity is attributed mainly to an increased ROS production causing oxidative stress and promoting the activation of inflammatory, autophagic, and apoptotic pathways (Pal *et al*, 2015; Wang *et al*, 2015). Chronically elevated oxidative stress is likely to

cause complications in all normal cellular functioning and signalling, and possible eventual organ failure.

A patient undergoing statin treatment is likely to have other metabolic aberrations apart from dyslipidaemia. The presence of this risky metabolic profile could potentiate statin-induced hepatotoxicity (Koh *et al*, 2011). The hyperlipidaemic condition, characterised by chronic high plasma concentrations of free fatty acids and triglycerides, is also associated with hepatic conditions such as steatosis and Non-Alcoholic Fatty Liver Disease (NAFLD). In this study, to mimic hyperlipidaemic conditions *in vitro*, palmitate, a naturally occurring long chain saturated fatty acid, was added to the culture media. The addition of palmitate has been used to study, for example, induced: insulin resistance in a) C3A cells by Abu Baker *et al* (2017); b) C2C12 myotubes by Abu Baker and Tan (2017); hyperlipidaemia, NAFLD, ER stress, and lipotoxicity in a) primary hepatocytes and H4IIEC3 cells by Egnatchik *et al* (2014), and b) primary mouse hepatocytes and HepG2 cells by Feldstein *et al* (2004); and as a model of CYP3A4 activity in Fa2N-4 and HepG2 cells by Hu *et al* (2014).

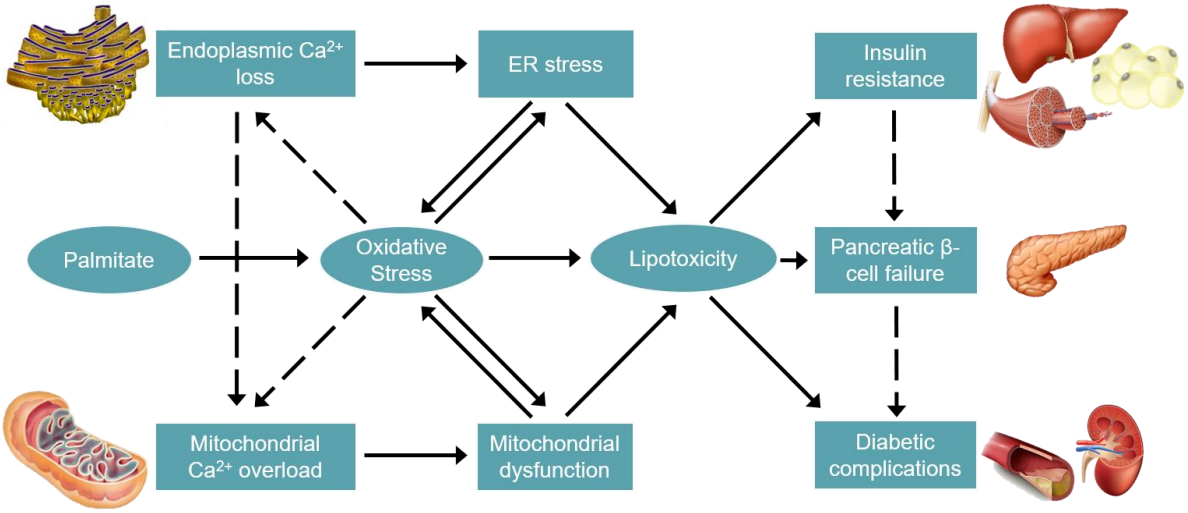

Figure 6.1.1: Proposed mechanism of lipotoxicity in Type 2 Diabetes. *Oxidative stress and calcium dysregulation form a vicious cycle that disturbs critical organelle function. Lipotoxicity resulting from ER stress and mitochondrial dysfunction contributes to pancreatic β-cell failure, insulin resistance in target tissues and diabetic complications. (Adapted from Ly et al, 2017).*

The hyperlipidaemic condition leads to altered liver function due to the onset of a pro-inflammatory state, increasing the activity of cell death mechanisms and promoting a state of excess ROS and oxidative stress (*Figure 6.1.1*). The relationship between CYP450 modulation and diabetes has been found to be time-dependent with long-term diabetes resulting in more significant CYP450 modulation, suggesting that treating cells with high levels

of fatty acids for a longer time may be more demonstrative when studying the effects of elevated concentrations of fatty acids in an *in vitro* study (Hu *et al*, 2014; Shu *et al*, 2016a; Shu *et al*, 2016b). The hyperlipidaemic condition has also been shown to increase the activity of CYP3A4 which is an enzyme responsible for atorvastatin metabolism. An increase in CYP3A4 activity would alter the metabolism and pharmacokinetics of atorvastatin, potentially resulting in an incorrect and/or ineffective concentration of atorvastatin in the circulation, leaving the liver susceptible to toxicity. Patel *et al* (2016) showed that GRT is metabolised by CYP3A4, suggesting that concurrent administration of GRT and ATV would result in competitive inhibition of CYP3A4 and altered pharmacokinetics of ATV. Patel *et al* (accepted manuscript) demonstrated a 300% increase in ATV serum concentrations in mice following concurrent administration of ATV and GRT.

Often, the philosophy of 'prevention is better than cure' is employed by patients and healthcare professionals alike. It is well-known that statins can result in unwanted side-effects, and it has been shown that patients stop using statins as a result of unwanted side-effects. A retrospective study (between 2000 and 2008) by Zhang *et al* (2013) showed that, of a cohort of 107 835 patients, 17.4% experienced statin-related side-effects, and 59.2% of which discontinued statin treatment as a result (Zhang *et al*, 2013). As such, patients with increased cholesterol levels will often supplement statin treatment with alternative "holistic" medication in order to prevent or lessen the side-effects associated with statin usage. Such preventative measures include dietary changes or the use of nutraceuticals, herbal, or indigenous medicines. Natural products, nutraceuticals, and herbal medicines are generally presumed to be safe. However, taken in conjunction with a therapeutic pharmaceutical agent may alter their metabolism and lead to adverse herb-drug interactions (reviewed by Awortwe *et al*, 2018).

Rooibos is traditionally consumed as a hot or cold beverage, favoured for its high polyphenol content and lack of caffeine, and has gained popularity not only for its taste but for its health promoting properties. As such, numerous health products containing Rooibos are available, including extracts with increased phenolic content. With the increased prevalence of metabolic perturbations, specifically dyslipidaemia, the likelihood of combining statin usage and Rooibos supplementation is increased as it is presumed that Rooibos will safely limit side-effects while positively modulating the lipid profiles of patients. These assumptions are based on pre-clinical publications in the public domain that demonstrate hepatoprotective effects of Rooibos against known hepatotoxins such as CCl_4^- (Kucharská *et al*, 2004), LPS (Ajuwon *et al*, 2014), and *t*-BHP (Canda *et al*, 2014).

Given the increase in probability of the concomitant therapy of statins and Rooibos, the effects of Rooibos on statin-induced hepatotoxicity warrants investigation as two cases exist that show chronic Rooibos consumption, with atorvastatin or maintenance treatment of rituximab and daily administration of prednisolone, was associated with hepatotoxicity. Statin-induced hepatotoxicity is rare, but it has occurred. This study aimed to assess whether the addition of GRT would improve or worsen induced toxicity, especially in patients with dyslipidaemia.

6.2 Toxicity Study

The human-derived hepatocarcinoma cell line C3A is a derivative of the HepG2 cell line and has been shown to express human proteins, secrete albumin, and have increased CYP450 activity compared to HepG2 cells (Baquerizo *et al*, 2015). For the *in vitro* toxicity study, HepG2/C3A cells were used to establish a model of hepatotoxicity in a normal and an induced hyperlipidaemic state. HepG2/C3A cells are frequently used in toxicity studies (reviewed by Baquerizo *et al*, 2015) and have also successfully been used in the culturing of 3D spheroids (Wrzesinski *et al*, 2013; Wrzesinski *et al*, 2014; Wrzesinski & Fey, 2018; reviewed by Calitz *et al*, 2018).

Atorvastatin was assessed for potential toxicity and doses above 25 µM (50 µM and 100 µM) showed significant toxicity as early as 6 hours after treatment, which decreased cell viability in a dose- and time-dependent manner. These results complement data published by Dorcat *et al* (2018) showing that ATV treatment dose-dependently decreases cell viability in terms of MTT activity in HepG2 cells at a concentration of 1.2 mM. Tolosa *et al* (2015) showed that 24 hours treatment with of six different statins (atorvastatin, cerivastatin, fluvastatin, lovastatin, pravastatin, and simvastatin) showed a significant decrease in cell viability, and a significant increase in mitochondrial mass at doses of above 50 µM in HepG2 cells. In this study, doses of under 25 µM showed no toxicity at 24 hours. Subsequent IC_{50} values were calculated to be 48.13 µM ± 2.08 and 41.41 µM ± 3.67 at 12 and 24 hours respectively. Two intermediate concentrations (10 µM and 25 µM) were thus chosen for future experiments.

A 2011 letter to the editor of the British Journal of Clinical Pharmacology by Björkhem-Bergman *et al* highlighted a discrepancy in the ATV concentrations tested *in vivo* and *in vitro* compared to human serum concentrations and C_{max} values. It was shown that toxicity studies and studies assessing the pleiotropic effects of statins, made use of concentrations typically >1000-fold than those found in humans. Although there are differences between the

metabolism in humans, rodents, and cultured cells, it is still important to note that these differences exist (Björkhem-Bergman *et al*, 2011). The C_{max} of ATV has been shown to range between 1.95 µg/L and 252 µg/L in dosages between 2.5 mg and 80 mg (Lea & McTavish, 1997; Lennernäs, 2003). Both 10 µM and 25 µM are more than twice the maximum recorded C_{max} values. However, as this study was an assessment of acute toxicity, the concentrations and time points of ATV used were acceptable and aligned with those used in previous studies (Youssef *et al*, 2002; Hoffart *et al*, 2011; Phulukdaree *et al*, 2015; Tolosa *et al*, 2015; Kim *et al*, 2016; Shu *et al*, 2016a). Youssef *et al* (2002) found that treatment with 10 µM ATV exerted immunomodulatory pleiotropic effects on microglia EOC 20 cells and may be beneficial for multiple sclerosis or other Th1-mediated autoimmune diseases. Hoffart *et al* (2011) found that 30 µM ATV and its metabolites are PXR ligands and induce various metabolising enzymes. Gaunidinoaceto-N-methyltranserase is a critical enzyme in the creatine synthesis pathway and its expression in hepatocytes is regulated by miR-124a. Phulukdaree *et al* (2015) found that 20 µM ATV treatment upregulated miR-124a levels in HepG2 cells. Tolosa *et al* (2015) assessed a range of statin concentrations (5 µM to 100 µM) and the consequent drug-induced mitochondrial impairment in HepG2 cells, and found that ATV resulted in mitochondrial membrane hyperpolarisation, decreased calcein levels, and increased superoxide production. Kim *et al* (2016) found that treatment of glomerular mesangial cell line SV40 MES 13 with 10 µM rosuvastatin decreased plasminogen activator inhibitor-1 (PAI-1); a protein that, when present in high levels, has been linked to the development of atherosclerosis and thrombosis. Shu *et al* (2016a) showed that treatment of HepG2 cells with 10 µM and 30 µM ATV resulted in oxidative stress-induced hepatotoxicity. The same study by Shu *et al* (2016a) used a low (10 mg/kg), medium (20 mg/kg), and high dose (40 mg/kg) of atorvastatin in a single dose streptozotocin-induced diabetic Sprague-Dawley rat model. Within 8 days of atorvastatin treatment, all the high dose atorvastatin rats died and suffered from hepatomegaly and hepatorrhagia. The low and medium doses also caused severe liver damage, however this was not lethal (Shu *et al*, 2016a). It is important to note the lethality of the dosage of atorvastatin; however it is also important to note that STZ is hepatotoxic specifically to rodents and could also contribute to the toxicity of atorvastatin.

Similar to what has been described above, in this study, GRT was assessed for potential toxicity at a range of doses from 0 mg/mL to 2 mg/mL on C3A cells. The cell viability results suggested that mild toxicity occurred only at the highest dose after 24 hours of treatment. Literature relevant concentrations of 0.01 mg/mL and 0.1 mg/mL GRT were chosen for further experiments (Muller *et al*, 2012; Mazibuko *et al*, 2013; Mazibuko *et al*, 2015).

As previously stated, the hyperlipidaemic state in animals and humans exerts its own toxic effects on the system. Therefore, in order to prevent a state of excessive lipotoxicity, the model was optimised for the induction of hepatic dysfunction as a result of hyperlipidaemia induced by palmitate allowing for the assessment of ATV toxicity. Optimisation of the hyperlipidaemic state was achieved through the evaluation of three palmitate concentrations (200 µM, 500 µM, and 750 µM). Zezina *et al* (2018) showed that treatment with 500 µM palmitate resulted in increased mitochondrial fragmentation in macrophages, however this was found to be a defence mechanism employed by the cells to reduce ROS production and lipotoxicity as opposed to being as a result of lipotoxicity itself. Further, it was shown that this fragmentation was neither toxic nor irreversible in the macrophages. In untreated cells in this study, it was shown that 750 µM resulted in a significant decrease ($p<0.001$) in cell viability (48.96% ± 22.16 compared to 100% ± 2.26 in the untreated control). A similar pattern of viability was shown in cells exposed to palmitate pre-treatment and then either of two concentrations of GRT or ATV monotherapy: 750 µM was deemed too toxic for the model. Abu Baker and Tan (2017) showed that exposure to 750 µM palmitate for 24 hours elicited numerous detrimental effects in C3A cells, such as oxidative stress, mitochondrial dysfunction, and impaired fatty acid oxidation. The present study showed that the addition of 500 µM palmitate greatly increased the toxicity of ATV. The difference in viability in both GRT treated groups as compared to the untreated control showed that GRT alone was not able to modulate the toxic effect of palmitate.

In the normal condition, in cells not pre-treated with palmitate, both 10 µM and 25 µM ATV caused a significant decrease in relative MTT activity, while GRT alone showed no difference at the concentrations used after 24 hours. In combination, GRT did not modulate the toxicity induced by ATV in terms of MTT activity. The same trend was noted in the hyperlipidaemic condition. Taken together, this suggests that GRT did not have a modulating effect on ATV-induced toxicity in terms of MTT activity.

6.3 Induction of Simulated Hyperlipidaemia

As mentioned previously, it has been shown that the presence of metabolic perturbations such as T2DM causes altered drug metabolism due to increased expression and activity of cytochrome P450 isozymes (Hu *et al*, Shu *et al*, 2016a; Shu *et al*, 2016b). Of particular importance, in terms of statin-induced hepatotoxicity, is CYP3A4, which has been shown to increase statin metabolism resulting in decreased plasma concentrations and accelerated

clearance of the CYP3A4-metabolised drugs (Nobuo *et al*, 1994; Xu *et al*, 2014; Shu *et al*, 2016a; Shu *et al*, 2016b). As such, the expression of CYP3A4 in C3A cells would allow for validation of CYP3A4 induction in the simulated hyperlipidaemic condition induced by 500 µM palmitate pre-treatment. Although present, CYP3A4 expression is significantly decreased in HepG2/C3A cells compared to primary hepatocytes (Barnett *et al*, 1990; Yu *et al*, 2005; Baek *et al*, 2006; Borbás *et al*, 2006; Westerink & Schoonen, 2007). However, rifampicin, a known potent CYP3A4 inducer (Lin & Lu, 1998; Lu & Li, 2001), was used as a positive control to induce CYP3A4 expression in C3A cells. Literature has shown that 14 hour treatment with a mixture of a high concentration of fatty acids, decreased CYP3A4 activity. However, Hu *et al* (2014) showed that a 48 hour treatment of hepatocytes with 100 and 200 µM palmitate induced CYP3A4 activity, demonstrating that CYP3A4 can be differentially expressed in a time- and concentration-dependent manner. Despite these high concentrations, fatty acids have been shown to induce apoptosis and the accumulation of lipids in hepatocytes, supported by the preliminary study by Hu *et al* (2014) showing that concentrations higher than 200 µM of palmitate could significantly decrease cell viability after 48 hours. As expected, the results of the present study showed that the untreated control cells showed low CYP3A4 expression, and the addition of rifampicin resulted in a >7-fold increase in CYP3A4 expression. The addition of palmitate alone resulted in a marked increase in CYP3A4 expression compared to the untreated control, and this appeared to be slightly increased, albeit not significantly, with the addition of rifampicin to the palmitate treatment. This shows that CYP activity, specifically CYP3A4 in this study, was up-regulated in palmitate-treated cells. As such, these results, in conjunction with the literature, suggest that the addition of 500 µM palmitate pre-treatment induced a simulated hyperlipidaemic condition in this model.

Pharmacokinetic and toxicity studies are performed in order to understand the therapeutic margin of a drug in pre-clinical trials, thereby decreasing the risk of adverse effects or toxicity and establishing effective therapeutic margins, consequently decreasing the risk of drug failure. Pharmacokinetic studies assess the absorption, distribution, metabolism, and excretion (ADME) of a drug to understand at which point the potential for adverse reactions lies in the overall metabolism of a drug. Increased understanding of the biochemistry of CYPs has altered the way ADME research is conducted. The CYP system plays an essential role in drug metabolism, and CYP phenotype, CYP inhibition, and CYP induction all alter drug pharmacokinetics (Vrbanac & Slauter, 2017). As such, *in vitro* analysis of these parameters provides early predictive information relative to drug metabolism, however *in vivo* assessment

of ADME processes, remains the gold standard for drug pharmacokinetic and pharmacodynamic assessment.

6.4 Oxidative Stress

The overproduction of ROS in the presence of insufficient antioxidant defences results in a state of oxidative stress, creating an environment where cells are particularly susceptible to injury. The fluorescence of DCF occurs due to the oxidation of the DCFDA substrate by free radicals and is a measure of the extent of ROS production in the cell.

Results of the toxicity study were supported by the oxidative stress experiments performed. In the normal condition, GRT alone at any concentration did not induce ROS production. The higher concentration of ATV (25 µM) induced significant amounts of ROS production, and co-treatment with 0.1 mg/mL GRT further exacerbated this effect. In the hyperlipidaemic condition, a similar trend was seen: GRT alone did not induce ROS production, however significant ROS production was found with 25 µM ATV treatment, both alone (1431.00% ± 504.20) and in combination with GRT (1493% ± 278.40). Shu *et al* (2016) showed that ATV-induced hepatotoxicity in the hyperlipidaemic condition is as a result of increased ROS production.

The antioxidant potential of Rooibos has been well documented and has been shown to increase the activity of endogenous antioxidant systems, as well as having ROS scavenging capabilities (Marnewick *et al*, 2003; Uličná *et al*, 2003, Kucharská *et al*, 2004; Ajuwon *et al*, 2013; Ajuwon *et al*, 2014). In this study, GRT was unable to ameliorate the ATV-induced ROS production in either condition, suggesting that GRT was unable to protect the cells against ATV-induced ROS production. ATV acts by inhibiting mevalonate which, apart from being a precursor of cholesterol, is also a precursor of the mitochondrial ubiquinone (CoQ_{10}), an important redox component of the mitochondrial electron transport chain, responsible for synthesising ATP. Reducing the biosynthesis of CoQ_{10} in the liver affects mitochondrial oxygen consumption and liver cell function, and increases cellular ROS production. Although GRT is known to affect cholesterol synthesis, it is likely that its mechanism of action does not involve the mevalonate pathway and, as such, does not protect against ATV-induced ROS production.

In terms of hepatotoxicity, it can be speculated that the contrast of the results of this study to those in other studies may be as a result of fundamental experimental differences. Carbon tetrachloride (CCl_4^-) (Kucharská *et al*, 2004), LPS (Ajuwon *et al*, 2014), and *t*-BHP (Canda *et al*, 2014) have been used to chemically induce hepatic injury, inflammation, and acute oxidative stress *in vivo*. Treatment with Rooibos has shown to modulate the induced hepatic injury in these models. Previously, Rooibos has been shown to protect against CCl_4^- induced toxicity. However, the mechanism of toxicity induced by CCl_4^- is different to that of ATV as it involves the production of trichloromethylperoxy radicals inducing lipid peroxidation, oxidising polyunsaturated fatty acids and phospholipids, and consequently affecting the permeability of the mitochondria, ER, and the cellular membrane. The endotoxins LPS are inducers of inflammation and cytokine-mediated cell damage, whereas *t*-BHP causes hydroperoxide-induced oxidative stress as it generates free radicals such as t-butoxyl and t-methyl radicals which cause DNA damage, depletion of glutathione, and cell membrane permeabilisation, via various mechanisms. It can be speculated that the mechanism of action of ATV-induced toxicity is due to the chronic inhibition of the mevalonate pathway, consequently hindering the fluidity and permeability of the mitochondrial membrane.

6.5 Mitochondrial Membrane Integrity

The dual emission JC-1 dye allows for the assessment of the formation of fluorescent red “J-aggregates” that accumulate in the mitochondria as a result of high mitochondrial membrane potential, and fluorescent green J monomers which form due to decreased mitochondrial membrane potential. The overall mitochondrial membrane integrity of the cells is measured in terms of the mean red fluorescence intensity, where an increased mean value is indicative of a stronger red fluorescence as a result of greater J-aggregate formation. The relative percentage of JC-1 inactive cells is indicative of the proportion of the population with increased green fluorescence as a result of the presence of J monomers and decreased membrane integrity.

In the normal condition, ATV dose-dependently decreased mean red fluorescence intensity, whereas GRT treatment alone showed no difference to mean red fluorescence intensity. Although insignificant, the co-treatment groups showed a similar range of results compared to the ATV monotherapy groups, suggesting that GRT could not attenuate the toxicity of the ATV in terms of mitochondrial membrane potential changes. In the hyperlipidaemic condition, in

comparison to ATV1, ATV2 significantly reduced mean fluorescence intensity. This effect was not ameliorated by GRT treatment.

Taken together, these results show that ATV has a negative effect on mitochondria. As mentioned previously, the ATV-induced oxidative stress was associated with mitochondrial alterations which, in terms of oxidative stress, was not ameliorated by GRT. In terms of membrane potential, these results support the previous findings whereby ATV reduced mitochondrial dehydrogenase activity, increased oxidative stress, in a dose-related fashion. These effects were not attenuated by the addition of GRT. To date, similar studies have not been performed.

Previously, Johnson *et al* (2016) showed that aspalathin, the major dihydrochalcone *C*-glucoside in Rooibos, was able to protect mitochondrial membrane integrity of H9c2 cells under hyperglycaemic conditions by shifting the substrate preference from fatty acid oxidation to glucose oxidation. It can be speculated that, in the present study, GRT is unable to overcome the damage caused by hyperlipidaemic condition, whereas a model of hyperglycaemia is more easily rectified by GRT.

6.6 Apoptosis Assessment

Annexin V and PI are used concurrently in order to assess plasma and nuclear membrane integrity. Annexin V and PI negative cells have intact plasma membranes and, as such, are deemed viable. Annexin positive, PI negative cells indicate a decrease in the integrity of the plasma membrane and are considered to be in early apoptosis. The membrane phospholipid phosphatidylserine (PS) is translocated out of the plasma membrane and exposed to the extracellular environment upon the loss of plasma membrane symmetry. In this early stage of cell death, the membrane is compromised and PS flipped, allowing for the conjugation of annexin V fluorochromes to the exposed PS. Propidium iodide is a DNA-intercalating dye. Propidium iodide positive cells are in a state of late apoptosis as the plasma membrane integrity is lost and the cells' ability to exclude PI dye is compromised. Results will be discussed in terms of viable, early apoptosis, and late apoptosis in the normal state and in the hyperlipidaemic state.

The value of flow cytometry is to assess the current rate of apoptosis from within the remaining "normal" population of C3A cells: cells are selected (gated) based on their

physical/morphological characteristics. The selection of cells based on their forward/side scatter characteristics means that cells in advanced stages of apoptosis, apoptotic bodies, karyorrhectic and necrotic cells are excluded from the analysis due to their reduced size and increased side scatter densities. Further, the gating was selected according to the dispersion of viable cells in an untreated, normal population, thereby excluding cells that had already been affected by the toxic effects of palmitate. Cells assessed in the hyperlipidaemic condition, therefore, allowed for the assessment of the viability status of the remaining cells falling into the parameters of “normal” cells. An MTT assay assesses cell viability in totality, considering the mitochondrial dehydrogenase activity of the entire cellular population as opposed to a select population. Cell viability, metabolism, and proliferation, as assessed by MTT assay, is a rudimentary indication of functional mitochondria within the cell. As such, the two methods should be regarded as complementary: MTT provides an overall impression of the toxicity and cell viability, whereas flow cytometry provides an indication of cell loss to apoptosis at a specific time i.e. 24 hours. Based on this, looking at the MTT, there were dramatic losses of cell viability, particularly in high dose ATV, while, after 24 hours, the effects of ATV and GRT on apoptosis was significantly different to the controls, suggesting that the cells exposed to palmitate were more susceptible and cells were lost to apoptosis before this time point.

In the normal condition, in terms of annexin V/PI assessment, the results of the viable cells (annexin neg., PI neg.) supported the MTT activity of different treatment groups. In terms of apoptotic cells, cells in early apoptosis (annexin V pos., PI neg.) showed no significant differences between the treatment groups and the control. The evaluation of late apoptosis confirmed results of the DCF assay where treatment with ATV, particularly 25 µM ATV, resulted in significant amounts of late apoptosis. After 24 hours with treatment, the increased number of cells in late apoptosis relative to those in early apoptosis indicates that the toxic effects of ATV (especially at a high dose 25uM) had a rapid onset. This is evident by the number of viable cells, which are almost depleted (18.00% ± 5.62 for ATV2 vs 57.67% ± 10.41 for ATV1), cells entering apoptosis (0.33% ± 0.52 for ATV2 vs 5.67% ± 2.50 for ATV1), and those in late apoptosis (81.67% ± 5.57 for ATV2 vs 36.50% ± 10.93 for ATV1) after 24 hours. GRT was unable to modulate the apoptotic effects of 10 µM or 25 µM ATV on hepatocytes. Taken together, these results are consistent with previous results, supporting the idea that ATV-induced hepatotoxicity is dose-dependent in the normal condition.

The hyperlipidaemic condition showed contrasting results to the normal condition, in terms of cell viability where the majority of the assessed gated population under all treatment conditions

were viable, further highlighting the experimental design in terms of assessing a population that is considered “normal” or healthy according to morphological characteristics alone. The results of the apoptotic cells, however, showed complementary results to that found in the normal condition, where cells treated with ATV2 showed the fewest early apoptotic cells, although differences were insignificant. There was no significant difference between any of the treatment groups in terms of late apoptotic cells, however the ATV2 group showed the greatest percentage thereof (30.75% ± 13.45). To date, similar studies have not been performed.

The discrepancy between these results and those of the MTT assay illustrates limitations of different experimental designs, although the results should be considered complementary.

6.7 Caspase Assessment

Apoptosis can be initiated through either the extrinsic or intrinsic pathways. Caspase-3, -7, and -9 are executioner caspases and activated by both the intrinsic and extrinsic apoptotic pathways in the final part of each pathway, committing the cell to apoptosis. As such, the activity of these caspases is an indication of the state of apoptosis of the cells and, therefore, an overall measurement of cell viability.

Caspase 3/7 activity was significantly increased by ATV, particularly 25 µM. These results are in agreement with the 2015 study by Pal *et al* that showing a significant increase in caspase activation in healthy rats from ATV concentrations of 10 mg/kg/day. Similarly, Docrat *et al* (2018) noted a significant increase in ATV-induced caspase activation in HepG2 cells, of which C3A cells are a sub-clone, treated with 1.2 mM ATV. Further, Docrat *et al* (2018) made use of a similar assay to assess caspase activity. The combination of ATV2 + GRT2 showed significantly less caspase 3/7 activity compared to the ATV2 group alone, suggesting that GRT had a modulating effect on caspase activity in the normal condition. GRT alone did not activate caspase activity.

In the hyperlipidaemic condition, although there are significant differences and GRT dose-dependently increases caspase activity, the increase is relatively small (<1-fold), which is below a biologically significant change, generally regarded as >1.5-fold. Further, it is important to consider the activity relative to the time point assessed. Another variable compared to the cells in the normal condition is that the cells had already been pre-treated with palmitate which

could account for the differences observed in terms of ATV toxicity in the cells in the normal condition relative to the cells in the hyperlipidaemic condition. Further, GRT at the relatively high dose of 0.1 mg/mL could have pro-oxidant effects under the hyperlipidaemic condition. The antiapoptotic/antioxidant effects of Rooibos and aspalathin has been previously shown to be optimal at doses of 0.001 mg/mL and 0.01 mg/mL.

As with an MTT assay, the fluorescent measurement of caspase activity allows an average at a specific time-point as opposed to a cell-specific result. The experimental time point may miss the point at which the caspase cascade is initiated. Further, the preference of necrosis as a mechanism of cell death results in caspase activation being avoided altogether.

6.8 3D Spheroid Culturing of C3A Cells

Three-dimensional culturing has become increasingly popular for assessing pharmacokinetics *in vitro* as a means of an intermediate technology between cell culture and animal studies. This form of culturing C3A cells allows for the regaining of functionality after trypsinisation, specific to hepatocytes, in an *in vitro* model, and allows the culture to grow "undisturbed" and unharmed by trypsinisation, with a constant "flow" of nutrients. These culturing conditions mean that hepatocellular specialisation, within the spheroids, occurs. Further, multiple spheroids are produced in each experimental repeat (approximately 600 in this study). As a result, even one experimental repeat yields multiple technical repeats per subsequent assay or analysis.

Transmission electron micrographs of an untreated control spheroid showed the specialisation of the cells within the spheroid. Microvilli increase the cellular surface area, increasing the efficiency of nutrient transfer, while tight junctions and desmosomes increase cellular strength and integrity. The presence of rough endoplasmic reticulum, autophagosomes, and polyribosomes showed normal cellular protein synthesis and turnover, further supported by the presence of heterochromatic and euchromatic DNA. As further confirmation of the specialisation of the hepatocytes, lipid droplets were present intracellularly due to restored hepatocellular cholesterol synthesis.

The C3A spheroids produced followed the growth and doubling time as previously observed by Wrzesinski, *et al* (2013) and Wrzesinski & Fey (2013). Growth and cellular function of the spheroids was measured in terms of average spheroid size as well as in terms of glucose utilisation. In this study, spheroids grew at a constant rate from approximately 250 µm at Day 0 to approximately 800 µm at Day 18, the first day of treatment. By Day 36, spheroids were approximately 1500 µm. Similar results were found in the study by Wrzesinski, *et al* (2013). In terms of projected growth, the growth curve of the spheroids would tend towards a plateau from Day 35 onward. Due to time constraints, it was not possible to assess this further in the current study. In this study, the addition of the various treatments resulted in alterations in the macroscopic appearance of the treated spheroids, suggesting changes in the structural integrity of the spheroids. Palmitate treatment adversely effected the spheroids in terms of their spherical shape and surface morphology, with potential loss of cells or cell clusters from the spheroids, which was confirmed with increased cell debris within the surrounding media. This is in keeping with the MTT which showed that there is significant cell loss with the addition

of palmitate and ATV, and, by implication, a loss of cluster integrity in 3D culture. The ATV treated spheroids showed the most severe alterations as was evident in the compromised structural integrity of the spheroids. This resulted in a significant overall increase in the average diameter measured in the ATV treated spheroids as compared to all other treatments after 18 days of treatment. Although there were slight differences in the average diameter measured for the other treatment groups, there was no significant difference in the average diameters.

Glucose is used for the maintenance of normal cellular functions. As such, changes in the utilisation of glucose rudimentarily indicates alterations in normal cellular function. Glucose concentration was measured at each medium change and calculated relative to the glucose concentration of the fresh treatment, set at 100%. The changes in the remaining glucose were a simple indication of metabolism and the viability. The glucose utilisation fluctuated, but the remaining concentration was always less than the fresh medium. The addition of the treatments decreased the average glucose utilisation, suggesting a decrease in spheroid integrity and viability as a result of the treatment. This was further confirmed by the assessment of glucose utilisation measurement of each treatment bioreactor. By Day 7, the ATV+GRT treated spheroids showed decreased glucose utilisation (86.16%), which decreased further by Day 14 (94.68%). Day 14 also showed a decreased utilisation by the ATV-treated spheroids (91.84%).

6.9 ATP

As with glucose utilisation, ATP is indicative of normal cellular functioning, with a decrease in ATP production suggesting compromised cellular functioning and consequently decreased viability of the spheroids. The results of ATP production as shown by Wrzesinski, *et al* (2013), showed fluctuations in the initial growth phase of the spheroids, followed by a trend towards a plateau after 25 days of growth. In the present study, the ATP production was normalised to the spheroid size. A similar trend in ATP production was noted in the present study for the Control and Palmitate-treated spheroids. At Day 0 of treatment, the ATP levels were comparable between all the different groups. The Control and Palmitate-treated spheroids fluctuated marginally, although insignificantly, but overall maintained a stable, almost plateaued, rate of ATP production. At Day 3, there was an increase in the ATP production in the GRT, ATV, and ATV+GRT spheroids. Day 7 showed a notable increase in ATP production in the GRT, ATV, and ATV+GRT spheroids, with the ATV treated spheroids showing a

significant difference compared to the control spheroids. Day 14 showed a severe decline in the ATP production in the GRT, ATV, and ATV+GRT spheroids, all with values approaching 0. These results support the results of the average glucose utilisation as well as the ultrastructural changes in the spheroids, confirming that there is a decline in the viability and integrity of the spheroids as a result of the treatments administered, supporting, preliminarily, the two-dimensional *in vitro* results.

6.10 Adenylate Kinase

The degradation of the mitochondrial membrane causes the leakage of the mitochondrial intermembrane enzyme, adenylate kinase, into the cytosol. A study by Wrzesinski & Fey (2013) showed that the extension of culturing time decreased the adenylate production of the spheroids, however insignificant erratic fluctuations were noted occasionally. In the present study, adenylate kinase production decreased exponentially over the initial 18-day growth period. The Control spheroids continued to decrease towards a plateau, in keeping with the study by Wrzesinski & Fey (2013). The addition of palmitate pre-treatment significantly increased adenylate kinase production for the first two days, before decreasing to levels comparable with the Control spheroids. The addition of the various treatments increased the adenylate kinase production at Day 3, before decreasing at Day 7 and Day 14. This insignificant erratic fluctuation is in keeping with those found by Wrzesinski & Fey (2013). Control, GRT, and Palmitate spheroids had the lowest adenylate kinase production by the end of the treatment period, although this was statistically insignificant.

7 Conclusion

This study hypothesised that an aspalathin-enriched Rooibos extract (GRT) ameliorates statin-induced hepatotoxicity and aimed to investigate the potential hepatoprotective effects of Rooibos against statin-induced hepatotoxicity *in vitro.*

ATV was dose- and time-dependently hepatotoxic and this hepatotoxic effect was exacerbated by the addition of palmitate pre-treatment. ATV toxicity was associated with decreased mitochondrial membrane potential, and increased ROS production as well as caspase 3/7 activity. Increased cell death was confirmed by MTT and annexin V. GRT on its own was not toxic but could not mitigate the toxicity induced by palmitate or ATV. The findings from the current study suggest that concurrent supplementation with GRT appears to be less effective at protecting hepatocytes against ATV- and/or palmitate-induced toxicity as compared to the toxicity of other exogenous toxins.

A single observational 3D culture experiment was conducted, acting as basic confirmation of the use of a chronic model without using animals. The results of 3D culturing should be reviewed in conjunction with the 2D model as it is not possible to infer possible conclusions drawn from the above work alone. It is not possible to make assumptions after Day 7 of ATV or ATV+GRT treatment as it was shown that the spheroids started dying from Day 7. This could be due to the ATV dosages used being too great or too toxic for chronic exposure *in vitro*. At the concentrations tested, palmitate and ATV treatment, as a monotherapy and in combination with GRT, decreased viability. In the parameters assessed, GRT was unable to attenuate the ATV-induced toxicity.

This study found that GRT alone was not toxic. However, even at the highest concentration tested, GRT was unable to protect against the ATV-induced mitochondrial dysfunction and the consequent induced toxicity. These findings were observed in the normal and hyperlipidaemic conditions. However, GRT did not exacerbate the effects of ATV, suggesting that concomitant use of GRT and ATV is safe in terms of hepatotoxicity. These results are in contrast with studies on the hepatoprotective effects of Rooibos (Marnewick *et al*, 2003; Uliĉná *et al*, 2003, Kucharská *et al*, 2004; Ajuwon *et al*, 2013; Ajuwon *et al*, 2014), however it is speculated that this is because ATV induces mitochondrial dysfunction and toxicity through a different mechanism of action to other hepatotoxins. By extension, the mechanism by which GRT

exerts its antioxidant and hepatoprotective effects is not associated with the mechanism of ATV-induced hepatotoxicity.

The present study assessed ATV (10 µM and 25 µM) as a hepatotoxin and the effects that the hepatoprotectant GRT (0.01 mg/mL and 0.1 mg/mL) could have on the induced toxicity, under normal and hyperlipidaemic conditions. It was shown that GRT was unable to modulate the hepatotoxic effects induced by ATV or palmitate in an acute or a chronic model. These findings support the null hypothesis of this study.

8 Limitations & Future Outlook

The present study focused on the hepatotoxic effects of ATV in C3A cells exposed to standard media conditions and cells exposed to media treated with palmitate. The palmitate treatment served as an *in vitro* model mimicking a hyperlipidaemic condition. To achieve this aim, it was essential to select ATV dose concentrations that were “safe”. The lower ATV dose (10 µM) did not induce significant toxicity whilst the higher dose (25 µM) induced significant cytotoxicity after 24 hours. Based on MTT mitochondrial dehydrogenase activity and CYP3A4 activity, pre-treatment with 500 µM palmitate for 24 hours followed by 24 hours’ treatment with 10 µM and 25 µM ATV was selected. However, the addition of a low dose of ATV in conjunction with the palmitate pre-treatment decreased viability significantly. A more toxic effect was seen with the addition of high dose ATV. Whilst GRT slightly increased cell survival, this was not significant. As such, the study could have benefitted from reducing the palmitate concentration, shifting the primary hepatotoxic effect to ATV toxicity rather than palmitate toxicity.

Based on initial MTT results, the addition of GRT treatment (0.01 mg/mL and 0.1 mg/mL) had no effect on ATV-induced toxicity at 10 µM or 25 µM ATV. Therefore, for technical reasons, such as fitting treatments and controls onto a single 96-well multiplate to ensure standard culture conditions per experiment, only the highest concentration GRT was used as a combination treatment with ATV2.

Moving forward with the study, it would be beneficial to assess cholesterol synthesis ([^{14}C] acetate incorporation), mitochondrial activity and biosynthesis (CoQ_{10} synthesis and activity), several markers of apoptosis (e.g. PARP and caspase-1), and to assess parameters of endogenous antioxidant defence systems (SOD and GSH/GSSG activity). Evaluation of the mevalonate pathway could also elucidate potential mechanism(s) by which ATV induces toxicity, as well as the potential influence GRT may have on cholesterol synthesis at a mechanistic level. This elucidation could be relevant not only in liver cells, but also in skeletal muscle cells, and could illustrate the potential influence GRT may have on mitochondrial electron transport chain function. Understanding these parameters could provide insight into the serious muscular side-effects of ATV treatment. Assessing the bioenergetics of the mitochondria using a Seahorse platform would allow for the real time assessment of oxygen consumption rate (OCR) and the extracellular acidification rate (ECAR), thereby dissecting the precise effects both on and of the mitochondria in this context.

It has been shown that GRT inhibits CYP3A4 and increases the C_{max} of ATV and its metabolites. As such, GRT interferes with ATV pharmacokinetics. This study investigated ATV cytotoxicity, and as such, therapeutic and/or realistic doses were not considered. Moving forward with the study, these aspects should be considered.

Although standard cell culture methodologies allow for the dissection of functional and mechanistic effects of drugs, a large gap exists between what can be achieved in culture and what happens in the *in vivo* environment (i.e. the ADME of the substances). Recently, the use of 3D culture as a tissue-specific intermediate has gained interest in pharmacology research which, due to ethical pressures, are exploring non-animal-based testing of drugs and cosmetics. Following the findings in 2D culture, the potential for applying this model in 3D culture was pursued as a single observational 3D culture experiment.

In terms of the model, it was possible to successfully grow multiple C3A liver spheroids over 36 days and recreate the conditions and treatments used in 2D culture. The results of this preliminary study would determine whether or not the research topic would be worth pursuing further (i.e. as part of a larger PhD study). The seeding and structure of the technique means that more than 600 spheroids were grown at a time, with multiple spheroids sampled per assay and time point, resulting in multiple technical repeats despite there only being a single experimental repeat. A shortcoming in the present study, however, was the limitation in the number of bioreactors available for the study, thereby limiting the treatments and combinations that could be assessed. The maintenance of bioreactors and spheroids is a reagent-heavy process, increasing the experimental cost. Further, the time constraints of an MSc limited the repetition of this experiment as one experimental repeat takes over a month to complete.

The adenylate kinase assessment showed that there was initial cell damage, however the spheroids were able to acclimatise to the culturing conditions and were able to adapt to palmitate concentration used. Thereafter, the spheroids remained viable for an extended period. This is important in terms of highlighting the stark differences between acute and chronic models and their associated toxicity as the models provide different insights. In the present study, the addition of ATV at the concentrations tested induced severe toxicity which proved to be fatal to the spheroids, both alone and in combination with GRT.

This study has shown that 3D culturing technology can be used as a model, and the presence of tissue-specification specialisations, crucial to tissue functioning and cellular viability, means that data generated is likely to be more reliable than that of 2D culturing. This cellular specialisation allowed the spheroids to better adapt to the treatment environment created. Three-dimensional culturing, as an intermediate between *in vitro* and *in vivo* models, allows for refinement prior to *in vivo* experimentation in a model that is safer, more ethical to animals, as well as more cost-effective. Further, the 3D culturing technique allows for testing of drugs/substances in human-derived cells that express human metabolising enzymes such as CYP3A4. Rodents express a different isozyme of CYP3A, creating an uncertainty in the validity of assessing CYP3A metabolism in rodents and extrapolating the results to humans. The use of 3D culture and human-specific tissue narrows the translational gap between rodents and human metabolism of a drug/substance/ATV.

9 References

1. Abrahams, S., 2011. Gene expression of xenobiotic metabolising enzymes in rat liver and kidney: Differential effects of rooibos and honeybush herbal teas.

2. Abu Bakar, M.H., Tan, J.S., 2017. Improvement of mitochondrial function by celastrol in palmitate-treated C2C12 myotubes via activation of PI3K-Akt signaling pathway. Biomed. Pharmacother. 93, 903–912. https://doi.org/10.1016/j.biopha.2017.07.021

3. Adedinsewo, D., Taka, N., Agasthi, P., Sachdeva, R., Rust, G., Onwuanyi, A., 2016. Prevalence and Factors Associated With Statin Use Among a Nationally Representative Sample of US Adults: National Health and Nutrition Examination Survey, 2011-2012: Adedinsewo ET AL. Clin. Cardiol. 39, 491–496. https://doi.org/10.1002/clc.22577

4. Ahern, T.P., Lash, T.L., Damkier, P., Christiansen, P.M., Cronin-Fenton, D.P., 2014. Statins and breast cancer prognosis: Evidence and opportunities. Lancet Oncol. 15, e461–e468. https://doi.org/10.1016/S1470-2045(14)70119-6

5. Ajuwon, O.R. azaq, Oguntibeju, O.O. moniyi, Marnewick, J.L. ucasta, 2014. Amelioration of lipopolysaccharide-induced liver injury by aqueous rooibos (*Aspalathus linearis*) extract via inhibition of pro-inflammatory cytokines and oxidative stress. BMC Complement. Altern. Med. 14. https://doi.org/10.1186/1472-6882-14-392

6. Ajuwon, O.R., Katengua-Thamahane, E., Van Rooyen, J., Oguntibeju, O.O., Marnewick, J.L., 2013. Protective effects of rooibos (*Aspalathus linearis*) and/or red palm oil (*elaeis guineensis*) supplementation on *tert* -butyl hydroperoxide-induced oxidative hepatotoxicity in wistar rats. Evid. Based Complement. Alternat. Med. 2013. https://doi.org/10.1155/2013/984273

7. Akhmedov, D., Berdeaux, R., 2013. The effects of obesity on skeletal muscle regeneration. Front. Physiol. 4. https://doi.org/10.3389/fphys.2013.00371

8. Alkhouri, N., 2009. Lipotoxicity in nonalcoholic fatty liver disease: not all lipids are created equal. Expert Rev Gastroenterol Hepatol 3, 445–51. https://doi.org/10.1586/egh.09.32.Lipotoxicity

9. Alkhouri, N., Carter-Kent, C., Feldstein, A.E., 2011. Apoptosis in nonalcoholic fatty liver disease: diagnostic and therapeutic implications. Expert Rev. Gastroenterol. Hepatol. 5, 201–212. https://doi.org/10.1586/egh.11.6

10. Anton, D., Burckel, H., Josset, E., Noel, G., 2015. Three-dimensional cell culture: A breakthrough in vivo. Int. J. Mol. Sci. 16, 5517–5527. https://doi.org/10.3390/ijms16035517

11. Antwi-Baffour, S.S., Bello, A.I., Adjei, D.N., Mahmood, S.A., and Ayeh-Kumi, P.F., 2014. The Place of Traditional Medicine in the African Society: The Science, Acceptance and Support. American Journal of Health Research. Vol. 2, No. 2, 2014, pp. 49-54. doi: 10.11648/j.ajhr.20140202.13

12. Awortwe, C., Makiwane, M., Reuter, H., Muller, C., Louw, J., Rosenkranz, B., 2018. Critical Evaluation of Causality Assessment of Herb-Drug Interactions in Patients. Br. J. Clin. Pharmacol. 1–15. https://doi.org/10.1111/bcp.13490

13. Baek, H.W., Bae, S.K., Lee, M.G., Sohn, Y.T., 2006. Pharmacokinetics of chlorzoxazone in rats with diabetes: Induction of CYP2E1 on 6-hydroxychlorzoxazone formation. J. Pharm. Sci. 95, 2452–2462. https://doi.org/10.1002/jps.20698

14. Baquerizo, A., Bañares, R., Saliba, F., 2015. Current Clinical Status of the Extracorporeal Liver Support Devices. Elsevier, pp. 1463–1487. https://doi.org/10.1016/b978-1-4557-0268-8.00107-x

15. Barnett, C.R., Gibson, G.G., Wolf, C.R., Flatt, P.R., Ioannides, C., 1990. Induction of cytochrome P450III and P450IV family proteins in streptozotocin-induced diabetes. Biochem. J. 268, 765–9.

16. Barter, P.J., Caulfield, M., Eriksson, M., Grundy, S.M., Kastelein, J.J.P., Komajda, M., Lopez-Sendon, J., Mosca, L., Tardif, J.-C., Waters, D.D., Shear, C.L., Revkin, J.H., Buhr, K.A., Fisher, M.R., Tall, A.R., Brewer, B., 2007. Effects of Torcetrapib in Patients at High Risk for Coronary Events. New England Journal of Medicine 357, 2109–2122. https://doi.org/10.1056/NEJMoa0706628

17. Beltrán-Debón, R., Rull, A., Rodríguez-Sanabria, F., Iswaldi, I., Herranz-López, M., Aragonès, G., Camps, J., Alonso-Villaverde, C., Menéndez, J.A., Micol, V., Segura-Carretero, A., Joven, J., 2011. Continuous administration of polyphenols from aqueous rooibos (*Aspalathus linearis*) extract ameliorates dietary-induced metabolic disturbances in hyperlipidemic mice. Phytomedicine 18, 414–424. https://doi.org/10.1016/j.phymed.2010.11.008

18. Bhardwaj, R.K., 2002. Piperine, a Major Constituent of Black Pepper, Inhibits Human P-glycoprotein and CYP3A4. J. Pharmacol. Exp. Ther. 302, 645–650. https://doi.org/10.1124/jpet.102.034728

19. Björkhem-Bergman, L., Lindh, J.D., Bergman, P., 2011. What is a relevant statin concentration in cell experiments claiming pleiotropic effects? Br. J. Clin. Pharmacol. 72, 164–165. https://doi.org/10.1111/j.1365-2125.2011.03907.x

20. Björnsson, E., Jacobsen, E.I., Kalaitzakis, E., 2012. Hepatotoxicity associated with statins: Reports of idiosyncratic liver injury post-marketing. J. Hepatol. 56, 374–380. https://doi.org/10.1016/j.jhep.2011.07.023

21. Björnsson, E.S., 2016. Hepatotoxicity of statins and other lipid-lowering agents. Liver Int. 1–6. https://doi.org/10.1111/liv.13308

22. Borbás, T., Benko, B., Dalmadi, B., Szabó, I., Tihanyi, K., 2006. Insulin in flavin-containing monooxygenase regulation: Flavin-containing monooxygenase and cytochrome P450 activities in experimental diabetes. Eur. J. Pharm. Sci. 28, 51–58. https://doi.org/10.1016/j.ejps.2005.12.011

23. Borst, P., Elferink, R.O., 2002. Mammalian ABC Transporters in Health and Disease. Annual Review of Biochemistry 71, 537–592. https://doi.org/10.1146/annurev.biochem.71.102301.093055

24. Budzinski, J.W., Foster, B.C., Vandenhoek, S., Arnason, J.T., 2000. An in vitro evaluation of human cytochrome P450 3A4 inhibition by selected commercial herbal extracts and tinctures. Phytomedicine 7, 273–282. https://doi.org/10.1016/S0944-7113(00)80044-6

25. Bursill, C.A., Abbey, M., Roach, P.D., 2007. A green tea extract lowers plasma cholesterol by inhibiting cholesterol synthesis and upregulating the LDL receptor in the cholesterol-fed rabbit. Atherosclerosis 193, 86–93. https://doi.org/10.1016/j.atherosclerosis.2006.08.033

26. Calitz, C., Hamman, J.H., Fey, S.J., Wrzesinski, K., Gouws, C., 2018. Recent advances in three-dimensional cell culturing to assess liver function and dysfunction: from a drug biotransformation and toxicity perspective. Toxicol. Mech. Methods 0, 000. https://doi.org/10.1080/15376516.2017.1422580

27. Calitz, C., Plessis, L., Gouws, C., Steyn, D., Steenekamp, J., Muller, C., Hamman, S., 2015. Herbal hepatotoxicity: current status , examples , and challenges 1–15.

28. Canda, B.D., Oguntibeju, O.O., Marnewick, J.L., 2014. Effects of Consumption of Rooibos (Aspalathus *linearis*) and a Rooibos-Derived Commercial Supplement on Hepatic Tissue Injury by tert -Butyl Hydroperoxide in Wistar Rats 2014.

29. Cesaratto, L., Vascotto, C., Calligaris, S., Tell, G., 2004. The importance of redox state in liver damage. Ann. Hepatol. Off. J. Mex. Assoc. Hepatol. 3, 86–92.

30. Chan, L.M.., Lowes, S., Hirst, B.H., 2004. The ABCs of drug transport in intestine and liver: efflux proteins limiting drug absorption and bioavailability. European Journal of Pharmaceutical Sciences 21, 25–51. https://doi.org/10.1016/j.ejps.2003.07.003

31. Clarke, A.T., Mills, P.R., 2006. Atorvastatin associated liver disease. Dig. Liver Dis. 38, 772–777. https://doi.org/10.1016/j.dld.2006.04.013

32. Clarke AT, Johnson PCD, Hall GC, Ford I, Mills PR (2016) High Dose Atorvastatin Associated with Increased Risk of Significant Hepatotoxicity in Comparison to Simvastatin in UK GPRD Cohort. PLoS ONE 11(3): e0151587. doi:10.1371/journal.pone.0151587

33. Degli Esposti, D., Hamelin, J., Bosselut, N., Saffroy, R., Sebagh, M., Pommier, A., Martel, C., Lemoine, A., 2012. Mitochondrial roles and cytoprotection in chronic liver injury. Biochem. Res. Int. 2012. https://doi.org/10.1155/2012/387626

34. Deichmann, R., Lavie, C., Andrews, S., 2010. Coenzyme Q10 and Statin-Induced Mitochondrial Dysfunction. Ochsner J. 10, 16–21.

35. Del Rio, D., Rodriguez-Mateos, A., Spencer, J.P.E., Tognolini, M., Borges, G., Crozier, A., 2013. Dietary (Poly)phenolics in Human Health: Structures, Bioavailability, and Evidence of Protective Effects Against Chronic Diseases. Antioxidants & Redox Signaling 18, 1818–1892. https://doi.org/10.1089/ars.2012.4581

36. Di Lisa, F., Blank, P.S., Colonna, R., Gambassi, G., Silverman, H.S., Stern, M.D., Hansford, R.G., 1995. Mitochondrial membrane potential in single living adult rat cardiac myocytes exposed to anoxia or metabolic inhibition. J Physiol 486 (Pt 1, 1–13.

37. Dludla, P.V., Muller, C.J.F., Louw, J., Joubert, E., Salie, R., Opoku, A.R., Johnson, R., 2014. The cardioprotective effect of an aqueous extract of fermented rooibos (Aspalathus linearis) on cultured cardiomyocytes derived from diabetic rats. Phytomedicine 21, 595–601. https://doi.org/10.1016/j.phymed.2013.10.029

38. Docrat, T.F., Nagiah, S., Krishnan, A., Naidoo, D.B., Chuturgoon, A.A., 2018. Atorvastatin induces MicroRNA-145 expression in HEPG2 cells via regulation of the PI3K/AKT signalling pathway. Chem. Biol. Interact. 287, 32–40. https://doi.org/10.1016/j.cbi.2018.04.005

39. Edmondson, R., Broglie, J.J., Adcock, A.F., Yang, L., 2014. Three-dimensional cell culture systems and their applications in drug discovery and cell-based biosensors. Assay Drug Dev. Technol. 12, 207–18. https://doi.org/10.1089/adt.2014.573

40. Egnatchik, R.A., Leamy, A.K., Jacobson, D.A., Shiota, M., Young, J.D., 2014. ER calcium release promotes mitochondrial dysfunction and hepatic cell lipotoxicity in response to palmitate overload. Molecular Metabolism 3, 544–553. https://doi.org/10.1016/j.molmet.2014.05.004

41. Engels, M., Wang, C., Matoso, A., Maidan, E., Wands, J., 2013. Tea not tincture: hepatotoxicity associated with Rooibos herbal tea. ACG Case Rep. J. 1, 58–60. https://doi.org/10.14309/crj.2013.20.

42. Feldstein, A.E., Werneburg, N.W., Canbay, A., Guicciardi, M.E., Bronk, S.F., Rydzewski, R., Burgart, L.J., Gores, G.J., 2004. Free fatty acids promote hepatic lipotoxicity by stimulating TNF-α expression via a lysosomal pathway. Hepatology 40, 185–194. https://doi.org/10.1002/hep.20283

43. *Forbes*, 2018. King, S. 07/15/2013. The Best Selling Drugs Since 1996 - Why AbbVie's Humira Is Set To Eclipse Pfizer's Lipitor, available at: https://www.forbes.com/sites/simonking/2013/07/15/the-best-selling-drugs-since-1996-why-abbvies-humira-is-set-to-eclipse-pfizers-lipitor/#6f49ab996a8d

44. Fugh-Berman, A., 2000. Herb-drug interactions. Lancet 355, 134–138. https://doi.org/10.1016/S0140-6736(99)06457-0

45. Gelderblom, W.C.A., Joubert, E., Gamieldien, K., Sissing, L., Malherbe, C.J., Maritz, G., 2017. Rooibos (*Aspalathus linearis*), honeybush (*Cyclopia intermedia*) and cancer bush (*Sutherlandia frutescens* subsp. *microphylla*) protect against tobacco-specific mutagenesis in vitro. South Afr. J. Bot. 110, 194–200. https://doi.org/10.1016/j.sajb.2016.06.004

46. Giboney, P.T., 2005. Mildly Elevated Liver Transaminase Levels in the Asymptomatic Patient 71, 6.

47. Gouws, C., Hamman, J.H., 2018. Recent developments in our understanding of the implications of traditional African medicine on drug metabolism. Expert Opin. Drug Metab. Toxicol. 14. https://doi.org/10.1080/17425255.2018.1421171

48. Gum, S.I., Nguyen, P.A., Lee, J.R., Han, Y.H., Cho, M.K., 2017. The physico-chemical alteration of lovastatin and enhanced antioxidant effect of Bacillus subtilis fermented-red yeast rice product. Food Chem. 232, 203–209. https://doi.org/10.1016/j.foodchem.2017.04.023

49. Hayat, M.A., 1986. Preface, in: Hayat, M.A. (Ed.), Basic Techniques for Transmission Electron Microscopy. Academic Press, pp. xxv–xxvii. https://doi.org/10.1016/B978-0-12-333926-3.50003-8

50. Hillis, W.E., Inoue, T., 1967. The polyphenols of Nothofagus species—II.The heartwood of *Nothofagus fusca*. Phytochemistry 6, 59–67. https://doi.org/10.1016/0031-9422(67)85008-8

51. Ho, R., Kim, R., 2005. Transporters and drug therapy: Implications for drug disposition and disease. Clinical Pharmacology & Therapeutics 78, 260–277. https://doi.org/10.1016/j.clpt.2005.05.011

52. Hoffart, E., Ghebreghiorghis, L., Nussler, A.K., Thasler, W.E., Weiss, T.S., Schwab, M., Burk, O., 2012. Effects of atorvastatin metabolites on induction of drug-metabolizing enzymes and membrane transporters through human pregnane X receptor. Br. J. Pharmacol. 165, 1595–1608. https://doi.org/10.1111/j.1476-5381.2011.01665.x

53. Houten, S.M., Wanders, R.J.A., 2010. A general introduction to the biochemistry of mitochondrial fatty acid β-oxidation. J. Inherit. Metab. Dis. 33, 469–477. https://doi.org/10.1007/s10545-010-9061-2

54. Hu, N., Hu, M., Duan, R., Liu, C., Guo, H., Zhang, M., … Liu, X. (2014). Increased levels of fatty acids contributed to induction of hepatic CYP3A4 activity induced by diabetes - *in vitro* evidence from HepG2 cell and Fa2N-4 cell lines. Journal of Pharmacological Science, 124(4), 433–444. https://doi.org/10.1254/jphs.13212FP

55. Huang, C.F., Gan†, X.W., Bai, H.Y., Ma, L., Hu, L.H., 2008. Schoepfin A, B, C: three new chalcone C-glycosides from *Schoepfia chinensis*. Nat. Prod. Res. 22, 623–627. https://doi.org/10.1080/14786410701614184

56. Jiménez-Santos, M.A., Juárez-Rojop, I.E., Tovilla-Zárate, C.A., Espinosa-García, M.T., Juárez-Oropeza, M.A., Ramón-Frías, T., Bermúdez-Ocaña, D.Y., Díaz-Zagoya, J.C., 2014. Coenzyme Q10 supplementation improves metabolic parameters, liver function and mitochondrial respiration in rats with high doses of atorvastatin and a cholesterol-rich diet. Lipids Health Dis. 13, 22. https://doi.org/10.1186/1476-511X-13-22

57. Jodoin, J., Demeule, M., Béliveau, R., 2002. Inhibition of the multidrug resistance P-glycoprotein activity by green tea polyphenols. Biochim. Biophys. Acta - Mol. Cell Res. 1542, 149–159. https://doi.org/10.1016/S0167-4889(01)00175-6

58. Johnson, R., Dludla, P., Joubert, E., February, F., Mazibuko, S., Ghoor, S., Muller, C., Louw, J., 2016. Aspalathin, a dihydrochalcone *C*-glucoside, protects H9c2 cardiomyocytes against high glucose induced shifts in substrate preference and apoptosis. Mol. Nutr. Food Res. 60, 922–934. https://doi.org/10.1002/mnfr.201500656

59. Joubert, E., de Beer, D., 2011. Rooibos (*Aspalathus linearis*) beyond the farm gate: From herbal tea to potential phytopharmaceutical. South Afr. J. Bot. 77, 869–886. https://doi.org/10.1016/j.sajb.2011.07.004

60. Kalyanaraman, B., Darley-Usmar, V., Davies, K., Dennery, P., Forman, H., Grisham, M., Mann, G., Moore, K., Roberts II, L., Ischiropoulos, H., 2012. Measuring reactive oxygen and nitrogen species with fluorescent probes: challenges and limitations. Free Radic Biol Med 52, 1–6. https://doi.org/10.1016/j.freeradbiomed.2011.09.030.Measuring

61. Kamakura, R., Son, M.J., de Beer, D., Joubert, E., Miura, Y., Yagasaki, K., 2015. Antidiabetic effect of green rooibos (*Aspalathus linearis*) extract in cultured cells and type 2 diabetic model KK-Ay mice. Cytotechnology 67. https://doi.org/10.1007/s10616-014-9816-y

62. Kawano, A., Nakamura, H., Hata, S. ichi, Minakawa, M., Miura, Y., Yagasaki, K., 2009. Hypoglycemic effect of aspalathin, a rooibos tea component from *Aspalathus linearis*, in type 2 diabetic model db/db mice. Phytomedicine 16, 437–443. https://doi.org/10.1016/j.phymed.2008.11.009

63. Kim, D., Choi, B., Ku, S.-K., Park, J., Oh, E., Kwak, M.-K., 2016. Beneficial Effects of Sarpogrelate and Rosuvastatin in High Fat Diet/Streptozotocin-Induced Nephropathy in Mice. PLOS ONE 11, e0153965. https://doi.org/10.1371/journal.pone.0153965

64. Kinae, N., Shimoi, K., Masumori, S., Harusawa, M., Furugori, M., 1994. Suppression of the Formation of Advanced Glycosylation Products by Tea Extracts, in: Ho, C.-T., Osawa, T., Huang, M.-T., Rosen, R.T. (Eds.), Food Phytochemicals for Cancer Prevention II. American Chemical Society, Washington, DC, pp. 68–75. https://doi.org/10.1021/bk-1994-0547.ch007

65. Knutsen, H.K. et al., 2017. Risks for human health related to the presence of pyrrolizidine alkaloids in honey, tea, herbal infusions and food supplements. *EFSA Journal*, 15(7). Available at: http://doi.wiley.com/10.2903/j.efsa.2017.4908.

66. Kocaman, O., Hulagu, S., Senturk, O., 2008. Echinacea-induced severe acute hepatitis with features of cholestatic autoimmune hepatitis. European Journal of Internal Medicine 19, 148. https://doi.org/10.1016/j.ejim.2007.04.014

67. Koh, K.K., Sakuma, I., Quon, M.J., 2011. Differential metabolic effects of distinct statins. Atherosclerosis 215, 1–8. https://doi.org/10.1016/j.atherosclerosis.2010.10.036

68. Köhler, C., Gahm, A., Noma, T., Nakazawa, A., Orrenius, S., and Zhivotovsky, B., 1999. Release of adenylate kinase 2 from the mitochondrial intermembrane space during apoptosis. FEBS Letters 447 (1999) 10-12

69. Koo, S.I. & Noh, S.K. (2007). Green tea as inhibitor of the intestinal absorption of lipids: potential mechanism for its lipid-lowering effect. *Journal of Nutritional Biochemistry,* 18(3), 179-183.

70. Kucharská, J., Uličná, O., Gvozdjáková, A., Sumbalová, Z., Vančová, O., Božek, P., Nakano, M., Greksák, M., 2004. Regeneration of coenzyme Q9 redox state and inhibition of oxidative stress by Rooibos tea (*Aspalathus linearis*) administration in carbon tetrachloride liver damage. Physiol. Res. 53, 515–521.

71. Kullak-Ublick, G.A., Ismair, M.G., Stieger, B., Landmann, L., Huber, R., Pizzagalli, F., Fattinger, K., Meier, P.J., Hagenbuch, B., 2001. Organic anion-transporting polypeptide B (OATP-B) and its functional comparison with three other OATPs of human liver. Gastroenterology 120, 525–533. https://doi.org/10.1053/gast.2001.21176

72. Kwakye, G.F., Jiménez, J., Jiménez, J.A., Aschner, M., 2018. *Atropa belladonna* neurotoxicity: Implications to neurological disorders. Food Chem. Toxicol. 116, 346–353. https://doi.org/10.1016/j.fct.2018.04.022

73. The Lancet, 2011. Lessons from Lipitor and the broken blockbuster drug model. The Lancet 378, 1976. https://doi.org/10.1016/S0140-6736(11)61858-8

74. Lea, A.P., McTavish, D., 1997. Atorvastatin. Drugs 53, 828–847. https://doi.org/10.2165/00003495-199753050-00011

75. Lee, J., Lee, M.S., Nam, K.W., 2014. Acute Toxic Hepatitis Caused by an *Aloe Vera* Preparation in a Young Patient: A Case Report with a Literature Review. The Korean Journal of Gastroenterology 64, 54. https://doi.org/10.4166/kjg.2014.64.1.54

76. Lee, W., Bae, J.S., 2015. Anti-inflammatory Effects of Aspalathin and Nothofagin from Rooibos (*Aspalathus linearis*) *In Vitro* and *In Vivo*. Inflammation 38, 1502–1516. https://doi.org/10.1007/s10753-015-0125-1

77. Lennernas, H., n.d. Clin Pharmacokinet 2003; 42 (13): 1141-1160. Clin Pharmacokinet 20.

78. Li, S., Tan, H.-Y., Wang, N., Zhang, Z.-J., Lao, L., Wong, C.-W., Feng, Y., 2015. The Role of Oxidative Stress and Antioxidants in Liver Diseases. Int. J. Mol. Sci. 16, 26087–26124. https://doi.org/10.3390/ijms161125942

79. Li, Y., Park, J.-S., Deng, J.-H., Bai, Y., 2006. Cytochrome c Oxidase Subunit IV is Essential for Assembly and Respiratory Function of the Enzyme Complex. J. Bioenerg. Biomembr. 38, 283–291. https://doi.org/10.1007/s10863-006-9052-z

80. Li, Z., Berk, M., McIntyre, T.M., Gores, G.J., Feldstein, A.E., 2008. The lysosomal-mitochondrial axis in free fatty acid–induced hepatic lipotoxicity. Hepatology 47, 1495–1503. https://doi.org/10.1002/hep.22183

81. Lin, J.H., Lu, A.Y.H., 1998. Inhibition and Induction of Cytochrome P450 and the Clinical Implications: Clinical Pharmacokinetics 35, 361–390. https://doi.org/10.2165/00003088-199835050-00003

82. Lodish, H., Berk, A., Zipursky, S.L., Matsudaira, P., Baltimore, D., Darnell, J., 2000. Electron Transport and Oxidative Phosphorylation. Mol. Cell Biol. 4th Ed.

83. Lu, C., Li, A.P., 2001. Species comparison in P450 induction: effects of dexamethasone, omeprazole, and rifampin on P450 isoforms 1A and 3A in primary cultured hepatocytes

from man, Sprague–Dawley rat, minipig, and beagle dog. Chemico-Biological Interactions 134, 271–281. https://doi.org/10.1016/S0009-2797(01)00162-4

84. Ly, L.D., Xu, S., Choi, S.-K., Ha, C.-M., Thoudam, T., Cha, S.-K., Wiederkehr, A., Wollheim, C.B., Lee, I.-K., Park, K.-S., 2018. Oxidative stress and calcium dysregulation by palmitate in type 2 diabetes. Experimental & Molecular Medicine 49, e291. https://doi.org/10.1038/emm.2016.157

85. Marnewick, J.L., Joubert, E., Swart, P., van der Westhuizen, F., Gelderblom, W.C., 2003. Modulation of hepatic drug metabolism enzymes and oxidative status by rooibos (*Aspalathus linearis*) tea, honeybush (*Cyclopia intermedia*) tea, as well as green and black (*Camellia sinensis*) teas in rats. J. Agric. Food Chem. 51, 8113–8119. https://doi.org/10.1021/jf0344643

86. Marnewick, J.L., Rautenbach, F., Venter, I., Neethling, H., Blackhurst, D.M., Wolmarans, P., MacHaria, M., 2011. Effects of rooibos (*Aspalathus linearis*) on oxidative stress and biochemical parameters in adults at risk for cardiovascular disease. J. Ethnopharmacol. 133, 46–52. https://doi.org/10.1016/j.jep.2010.08.061

87. Matsuda, K., Nishimura, Y., Kurata, N., Iwase, M., Yasuhara, H., 2007. Effects of continuous ingestion of herbal teas on intestinal CYP3A in the rat. J. Pharmacol. Sci. 103, 214–221. https://doi.org/10.1254/jphs.FP0061311

88. Mazibuko, S.E., Joubert, E., Johnson, R., Louw, J., Opoku, A.R., Muller, C.J.F., 2015. Aspalathin improves glucose and lipid metabolism in 3T3-L1 adipocytes exposed to palmitate. Mol. Nutr. Food Res. 59, 2199–2208. https://doi.org/10.1002/mnfr.201500258

89. Mazibuko, S.E., Muller, C.J.F., Joubert, E., De Beer, D., Johnson, R., Opoku, A.R., Louw, J., 2013. Amelioration of palmitate-induced insulin resistance in C2C12 muscle cells by rooibos (*Aspalathus linearis*). Phytomedicine 20, 813–819. https://doi.org/10.1016/j.phymed.2013.03.018

90. McKay, D.L., Blumberg, J.B., 2009. A Review of the Bioactivity of South African Herbal Teas: Rooibos (*Aspalathus linearis*) and Honeybush (Cyclopia intermedia). Phytother. Res. 22, 557–559. https://doi.org/10.1002/ptr

91. Mertens-Talcott, S.U., Zadezensky, I., Castro, W.V.D., Derendorf, H., Butterweck, V., 2006. Grapefruit-Drug Interactions: Can Interactions With Drugs Be Avoided? The Journal of Clinical Pharmacology 46, 1390–1416. https://doi.org/10.1177/0091270006294277

92. Michalik, M., Soczek, E., Kosińska, M., Rak, M., Wójcik, K.A., Lasota, S., Pierzchalska, M., Czyz, J., Madeja, Z., 2013. Lovastatin-induced decrease of intracellular cholesterol level attenuates fibroblast-to-myofibroblast transition in bronchial fibroblasts derived from asthmatic patients. Eur. J. Pharmacol. 704, 23–32. https://doi.org/10.1016/j.ejphar.2013.02.023

93. Mira, E., Carmona-Rodríguez, L., Tardáguila, M., Azcoitia, I., González-Martín, A., Almonacid, L., Casas, J., Fabriás, G., Mañes, S., 2013. A lovastatin-elicited genetic program inhibits M2 macrophage polarization and enhances T cell infiltration into spontaneous mouse mammary tumors. Oncotarget 4, 2288–2301. https://doi.org/10.18632/oncotarget.1376

94. Monsees, T.K., Opuwari, C.S., 2017. Effect of rooibos (*Aspalathus linearis*) on the female rat reproductive tract and liver and kidney functions in vivo. South Afr. J. Bot. 110, 208–215. https://doi.org/10.1016/j.sajb.2016.11.013

95. Mooradian, A., 2009. Dyslipidemia in type 2 diabetes mellitus. Nat. Clin. Pract. Endocrinol. Metab. 5, 150–9. https://doi.org/10.1038/ncpendmet

96. Mosmann, T., 1983. Rapid colorimetric assay for cellular growth and survival: Application to proliferation and cytotoxicity assays. J. Immunol. Methods 65, 55–63. https://doi.org/10.1016/0022-1759(83)90303-4

97. Muller, C.J.F., Joubert, E., De Beer, D., Sanderson, M., Malherbe, C.J., Fey, S.J., Louw, J., 2012. Acute assessment of an aspalathin-enriched green rooibos (*Aspalathus linearis*) extract with hypoglycemic potential. Phytomedicine 20, 32–39. https://doi.org/10.1016/j.phymed.2012.09.010

98. Na, D.H., Ji, H.Y., Park, E.J., Kim, M.S., Liu, K.H., Lee, H.S., 2011. Evaluation of metabolism-mediated herb-drug interactions. Arch. Pharm. Res. 34, 1829–1842. https://doi.org/10.1007/s12272-011-1105-0

99. Nehra, V., Angulo, P., Buchman, A.L., Lindor, K.D., 2001. Nutritional and Metabolic Considerations in the Etiology of Nonalcoholic Steatohepatitis. Dig. Dis. Sci. 46, 6.

100. Nobuo, S., 1994. Cytochrome P450 changes in rats with streptozocin-induced diabetes. Int. J. Biochem. 26, 1261–1268. https://doi.org/10.1016/0020-711x(94)90095-7

101. Olsson, T., Gulliksson, H., Palmeborn, M., Bergström, K., and Thore, A. (1983). Leakage of adenylate kinase from stored blood cells. Journal of Applied Biochemistry. Dec: 5(6), pp. 437-445.

102. Ott, M., Fricker, G., Bauer, B., 2009. Pregnane X Receptor (PXR) Regulates P-Glycoprotein at the Blood-Brain Barrier: Functional Similarities between Pig and Human PXR. J. Pharmacol. Exp. Ther. 329, 141–149. https://doi.org/10.1124/jpet.108.149690

103. Pal, S., Ghosh, M., Ghosh, S., Bhattacharyya, S., Sil, P.C., 2015. Atorvastatin induced hepatic oxidative stress and apoptotic damage via MAPKs, mitochondria, calpain and caspase12 dependent pathways. Food Chem. Toxicol. 83, 36–47. https://doi.org/10.1016/j.fct.2015.05.016

104. Patel, J., Buddha, B., Dey, S., Pal, D., Mitra, A.K., 2004. In Vitro Interaction of the HIV Protease Inhibitor Ritonavir with Herbal Constituents: Changes in P-gp and CYP3A4 Activity 277, 262–277.

105. Patel, O., Muller, C., Joubert, E., Louw, J., Rosenkranz, B., Awortwe, C., 2016. Inhibitory interactions of *Aspalathus linearis* (rooibos) extracts and compounds, aspalathin and Z-2-(??-D-glucopyranosyloxy)-3-phenylpropenoic acid, on cytochromes metabolizing hypoglycemic and hypolipidemic drugs. Molecules 21, 1–13. https://doi.org/10.3390/molecules21111515

106. Patil L, Kulkarni K, Khanvilkar V, et al. *In vitro* evaluation of herb-drug interactions: a review. Int J Pharm Pharm Sci. 2014; 6:9-12

107. Phulukdaree, A., Moodley, D., Khan, S., Chuturgoon, A.A., 2015. Atorvastatin Increases miR-124a Expression: A Mechanism of Gamt Modulation in Liver Cells. J. Cell. Biochem. 116, 2620–2627. https://doi.org/10.1002/jcb.25209

108. Plant, N., 2007. The human cytochrome P450 sub-family: Transcriptional regulation, inter-individual variation and interaction networks. Biochim. Biophys. Acta - Gen. Subj. 1770, 478–488. https://doi.org/10.1016/j.bbagen.2006.09.024

109. Rai, Y., Pathak, R., Kumari, N., Sah, D.K., Pandey, S., Kalra, N., Soni, R., Dwarakanath, B.S., Bhatt, A.N., 2018. Mitochondrial biogenesis and metabolic hyperactivation limits the application of MTT assay in the estimation of radiation induced growth inhibition. Sci. Rep. 8, 1531. https://doi.org/10.1038/s41598-018-19930-w

110. Reers, M., Smith, T.W., Chen, L.B., 1991. J-Aggregate Formation of a Carbocyanine as a Quantitative Fluorescent Indicator of Membrane Potential. Biochemistry 30, 4480–4486. https://doi.org/10.1021/bi00232a015

111. Research and Markets, 2018. Global Nutraceutical Ingredients Market Analysis & Trends - Industry Forecast to 2025; ID: 4115183, February 2018.

112. Savas, U., Griffin, K.J., Johnson, E.F., 1999. Molecular mechanisms of cytochrome P-450 induction by xenobiotics: An expanded role for nuclear hormone receptors. Mol. Pharmacol. 56, 851–7.

113. Schaefer, E.J., Asztalos, B.F., 2006. The effects of statins on high-density lipoproteins. Curr. Atheroscler. Rep. 8, 41–49. https://doi.org/10.1007/s11883-006-0063-3

114. Schenk, S., Saberi, M., Olefsky, J.M., 2008. Insulin sensitivity: Modulation by nutrients and inflammation. J. Clin. Invest. 118, 2992–3002. https://doi.org/10.1172/JCI34260

115. Selzner, M., RüDiger, H.A., Sindram, D., Madden, J., Clavien, P.-A., 2000. Mechanisms of ischemic injury are different in the steatotic and normal rat liver. Hepatology 32, 1280–1288. https://doi.org/10.1053/jhep.2000.20528

116. Shu, N., Hu, M., Ling, Z., Liu, P., Wang, F., Xu, P., Zhong, Z., Sun, B., Zhang, M., Li, F., Xie, Q., Liu, X., Liu, L., 2016a. The enhanced atorvastatin hepatotoxicity in diabetic rats was partly attributed to the upregulated hepatic Cyp3a and SLCO1B1. Sci. Rep. 6, 33072. https://doi.org/10.1038/srep33072

117. Shu, N., Hu, M., Liu, C., Zhang, M., Ling, Z., Zhang, J., Xu, P., Zhong, Z., Chen, Y., Liu, L., Liu, X., 2016b. Decreased exposure of atorvastatin in diabetic rats partly due to induction of hepatic Cyp3a and Oatp2. Xenobiotica Fate Foreign Compd. Biol. Syst. 8254, 1–7. https://doi.org/10.3109/00498254.2016.1141437

118. Singh, D.K., Banerjee, S., Porter, T.D., 2009. Green and black tea extracts inhibit HMG-CoA reductase and activate AMP kinase to decrease cholesterol synthesis in hepatoma cells. J. Nutr. Biochem. 20, 816–822. https://doi.org/10.1016/j.jnutbio.2008.07.011

119. Single, B., Leist, M., Nicotera, P., 1998. Simultaneous release of adenylate kinase and cytochrome c in cell death. Cell Death Differ. 5, 1001–1003. https://doi.org/10.1038/sj.cdd.4400462

120. Sinisalo, M., Enkovaara, A.L., Kivistö, K.T., 2010. Possible hepatotoxic effect of rooibos tea: A case report. Eur. J. Clin. Pharmacol. 66, 427–428. https://doi.org/10.1007/s00228-009-0776-7

121. Son, M.J., Minakawa, M., Miura, Y., Yagasaki, K., 2013. Aspalathin improves hyperglycemia and glucose intolerance in obese diabetic ob/ob mice. Eur. J. Nutr. 52, 1607–1619. https://doi.org/10.1007/s00394-012-0466-6

122. Soory, M., 2009. Relevance of nutritional antioxidants in metabolic syndrome, ageing and cancer: potential for therapeutic targeting. Infect. Disord. Drug Targets 9, 400–414. https://doi.org/10.2174/187152609788922537

123. Thomford, N.E., Awortwe, C., Dzobo, K., Adu, F., Chopera, D., Wonkam, A., Skelton, M., Blackhurst, D., and Dandara, C., 2016. Inhibition of CYP2B6 by Medicinal Plant Extracts: Implication for Use of Efavirenz and Nevirapine-Based Highly Active Anti-

Retroviral Therapy (HAART) in Resource-Limited Settings. *Molecules.* 21, 211; doi:10.3390/molecules21020211

124. Tolosa, L., Carmona, A., Castell, J.V., Gómez-Lechón, M.J., Donato, M.T., 2015. High-content screening of drug-induced mitochondrial impairment in hepatic cells: effects of statins. Arch. Toxicol. 89, 1847–1860. https://doi.org/10.1007/s00204-014-1334-3

125. Ulicná, O., Greksák, M., Vancová, O., Zlatos, L., Galbavý, S., Bozek, P., Nakano, M., 2003. Hepatoprotective effect of rooibos tea (*Aspalathus linearis*) on CCl4-induced liver damage in rats. Physiol. Res. Acad. Sci. Bohemoslov. 52, 461–466.

126. Uličná, O., Vančová, O., Božek, P., Čársky, J., Šebeková, K., Boor, P., Nakano, M., Greksák, M., 2006. Rooibos tea (*Aspalathus linearis*) partially prevents oxidative stress in streptozotocin-induced diabetic rats. Physiol. Res. 55, 157–164. https://doi.org/778 [pii]

127. Unger, R.H., Scherer, P.E., 2010. Gluttony, Sloth and the Metabolic Syndrome: A Roadmap to Lipotoxicity. Trends Endocrinol. Metab. TEM 21, 345–352. https://doi.org/10.1016/j.tem.2010.01.009

128. Van Engeland, M., Ramaekers, F.C.S., Schutte, B., Reutelingsperger, C.P.M., 1996. A novel assay to measure loss of plasma membrane asymmetry during apoptosis of adherent cells in culture. Cytometry 24, 131–139. https://doi.org/10.1002/(SICI)1097-0320(19960601)24:2<131::AID-CYTO5>3.0.CO;2-M

129. Van Wyk, B.E., Stander, M.A. & Long, H.S., 2017. *Senecio angustifolius* as the major source of pyrrolizidine alkaloid contamination of rooibos tea (*Aspalathus linearis*). *South African Journal of Botany*, 110, pp.124–131. Available at: http://dx.doi.org/10.1016/j.sajb.2017.01.013.

130. Vermes, I., Clemens, Haanen, C., Steffens-Nakken, H., & Reutelingsperger, C., 1995. A novel assay for apoptosis Flow cytometric detection of phosphatidylserine early apoptotic cells using fluorescein labelled expression on Annexin V. Ournal Immunol. Methods 184, 39–51.

131. Vrbanac, J., Slauter, R., 2017. ADME in Drug Discovery, in: A Comprehensive Guide to Toxicology in Nonclinical Drug Development. Elsevier, pp. 39–67. https://doi.org/10.1016/B978-0-12-803620-4.00003-7

132. Walsh, J.G., Cullen, S.P., Sheridan, C., Luthi, A.U., Gerner, C., Martin, S.J., 2008. Executioner caspase-3 and caspase-7 are functionally distinct proteases. Proc. Natl. Acad. Sci. 105, 12815–12819. https://doi.org/10.1073/pnas.0707715105

133. Wang, D., Wei, Y., Pagliassotti, M.J., 2006. Saturated Fatty Acids Promote Endoplasmic Reticulum Stress and Liver Injury in Rats with Hepatic Steatosis. Endocrinology 147, 943–951. https://doi.org/10.1210/en.2005-0570

134. Wang, H. J., Park, J. Y., Kwon, O., Choe, E. Y., Kim, C. H., Hur, K. Y., … Kang, E. S. (2015). Chronic HMGCR/HMG-CoA reductase inhibitor treatment contributes to dysglycemia by upregulating hepatic gluconeogenesis through autophagy induction. *Autophagy*, *11*(11), 2089–2101. https://doi.org/10.1080/15548627.2015.1091139

135. Wang, Y., Hekimi, S., 2016. Understanding Ubiquinone. Trends Cell Biol. 26, 367–378. https://doi.org/10.1016/j.tcb.2015.12.007

136. Wei, Y., Wang, D., Pagliassotti, M.J., 2007. Saturated fatty acid-mediated endoplasmic reticulum stress and apoptosis are augmented by trans-10, cis-12-conjugated linoleic acid in liver cells. Mol. Cell. Biochem. 303, 105–113. https://doi.org/10.1007/s11010-007-9461-2

137. Wei, Y., Wang, D., Topczewski, F., Pagliassotti, M.J., 2006. Saturated fatty acids induce endoplasmic reticulum stress and apoptosis independently of ceramide in liver cells. Am. J. Physiol.-Endocrinol. Metab. 291, E275–E281. https://doi.org/10.1152/ajpendo.00644.2005

138. Westerink, W.M.A., Schoonen, W.G.E.J., 2007. Cytochrome P450 enzyme levels in HepG2 cells and cryopreserved primary human hepatocytes and their induction in HepG2 cells. Toxicol. In Vitro 21, 1581–1591. https://doi.org/10.1016/j.tiv.2007.05.014

139. Wrzesinski, K., Fey, S., 2018. Metabolic Reprogramming and the Recovery of Physiological Functionality in 3D Cultures in Micro-Bioreactors. Bioengineering 5, 22. https://doi.org/10.3390/bioengineering5010022

140. Wetzel, L.T., Luempert, L.G., Breckenridge, C.B., Tisdel, M.O., Stevens, J.T., Thakur, A.K., Extrom, P.J., Eldridge, J.C., 1994. Chronic effects of atrazine on estrus and mammary tumor formation in female Sprague-Dawley and Fischer 344 rats. J Toxicol Environ Health 43, 169–182. https://doi.org/10.1080/15287399409531913

141. World Health Organization - Noncommunicable Diseases (NCD) Country Profiles, 2018, South Africa. Available at: http://www.who.int/nmh/countries/zaf_en.pdf?ua=1

142. Wrzesinski, K., Magnone, M.C., Hansen, L.V., Kruse, M.E., Bergauer, T., Bobadilla, M., Gubler, M., Mizrahi, J., Zhang, K., Andreasen, C.M., Joensen, K.E., Andersen, S.M., Olesen, J.B., Schaffalitzky de Muckadell, O.B., Fey, S.J., 2013. HepG2/C3A 3D spheroids exhibit stable physiological functionality for at least 24 days after recovering from trypsinisation. Toxicol. Res. 2, 163. https://doi.org/10.1039/c3tx20086h

143. Wrzesinski, K., Rogowska-Wrzesinska, A., Kanlaya, R., Borkowski, K., Schwämmle, V., Dai, J., Joensen, K.E., Wojdyla, K., Carvalho, V.B., Fey, S.J., 2014. The cultural divide: Exponential growth in classical 2D and metabolic equilibrium in 3D environments. PLoS ONE 9. https://doi.org/10.1371/journal.pone.0106973

144. Xu, D., Li, F., Zhang, M., Zhang, J., Liu, C., Hu, M., Zhong, Z., Jia, L., Wang, D., Wu, J., Liu, L., Liu, X., 2014. Decreased exposure of simvastatin and simvastatin acid in a rat model of type 2 diabetes. Acta Pharmacol. Sin. 35, 1215–1225. https://doi.org/10.1038/aps.2014.39

145. Yang, H.N., Kim, D.J., Kim, Y.M., Kim, B.H., Sohn, K.M., Choi, M.J., Choi, Y.H., 2010. Aloe-induced Toxic Hepatitis. J Korean Med Sci 25, 492–495. https://doi.org/10.3346/jkms.2010.25.3.492

146. Yang, S., Zhu, H., Li, Y., Lin, H., Gabrielson, K., Trush, M.A., Diehl, A.M., 2000. Mitochondrial Adaptations to Obesity-Related Oxidant Stress. Arch. Biochem. Biophys. 378, 259–268. https://doi.org/10.1006/abbi.2000.1829

147. Youssef, S., Stüve, O., Patarroyo, J.C., Ruiz, P.J., Radosevich, J.L., Hur, E.M., Bravo, M., Mitchell, D.J., Sobel, R.A., Steinman, L., Zamvil, S.S., 2002. The HMG-CoA reductase inhibitor, atorvastatin, promotes a Th2 bias and reverses paralysis in central nervous system autoimmune disease. Nature 420, 78–84. https://doi.org/10.1038/nature01158

148. Yu, C. K., Ae, K. L., Joo, H. L., Lee, I., Duk, C. L., So, H. K., … Myung, G. L. (2005). Pharmacokinetics of theophylline in diabetes mellitus rats: Induction of CYP1A2 and CYP2E1 on 1,3-dimethyluric acid formation. *European Journal of Pharmaceutical Sciences*, *26*(1), 114–123. https://doi.org/10.1016/j.ejps.2005.05.004

149. Zezina, E., Snodgrass, R.G., Schreiber, Y., Zukunft, S., Schürmann, C., Heringdorf, D.M. zu, Geisslinger, G., Fleming, I., Brandes, R.P., Brüne, B., Namgaladze, D., 2018. Mitochondrial fragmentation in human macrophages attenuates palmitate-induced inflammatory responses. Biochim. Biophys. Acta - Mol. Cell Biol. Lipids 1863, 433–446. https://doi.org/10.1016/j.bbalip.2018.01.009

150. Zhang, H., Plutzky, J., Skentzos, S., Morrison, F., Mar, P., Shubina, M., Turchin, A., 2013. Discontinuation of statins in routine care settings. Ann Intern Med 158, 526–534. https://doi.org/10.7326/0003-4819-158-7-201304020-00004

10 Supplementary Data

Table 10-1: Quantification of JC-1 FACS analysis in the normal condition. *C3A cells were exposed to various treatments and combinations (24 hours). Vehicle control = media with 0.25% DMSO; GRT1 = 0.01 mg/mL; GRT2 = and 0.1 mg/mL; ATV1 = 10 µM; ATV2 = 25 µM; ATV1 + GRT1 = 10 µM ATV + 0.01 mg/mL GRT; ATV1 + GRT2 = 10 µM ATV + 0.1 mg/mL GRT; ATV2 + GRT2 = 25 µM ATV + 0.1 mg/mL GRT. Data are mean ± SD derived from three independent experiments each with two technical repeats (n = 3). All results were expressed as a percentage normalised to the vehicle control at 100%. A one-way Analysis of Variance was performed with a Tukey post hoc test.*

	Mean Red (FL2-A) Fluorescence Intensity
Vehicle Control	100.00% ± 8.76
GRT1	90.62% ± 21.45
GRT2	64.28% ± 13.16
ATV1	66.99% ± 22.73 [a]
ATV2	32.48% ± 11.55 [a]
ATV1 + GRT1	73.95% ± 19.46
ATV1 + GRT2	56.22% ±11.62
ATV2 + GRT2	38.44% ± 20.66
	[a] = $p<0.05$

Table 10-2: Quantification of JC-1 FACS analysis in the hyperlipidaemic condition. *C3A cells were exposed to various treatments and combinations (24 hours). Palmitate control = palmitate pre-treated cells with media with 0.25% DMSO; GRT1 = 0.01 mg/mL; GRT2 = and 0.1 mg/mL; ATV1 = 10 µM; ATV2 = 25 µM; ATV1 + GRT1 = 10 µM ATV + 0.01 mg/mL GRT; ATV1 + GRT2 = 10 µM ATV + 0.1 mg/mL GRT; ATV2 + GRT2 = 25 µM ATV + 0.1 mg/mL GRT. Data are mean ± SD derived from three independent experiments each with two technical repeats (n = 3). All results were expressed as a percentage normalised to the palmitate control at 100%. A one-way Analysis of Variance was performed with a Tukey post hoc test.*

	Mean Red (FL-2) Fluorescence Intensity
Palmitate Control	100.00% ± 17.52
GRT1	69.03% ± 22.77
GRT2	74.38% ± 25.03
ATV1	106.90% ± 20.81 [a]
ATV2	63.02% ± 16.17 [a]
ATV1 + GRT1	75.87% ± 20.28
ATV1 + GRT2	81.00% ± 20.27
ATV2 + GRT2	57.67% ± 11.79
	[a] = $p<0.01$

10.1 JC-1 staining in the hyperlipidaemic condition

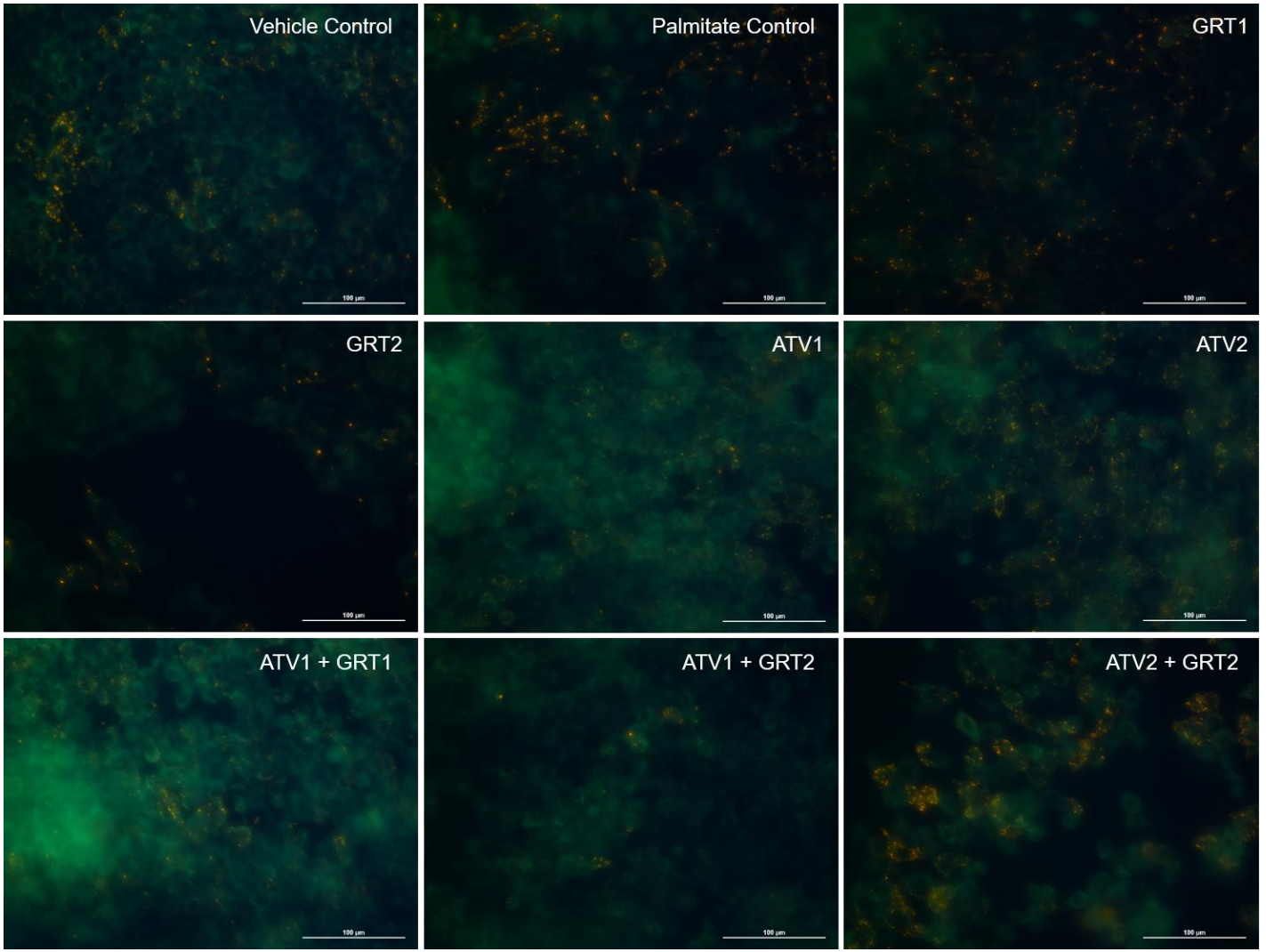

Figure 10.1.1: Representative images of JC-1 stained C3A cells in the hyperlipidaemic condition. *Images were captured at 40X magnification. Scale bar = 100 µm.*

Table 10-3: Quantification of annexin V/PI FACS analysis in the normal condition. *C3A cells were exposed to various treatments and combinations (24 hours). Vehicle control = media with 0.25% DMSO; GRT1 = 0.01 mg/mL; GRT2 = and 0.1 mg/mL; ATV1 = 10 µM; ATV2 = 25 µM; ATV1 + GRT1 = 10 µM ATV + 0.01 mg/mL GRT; ATV1 + GRT2 = 10 µM ATV + 0.1 mg/mL GRT; ATV2 + GRT2 = 25 µM ATV + 0.1 mg/mL GRT. Data are mean ± SD derived from three independent experiments each with two technical repeats (n = 3). A one-way Analysis of Variance was performed with a Tukey post hoc test.*

	Viable	Early Apoptosis	Late Apoptosis
Vehicle Control	86.33% ± 4.63	5.83% ± 2.04	7.83% ± 2.79
GRT1	86.83% ± 11.81 [a]	5.33% ± 2.50	8.00% ± 9.90 [a]
GRT2	78.17% ± 9.09 [b]	9.17% ± 3.25 [a]	12.50% ± 6.06 [b]
ATV1	57.67% ± 10.41 [c]	5.67% ± 2.50 [b]	36.50% ± 10.93 [c]
ATV2	18.00% ± 5.62 [c]	0.33% ± 0.52 [b]	81.67% ± 5.57 [c]
ATV1 + GRT1	56.67% ± 17.68 [a]	7.83% ± 3.76	35.17% ± 19.28 [a]
ATV1 + GRT2	68.67% ± 13.74	5.00% ± 0.89	26.33% ± 13.40
ATV2 + GRT2	34.67% ± 9.40 [b]	0.33% ± 0.52 [a]	64.83% ± 8.98 [b]
	[a] = p<0.001; [b] = p<0.001; [c] = p<0.001	[a] = p<0.001; [b] = p<0.01	[a] = p<0.01; [b] = p<0.001; [c] = p<0.001

Table 10-4: Quantification of annexin V/PI FACS analysis in the hyperlipidaemic condition*. Cells were exposed to various treatments and combinations (24 hours) subsequent to a 24 hour 500µM palmitate pre-treatment. Palmitate control = palmitate pre-treated cells exposed to media with 0.25% DMSO for 24 hours; GRT1 = 0.01 mg/mL; GRT2 = and 0.1 mg/mL; ATV1 = 10 µM; ATV2 = 25 µM; ATV1 + GRT1 = 10 µM ATV + 0.01 mg/mL GRT; ATV1 + GRT2 = 10 µM ATV + 0.1 mg/mL GRT; ATV2 + GRT2 = 25 µM ATV + 0.1 mg/mL GRT. Data are mean ± SD derived from three independent experiments each with two technical repeats (n = 3). A one-way Analysis of Variance was performed with a Tukey post hoc test.*

	Viable	Early Apoptosis	Late Apoptosis
Palmitate Control	67.00% ± 5.06	13.00% ± 5.73	19.83% ± 8.66
GRT1	65.00% ± 10.04	12.17% ± 4.92	23.00% ± 12.60
GRT2	73.33% ± 10.29	11.67% ± 2.58 [a]	14.67% ± 9.16
ATV1	72.00% ± 6.54	5.00% ± 2.45	22.83% ± 5.35
ATV2	67.75% ± 14.01	1.75% ± 0.50	30.75% ± 13.45
ATV1 + GRT1	71.17% ± 10.94	7.00% ± 5.55	21.83% ± 7.73
ATV1 + GRT2	82.50% ± 5.09	5.50% ± 3.21	11.67% ± 4.13
ATV2 + GRT2	76.33% ± 10.15	3.17% ±0.98 [a]	20.50% ± 9.81
		[a] = p<0.01	

11 Appendices

11.1 Tissue Culture

11.1.1 Aseptic Technique

- In order to maintain sterility, all experiments and procedures took place in a biosafety class 2 cabinet. Micropipette tips and serological pipettes used were filtered and sterile. Before being placed in the biosafety class 2 cabinet, all equipment (centrifuge tubes, flasks, etc.), as well as the surface of the hood itself, were sprayed down with 70% ethanol.

11.1.2 Maintenance of Cell Line

- Cell name: C3A [HepG2/C3A, derivative of HepG2 (ATCC HB-8065)] (ATCC® CRL-10741™)
- ATCC #: HB-8065
- Aggregating cell line, therefore care must be taken so as not to allow cultures to become over-confluent
- Growth medium: EMEM with 10% FBS and 0.1% 200 mM L-Glutamine (the combination of which referred to as complete growth medium)
- Temperature: 37°C and 5% CO_2
- Freeze medium: Complete growth medium supplemented with 7% DMSO
- Storage medium: Liquid nitrogen (vapour phase)
- Number of times the cells have been trypsinized and reseeded was indicated by passage numbers in order to avoid phenotypic drift.
- Complete growth medium, PBS, and treatments were always pre-warmed in a water bath at 37°C prior to use.

11.1.3 Preparation of Complete Growth Media

- 10% FBS (50 mL) was added to 500 mL EMEM
- 200 mM L-glutamine (5 mL) was added to 500 mL EMEM
- Complete medium was then aliquoted into 50 mL centrifuge tubes for routine use
- Aliquoted centrifuge tubes containing medium were stored at 4°C

11.1.4 Cell thawing

- 50 mL centrifuge tube of growth medium was pre-warmed in water bath at 37°C

- Cryopreservation vial storing C3A cells was removed from liquid nitrogen storage tank and allowed to thaw
    - NOTE: complete thawing of cells was not allowed
- Once partially thawed, cryopreservation vial was aseptically transferred the biosafety class 2 cabinet
- 14 – 18 mL pre-warmed growth medium was added to a T75 flask
- Cell suspension in the flask was slowly re-suspended and incubated (37°C with 5% CO_2)
- Confluency of the cells was assessed regularly and growth medium was refreshed every 2 days
- Cells were considered ready to be sub-cultured at 70% - 80% confluency

11.1.5 Cell sub-culturing and seeding

- Fresh growth medium and PBS is pre-warmed to 37°C in a water bath
- Trypsin was brought to room temperature
- Growth medium was aspirated from the cell monolayer
- The monolayer was washed with 5 mL pre-warmed PBS
- PBS was aspirated and 3 mL trypsin was added to the flask and incubated (37°C) for 5 minutes to ensure loosening of cells. Sufficient loosening of the cells was assessed using a microscope.
    - NOTE: cells were very adherent so gently tapping the culture flask against the base of one's palm helped to loosen the cells
- Once cells had sufficiently loosened, trypsin was inactivated with at least twice the volume of pre-warmed growth medium (i.e.: ≥6 mL)
- Cell suspension was aspirated from the flask and decanted into a 50 mL centrifuge tube and centrifuges for 5 minutes at 1500rpm
- Without disturbing the pellet, the supernatant was discarded and the pellet was re-suspended with pre-warmed medium
- A 10 µL sample of the cell suspension was counted and the required volume given the appropriate seeding density was calculated (See Counting of Cells)
- The calculated volume of cell suspension was added to the applicable growth surface (flask or plate) and the required volume of fresh growth medium was added
- Gently swirl plate or flask to ensure uniform cell distribution over growth surface
- Cells were then incubated as normal (37°C with 5% CO_2)

11.1.6 Counting of Cells

- Haemocytometer was cleaned with 70% ethanol before use
- 10 µL of cell suspension was added to 10 µL of Trypan blue
- 10 µL of the Trypan blue cell suspension was added to one half of the haemocytometer (covering one grid)
- Haemocytometer was placed on the stage of an Olympus CKX31 inverted light microscope
- Cells were counted in four of the nine quadrants (A, B, C, D see image below)

Example of a haemocytometer:

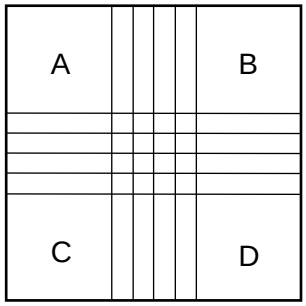

- Calculate the number of cells
  - Total volume of each quadrant = $10^{-4}cm^3$ therefore the conversion factor is 10 000

$$Cells\ per\ cm^3 = \left(\frac{\#\ cells\ tallied}{\#\ quadrants\ counted}\right) \times dilution\ factor\ \times 10\ 000$$

$$= x\ cells\ per\ ml$$

    - NOTE: multiplied by the Trypan blue dilution factor in order to calulate accurate number of cells relative to the volume
  - Cells resuspended in y µl of medium

$$Volume\ of\ cell\ suspension\ required = \frac{y}{x} \times required\ seeding\ density$$

    - NOTE: Seeding density for C3A cells is $1{,}10x10^5$ cells per millilitre

11.1.7 Freezing cells

- Cells were generally frozen at a concentration >$1X10^6$ cells/mL per cryopreservation vial
- After centrifugation, the supernatant was aspirated without disturbing the pellet
- Each pellet was carefully re-suspended in complete growth medium supplemented with 7% (v/v) DMSO

- 1 mL of cell suspension was added to each cryopreservation vial
- Vials were labelled with the cell line, passage number, and date
- Cryopreservation vials were stored at -80°C overnight
- The following day, cryopreservation vials were transferred to liquid nitrogen for proper storage for future use

11.2 Cytotoxicity and Cell Viability

11.2.1 MTT reagents

11.2.1.1 MTT

- 90 mg MTT was dissolved in 45 mL 1x PBS

11.2.1.2 Sorenson's Glycine Buffer

- 0.3755 g glycine (0.1 M)
- 0.292 g NaCl (0.1 M)
- 50 mL USP WFI
- pH to 10.5 with NaOH

11.2.2 MTT protocol

- PBS pre-warmed
- Medium aspirated
- Washed with 200 µL PBS
- Added 50 µL MTT to each well
- Incubated for 30 minutes at 37°C
- Aspirated MTT
- Added 200 µL DMSO and 25 µL Sorenson's Buffer
- Read at OD_{570nm} using Microtiter plate reader

11.3 Modulation of CYP3A4 activity

11.3.1 Western blot reagent preparation

11.3.1.1 10x Tris-buffered saline (TBS) stock solution

- 48.44 g Trizma-Base
- 160.12 g NaCl
- 1.8 L dH_2O
- pH to 7.6
- Made up to 2 L with dH_2O
- Stored at 4°C

11.3.1.2 1x TBS-T working solution

- 200 mL 10x TBS stock solution
- 1800 mL dH_2O

- 2 mL Tween-20
- Stored at 4°C

11.3.1.3 Transfer buffer

- 200 mL 5x Bio-Rad Transfer Buffer
- 200 mL absolute ethanol
- 600 mL d_2H_2O
- Stored at room temperature

11.3.2 Protein extraction

- Cells scraped in 300 µL radioimmunoprecipitation assay (RIPA) lysis buffer supplemented with phenylmethylsulfonyl fluoride (PMSF) and a protease inhibitor
- Lysate collected in Eppendorf microcentrifuge tube
- Lysate homogenised in a tissue ribolyser
    - Homogenise at 25 Hz for 60 seconds
    - Incubate 60 seconds on ice
    - Repeat 4 times
- Centrifuged at 30000 rpm at 4°C for 10 minutes
- Supernatant collected in new Eppendorf microcentrifuge tube

11.3.3 Protein concentration determination (RC DC protein assay)

- Samples were diluted 1:10 in nanopore water
- Samples were compared to a BSA standard curve
    - Standard curve concentrations were 0.0 mg/mL, 0.125 mg/mL, 0.25 mg/mL, 0.5 mg/mL, 0.75 mg/mL, 1.0 mg/mL, 1.5 mg/mL, and 2.0 mg/mL
- 25 µL of reagent A' + 200 µL of reagent B were added to each well containing standards and samples
- Multi-well plate was mixed on a plate shaker (500 rpm; 10 seconds) then incubated for 10 minutes at room temperature
- Absorbance was read on a SpectraMax i3x at OD_{630}
- Protein concentration of each sample was extrapolated from the BSA standard curve generated and multiplied by the dilution factor

11.3.4 Sample preparation and gel electrophoresis

- 4x SDS sample buffer was prepared (900 µL Laemmli Sample Buffer + 100 µL β-mercaptoethanol)

- 60 µg protein lysate was mixed with SDS sample buffer in a ratio of 1:4
- Samples were denatured by heating (5 minutes at 95°C)
- Samples were then immediately transferred to ice
- Mini-PROTEAN® TGX™ 12% Precast Gels placed in gel tank
- Tank and buffer dam filled with 1x Tris/Glycine/SDS running buffer
- 5 µL Precision Plus Protein™ Western C™ marker and 60 µg protein sample was loaded onto the gel
- PowerPac HC was run at 150 V for 70 minutes

11.3.5 Western blot analysis

11.3.5.1 Transfer to Nitrocellulose membrane

- Transfer sandwich and nitrocellulose membrane were submerged in 1x Transfer Buffer for 3 minutes
- Transfer sandwich was assembled in a Trans-Blot® Turbo™ transfer cassette
- Proteins were transferred to membrane by semi-dry transfer
    - Bio-Rad mixed molecular weight transfer for 10 minutes at 25 V and 2.5 A

11.3.5.2 Ponceau S stain

- Membrane was removed and submerged in Ponceau S stain to assess protein transfer
- Membrane was incubated on an orbital shaker for 10 minutes
- Membrane was rinsed in dH_2O until the background was clear
- Protein bands imaged on Bio-Rad ChemiDoc MP System
- Membrane was counterstained in TBS-T on an orbital shaker for 5 minutes at room temperature

11.3.5.3 Membrane labelling

- Membrane blocked in 5% (w/v) skim milk powder in TBS-T on an orbital shaker for 120 minutes at room temperature
- Membrane rinsed 3 x 10 minutes in TBS-T
- Membrane incubated in primary antibody overnight on an orbital shaker at 4°C
    - CYP3A4 1:500 in 5% (w/v) BSA in TBS-T
    - GAPDH 1:2500 in TBS-T
- Membrane rinsed 3 x 10 minutes in TBS-T
- Membrane blocked in HRP-conjugated secondary antibody (1:4000) + StrepTactin (1:10000) in 2.5% (w/v) skim milk powder in TBS-T on an orbital shaker for 90 minutes at room temperature

- Membrane rinsed 3 x 10 minutes in TBS-T
- Membrane immersed in ECL (1:1 parts A and B) and incubated for 5 minutes in the dark at room temperature
- Membrane imaged on Bio-Rad ChemiDoc MP System

11.4 Oxidative stress (DCF assay)

- 20 µM DCF added to each well
- Incubated for 30 minutes at 37°C
- Readings taken (Ex 485/20nm; Em 528/20nm)

11.5 Apoptosis assessment using flow cytometry

11.5.1 JC-1 mitochondrial membrane potential stain

- Aspirated treatment medium into Eppendorf micro centrifuge tubes in order to retain detached cells and stored at 4°C temporarily
- Added 200 µL trypsin to each well
- Incubated at 37°C for 15 minutes
- Neutralised the trypsin with 500 µL medium
- Added trypsinised cells to Eppendorf micro centrifuge tubes stored at 4°C
- Centrifuged at 200xg for 5 minutes
- Aspirated supernatant
- Re-suspended in 250 µL PBS
- Counted (untreated unstained control) with a Trypan blue stain
    - Calculated viability and adjusted to $1x10^6$ cells/mL
- Stained with 2 µM JC-1
    - NOTE: JC-1 is light-sensitive
- Incubated for 30 minutes at 37°C
- Centrifuged at 200xg for 5 minutes
- Washed with 300 µL PBS
- Centrifuged at 200xg for 5 minutes
- Re-suspended in 300 µL PBS
- Read on flow cytometer

11.5.2 Annexin V/propidium Iodide (PI) stain

- Aspirated treatment medium into Eppendorf micro centrifuge tubes in order to retain detached cells and stored at 4°C temporarily
- Added 200 µL trypsin to each well
- Incubated at 37°C for 15 minutes
- Neutralised the trypsin with 500 µL medium
- Added trypsinised cells to Eppendorf micro centrifuge tubes stored at 4°C
- Centrifuged at 200xg for 5 minutes
- Aspirated supernatant
- Re-suspended in 250 µL PBS
- Stained with 100 µL Annexin V/PI per sample
    - NOTE: Annexin V/PI is light-sensitive
    - 1.5 µL/100 µL Annexin V

- 10 µL/100 µL PI
  - Working concentration of PI is 100 µg/mL
- Incubated for 30 minutes at 37°C
- Centrifuged at 200xg for 5 minutes
- Washed with 300 µL PBS
- Centrifuged at 200xg for 5 minutes
- Re-suspended in 300 µL PBS
  - NOTE: Samples kept on ice
- Read on flow cytometer

11.6 Caspase 3/7 activation assessment

- 2 mM stock solution (made up in DMSO – 100 µL → already prepared)
- Diluted stock in complete medium to final concentration of 10 µM working solution
- Aspirated treatment
- Added 100 µL working solution to each well
- Read on SpectraMax i3x
  - Ex/Em: 502nm/530nm
  - Incubated for 60 minutes at 37°C
  - Read from the bottom of the well every 15 minutes

11.7 3D culturing

11.7.1 Day 0

Bioreactors and AggreWell™ plate were prepared

11.7.1.1 Setting up of 10 mL bioreactors

- Bioreactor was removed from sterile packaging in the hood
- Balanced in a sterile Petri dish, the bioreactor ports were plugged with appropriate plugs
- Humidity chamber was filled 40 mL with pre-warmed TC grade water
- Growth chamber was filled with 9 mL pre-warmed DPBS
- Apical growth chamber port area was cleaned with ~200 µL 70% ethanol
- Bioreactor was firmly attached to a rotor switched on to reverse

11.7.1.2 Preparation of AggreWell™ plate

- Centrifuge plate carrier was wiped with ethanol and appropriate programme was set
- 500 µL complete growth medium was added to two wells of the AggreWell™ plate
    - Used wells were marked accordingly
- AggreWell™ plate was centrifuged with an appropriately prepared counter balance plate at room temperature at 2200 RCF for 9 minutes
- Plate was carefully removed from the centrifuge and placed in the incubator until needed
- Semi-confluent cells were removed from T75 flask by trypsinisation
- Cells were gently re-suspended to achieve a single cell suspension
- A sample of approximately 100 µL of cell suspension was removed for quantification of cells with a haemocytometer
- Cells were centrifuged at room temperature in a sterile 50 mL centrifuge tube for 5 minutes at 100 RCF
- Cells were re-suspended at 4.8×10^6 cells/mL
    - A minimum of 2 mL of this cell suspension was prepared
- 500 µL of the cell suspension was added to each of the two previously prepared AggreWell™ plate wells. Caution was taken to disperse the cell suspension as evenly as possible throughout each well, as well as avoiding the formation of bubbles
- Each of the newly seeded wells was topped up with 1000 µL of pre-warmed growth medium

- AggreWell™ plate was centrifuged at room temperature at 100 RCF for 3 minutes
- Distribution of the cells and absence of bubbles was assessed visually with the aid of an inverted microscope
- AggreWell™ plate was carefully transferred to the incubator and the plate was left to incubate for approximately 20 hours

11.7.2 Day 1

- Heating blocks were pre-warmed to ~37°C
- Mother bioreactors were prepared as follows:
    - One bioreactor prepared on Day 0 was detached
    - PBS was aspirated from the growth chamber
    - 3.5 mL pre-warmed complete growth medium was added to the chamber
    - Bioreactor was reattached to the rotor and incubated at 37°C until required
- 500 µL pre-warmed complete growth medium was added to a Petri dish (on heating block; 35mm x 10mm; clearly labelled)
- AggreWell™ plate was placed on the second heating block. Spheroids were gently dislodged from within the micro-wells using a disposable Pasteur pipette.
    - NOTE: in order to be very gentle, a maximum volume equivalent to 2 cm from the tip of the pipette was taken up and pipetted incredibly slowly
- Process was observed continuously under the microscope
- Dislodged spheroids were transferred to the Petri dish when approximately 50% of the spheroids had been dislodged
- Fresh medium was added to the well to and remaining spheroids were dislodged and transferred to the Petri dish
- Spheroids were observed under the microscope for uniformity. Any distinctly aberrant spheroids or cell clusters were removed
- Petri dish was gently swirled to aggregate the spheroids in the centre. Using a disposable Pasteur pipette, spheroids were transferred to the growth chamber of the bioreactor via the large port on the face of the bioreactor
- The front port was securely fastened and the growth chamber was topped up via the apical port with pre-warmed complete growth medium using a 10 mL pipette
- Bioreactor was gently tapped to release any bubbles close to the apical port
- Excess medium was removed from the external apical port areas and bioreactor was checked again for bubbles.
- If no bubbles were found, external apical port was cleaning with ~200 µL 70% ethanol
- Bioreactor was returned to the incubator and rotated at the lowest speed (~14.5 rpm)

- Bioreactors were checked for bubbles approximately 1 hour later

11.7.3 Change of growth/treatment media

- For the first 18 days of growth, media was changed every two days. Treatment media was changed every day
- Media was carefully aspirated using a 10 mL syringe with an 18G hypodermic needle from the apical port of the bioreactor
- Fresh media/treatment added slowly using a 10 mL serological pipette
- The fastened apical port was cleaned thoroughly with 70% ethanol

11.7.4 Sampling of spheroids

- Approximately half of the media in the bioreactor was carefully aspirated using a 10 mL syringe with an 18G hypodermic needle from the apical port of the bioreactor
- Apical port was fastened and bioreactor placed with front port facing up
- Spheroids were sampled from the front port and transferred to applicable sample surface (plate or microcentrifuge tube) and front port was fastened
- Remaining media/treatment media was removed and replaced with fresh media/treatment media as previously described

11.8 ATP production

- Stored plate with sampled spheroids and CellTiter-Glo® detection kit left to equilibrate to room temperature before use
- Lyophilized CellTiter-Glo® Substrate reconstituted in CellTiter-Glo® buffer
- 125 µL CellTiter-Glo® Reagent added to each well
- Incubated for 60 minutes at 37°C on plate shaker
- Read on SpectraMax i3x

11.9 Adenylate kinase assessment

- All reagents equilibrated to room temperature before use
- Adenylate kinase detection reagent reconstituted in 10 mL assay buffer and allowed to equilibrate for 15 minutes (at room temperature)
- 5 µL of each treatment was added to a white-walled plate
- 100 µL reconstituted adenylate kinase detection reagent was added to each well
- Incubated at room temperature for 5 minutes
- Read on SpectraMax i3x

Turnitin Originality Report

17078334 DM MSc Thesis 2018

ORIGINALITY REPORT

13%	9%	11%	3%
SIMILARITY INDEX	INTERNET SOURCES	PUBLICATIONS	STUDENT PAPERS

PRIMARY SOURCES

1	"Systems Biology of Free Radicals and Antioxidants", Springer Nature America, Inc, 2014 Publication	1%
2	eprints.soton.ac.uk Internet Source	1%
3	core.ac.uk Internet Source	<1%
4	www.mdpi.com Internet Source	<1%
5	www.freepatentsonline.com Internet Source	<1%
6	www.salutebenessere.foundation Internet Source	<1%
7	Tirosh, O.. "Nutritional lipid-induced oxidative stress leads to mitochondrial dysfunction followed by necrotic death in FaO hepatocytes", Nutrition, 200902 Publication	<1%